Investigation of traffic characteristics in vehicular transport

A Thesis

submitted in partial fulfillment of the requirements for the award of the degree of

Doctor of Philosophy

in

School of Mathematics

by

Daljeet Kaur

Reg no: 901811001

under the supervison of

Dr. Sapna Sharma

Associate Professor

School of Mathematics

THAPAR INSTITUTE OF ENGINEERING AND TECHNOLOGY

PATIALA-147004, Punjab, India

DEDICATED
TO
THE ALMIGHTY
AND
MY PARENTS

Certificate

I hereby certify that the work, which is being presented in the thesis, entitled **Investigation of traffic characteristics in vehicular transport**, in partial fulfillment of the requirements for the award of the degree of **Doctor of Philosophy** and submitted to the institution is an authentic record of my own work carried out during the period **July 2018** to **February 2023** under the supervision of **Dr. Sapna Sharma**, Associate Professor, School of Mathematics, Thapar Institute of Engineering and Technology, Patiala.

Date: 29/05/23

Daljeet

(Daljeet Kaur)
Candidate

It is certified that the above statement made by the candidate is correct to the best of our knowledge.

Date: 29/5/23

Dr. Sapna Sharma
Supervisor

Acknowledgements

First and foremost, I would like to thank God. He has given me strength and encouragement throughout all the challenging moments of completing this thesis. I am truly grateful for His unconditional and endless love, mercy, and grace.

Thank you so much to everyone who has helped me along my student journey. So many people have been so kind. There are far too many to name but there are some people who I would like to especially thank.

I am extremely grateful to my supervisor **Dr. Sapna Sharma**, Associate Professor, School of Mathematics, Thapar Institute of Engineering and Technology, Patiala for her valuable guidance, consistent encouragement, understanding, and patience throughout my research work. I am thankful to **Dr. Arvind Kumar Gupta**, Associate Professor and Head, Department of Mathematics, Indian Institute of Technology, Ropar, for his unconditional support during my research work. He has made himself available to clarify my doubts despite his busy schedule, and I consider it as a great opportunity to work under his guidance as well and to learn from his positive disposition and research expertise.

I take this opportunity to express my deep sense of gratitude and respectful regards to Dr. Mahesh Kumar Sharma, Professor and Head, School of Mathematics. I am thankful to all the members of the doctoral committee Dr. Parimita Roy, Dr. Isha Dhiman, and Dr. Satish Kumar Sharma for their valuable comments and suggestions. I would like to express my gratitude to Dr. Harish Garg for his motivation. I am highly thankful to all other faculty members of the School of Mathematics and non-teaching staff members for providing me guidance and the necessary facilities for carrying out my research work.

This journey would not have been possible without the constant support from my friends. First of all, I would like to thank my best friend Ankit Sankhyan for his consistent support throughout these years and his selfless help when I was in trouble. You deserve a million thanks Rajwinder (elder sister by heart), love you a lot. I would also like to especially thank my friends Niyaz Ahmad Wani, Mandeep, Preet, Shaweta, and Uma Bharti for always support to me and believing in me. I would like to heartiest thank my seniors Raman and Madhu as well as my supportive juniors Tanvi and Muskan. I would like to thank my friend (badminton partner) Yash Jain. I would like to thank my fellow research scholars Kallal Pal, Nishtha, Mohit, Nikita, Rajvinder. I would like to thank all members of lab.

I would like to express my limitless thanks to my parents for their continuous and unparalleled love, motivation, support, faith and giving me the liberty to choose what I desired. I salute them for all the selfless love, care, pain and sacrifice they did to shape my life. To my brothers who turned out to be my best mates and to sisters-in-law, I can't express how much I love you guys and how appreciated you are. I would like to especially thank my nephews-nieces Rohan, Tanu, Prince, Prabh, Ginnu for bringing me so much happiness and you are actually the most wonderful part of my life.

Daljeet Kaur

Abstract

The number of automobiles increased as a result of population growth and economic expansion. The high availability of transportation complicates vehicle interaction, which may cause the occurrence of traffic congestion. Therefore, the traffic flow phenomenon has become one of the critical complex systems. Mathematical models can be used to understand and visualize traffic flow in mathematical terms. In this light, the current research puts up models and analyses of several actual traffic features by adopting a lattice hydrodynamic methodology (approach). The lattice hydrodynamic model has become the most famous because of its simpler approach. In this approach, space is discretized into lattice sites. The model comprises continuity and momentum equations that explain the aggregate behavior of traffic flow at each lattice site.

In this thesis, the effects of predictive effect have been examined on one-lane system when overtaking is permitted, two-lane system with rule of lane change, two-dimensional system having junction on road. Further, a new lattice model is developed by considering the influences of uncertainty of historical information on downstream. Furthermore, the factor area occupancy is included in lattice model which is related to heterogeneous traffic. All the models are analyzed theoretically by linear and nonlinear analysis. Theoretical findings are confirmed by numerical simulations. Additionally, the thesis is presented in seven chapters:

Based on traffic flow theory, **Chapter 1** reviews the literature regarding the general traffic system noted by the researchers, the potential hurdles to the transportation system, and possible solutions. Assumptions and requirements of traffic flow modeling are discussed. Various modeling approaches, such as microscopic models, macroscopic models, and lattice hydrodynamic models, are briefly discussed, describing important features of the traffic phenomenon. In addition, the scope and limitations of the existing models are presented.

The predictive effect and overtaking (passing) are interrelated in the traffic environment. When faster-moving vehicles receive prior information regarding the downstream circumstances, this information helps them decide whether to accelerate or slow down vehicle speed and also aids them in overtaking slower-moving vehicles. Therefore, motivated by the explained phenomenon, the investigation of the passing with predictive effect for a unidirectional single-lane highway is explored in **Chapter 2**. Further, the model is analyzed theoretically by employing stability analysis. The influence of the predictive effect is examined on traffic stream stability through linear stability analysis when passing is per-

mitted. It is shown that the accurate expected behavior of the vehicles ahead can enhance the stability of traffic flow for any rate of passing. Using nonlinear stability analysis, we obtained the critical value of the passing constant for which the kink soliton solution of the mKdV equation exists. When the passing constant is smaller than a critical value, the jamming transition occurs between uniform and kink flows. In contrast, for the higher value of passing constant, the jamming transitions occur from uniform flow to kink density wave flow through a chaotic phase. Numerical simulations verify the theoretical predictions, which show that traffic congestion can be suppressed efficiently by considering the predictive effect in a single-lane traffic system when passing is allowed. Finally, the results are summarized.

Chapter 3 aims to propose a new hydrodynamic lattice model by considering the predictive effect and the optimal current difference effect (OCDE) on a two-lane unidirectional traffic system. Stability analysis is used to conduct a theoretical investigation of the model. In a two-lane system with permitted lane changing, the contribution of the predictive effect, including consideration of OCDE, is examined on traffic stability by linear stability analysis. The mKdV equation is derived using nonlinear stability analysis, and the density wave in terms of the kink-antikink wave is obtained around the critical point. It is observed that the predictive effect plays an important role in enhancing traffic flow stability in a two-lane system. Numerical simulations are performed to validate the theoretical predictions, demonstrating that traffic jams can be alleviated more efficiently by considering the predictive effect in the vehicular system where lane change is permitted. At the end of the Chapter, the summary of the outcomes is presented with future scope.

In **Chapter 4**, a two-dimensional (2D) lattice model by incorporating the predictive effect with the junction on the road is proposed. According to the situation, drivers can change their driving behavior while using their skills in advance with the help of prior information, and they change their path through the turning point on the road. At the junction of the road, traffic can enter into various downstream lanes from the upstream. The intensity of downstream traffic may vary depending on the proportion of traffic. To analyze the proposed model, the stability condition is obtained without and with the control signal through the control method, which shows that the stable region increases when the control signal is considered into account. The theoretical findings indicate that the predictive effect could affect the stability of diverging traffic. Numerical simulations validate the theoretical findings, showing that the predictive effect for junction roads is beneficial in enhancing traffic flow stability. In the last section, the conclusion of the results and the possible future scope are given.

Several real-time feedback tactics have been presented and applied for traffic dynamics,

such as historical density information, historic flux information, etc. Moreover, complex uncertainties such as equipment malfunctions, network fluctuations, driver personality, and traffic disruption may affect traffic information. Therefore, **Chapter 5** is devoted to reflecting better the reality of traffic situations in the transportation system by considering uncertainty about historical information of density (UHDI) based on the lattice approach. The UHDI effect is probed using linear stability analysis and nonlinear stability analysis. The instability is found with an increased value of the UHDI coefficient. The modified Korteweg-de-Vries equation (mKdV) is obtained to describe the characteristics of traffic congestion. Finally, numerical simulations are implemented to analyze the results of theoretical findings. The numerical and hypothetical results show that the UHDI factor significantly affects traffic flow.

Chapter 6 deals with analyzing the impact of the heterogeneous behavior of vehicles on traffic dynamics. In developing countries, traffic not only consists of a wide range of vehicles, including automobiles, trucks, buses, motorbikes, etc. but is also disordered. Controlling and managing increasingly complex transport networks depend heavily on modeling the mechanics of mixed (heterogeneous) traffic. Vehicles having different speeds and sizes behave accordingly to their characteristics in traffic flow. Hence, a new lattice model is designed by considering the area occupancy of different vehicles in a heterogeneous disorder traffic system with a variable proportion of slow-moving to fast-moving automobiles. In addition, stability analysis is done to investigate the ability of a heterogeneous traffic model. The mixed traffic phase diagrams show a link between traffic stability and the fraction of vehicles. Moreover, a reduction perturbation approach is used to explore the behavior of the disordered traffic, and the mKdV equation is achieved near the critical point. It is demonstrated that larger vehicles cause traffic jams, whereas smaller ones are apt to ease traffic jams. Furthermore, numerical simulations are performed to verify the consistency of theoretical analysis. Results portray that a higher fraction of small vehicles is beneficial for stabilizing the traffic flow.

Further, **Chapter 7** summarizes the obtained results from the proposed models. The future scope is given based on some real traffic characteristics.

List of Publications

1. **D. Kaur** and S. Sharma. A new two-lane lattice model by considering predictive effect in traffic flow. *Physica A: Statistical Mechanics and Its Applications*, 539:122913, 2020. https://doi.org/10.1016/j.physa.2019.122913. (**SCI, Impact factor: 3.778**).

2. **D. Kaur** and S. Sharma. The impact of the predictive effect on traffic dynamics in a lattice model with passing. *The European Physical Journal B*, 93(3):1-10, 2020. https://doi.org/10.1140/epjb/e2020-100469-5. (**SCI, Impact factor: 1.398**).

3. **D. Kaur** and S. Sharma. Prior information affecting traffic dynamics in a two dimensional (2D) network. *The European Physical Journal B*, 94(9):1-12, 2021. https://doi.org/10.1140/epjb/s10051-021-00187-8. (**SCI, Impact factor: 1.398**).

4. **D. Kaur**, S. Sharma and A. K. Gupta. Analyses of lattice hydrodynamic area occupancy model for heterogeneous disorder traffic. *Physica A: Statistical Mechanics and Its Applications*, 607:128184, 2022. https://doi.org/10.1016/j.physa.2022.128184. (**SCI, Impact factor: 3.778**).

5. **D. Kaur** and S. Sharma. The impact of uncertain density information on traffic dynamics. (**Communicated**).

Table of Contents

Page No.

Acknowledgements . . . . . **v**

Abstract . . . . . **vii**

List of Publications . . . . . **xi**

Table of Contents . . . . . **xiii**

List of Figures . . . . . **xv**

List of Tables . . . . . **xix**

List of Abbreviations/Notations . . . . . **xxi**

Chapter 1 Introduction **1**

1.1 Traffic flow models 2

1.1.1 Components 3

1.1.2 Classifications 3

1.2 Formation of traffic jams 8

1.3 Lattice Hydrodynamic (LH) Model 10

1.3.1 Role of ITS 13

1.3.2 Extensions of LH model 14

1.4 Thesis contribution 16

Chapter 2 Influence of predictive effect in overtaking on traffic dynamics 19

2.1 Proposed LH model 20

2.2 Linear stability analysis 22

2.3 Nonlinear stability analysis 25

2.4 Numerical simulations 29

2.5 Conclusion 37

Chapter 3 Two-Lane traffic based on predictive effect **39**

3.1 Lattice model 40

3.2 Linear stability analysis 42

3.3 Nonlinear stability analysis . . . 44
3.4 Simulation . . . 48
3.5 Conclusion and future scope . . . 50

Chapter 4 Impact of prior information on two-dimensional vehicular system . . . 53
4.1 Two dimensional (2D) lattice model with junction road . . . 55
4.2 Linear stability analysis . . . 58
4.3 Stability analysis with control signal . . . 60
4.4 Results discussion . . . 64
4.5 Conclusion . . . 72
4.5.1 Outcomes: . . . 72
4.5.2 Future scope: . . . 72

Chapter 5 Effects of uncertainty about historical information on traffic dynamics . . . 73
5.1 Lattice model . . . 74
5.2 Linear stability analysis . . . 76
5.3 Nonlinear stability analysis . . . 78
5.4 Numerical simulations . . . 81
5.5 Conclusion and future scope . . . 83

Chapter 6 Lattice hydrodynamic area occupancy model . . . 87
6.1 Lattice Hydrodynamic Traffic Flow Models . . . 89
6.1.1 Basic Lattice Model . . . 89
6.1.2 Area Occupancy (AO) . . . 90
6.2 Lattice Hydrodynamic Area Occupancy (LHAO) Model . . . 92
6.3 Linear Stability Analysis (Effect of small amplitude deviation) . . . 95
6.4 Nonlinear Stability Analysis (Effect of long-wavelength deviation) . . . 96
6.5 Numerical Simulations . . . 100
6.6 Conclusion . . . 104
6.6.1 Research outcomes . . . 104
6.6.2 Future scope . . . 105

Chapter 7 Summary and future scope . . . 107
7.1 Summary . . . 107
7.2 Future scope . . . 109

Bibliography . . . 111

List of Figures

Figure No.	Title	Page No.
1.1	Illustrations of a simple microscopic approach in a one-dimensional system.	5
1.2	Illustrations of a simple macroscopic approach in a one-dimensional system [1].	6
1.3	Categories of traffic flow models and their connection [2]; $\langle\ \rangle$ denotes the mean value.	7
1.4	The schematic illustration of lattice hydrodynamic model.	11
1.5	Diagram of Density (ρ) versus Optimal velocity (V).	12
1.6	Illustration of receiving information on ahead traffic through ITS.	14
2.1	Phase diagram in parameter space (ρ, a) for different values of β with $t_0 = 0.1$ when (a) $\eta = 0.05$, and (b) $\eta = 0.3$. The solid lines in (a) and (b) show neutral stability curves, whereas the dashed lines in (a) represent the coexisting stability curves. The coexisting curves do not exist for $\eta = 0.3$ in (b).	23
2.2	Phase diagram in parameter space (ρ, a) for different values of t_0 with $\beta = 0.5$ when (a) $\eta = 0.05$, and (b) $\eta = 0.3$. The solid lines in (a) and (b) show neutral stability curves, whereas the dashed lines in (a) represent the coexisting stability curves. The coexisting curves do not exist for $\eta = 0.3$ in (b).	24
2.3	Phase diagram in (η, a) space	25
2.4	Spatiotemporal evolutions of density waves after time $t = 2 \times (10^4)s$ when $\eta = 0.05$, $a = 2.0$, and $t_0 = 0.1$ for (a) $\beta = 0$, (b) $\beta = 0.2$, (c) $\beta = 0.4$, and (d) $\beta = 0.6$, respectively.	26
2.5	Density profiles at time $t = 20000s$ when $\eta = 0.05$, $a = 2.0$, and $t_0 = 0.1$ for (a) $\beta = 0$, (b) $\beta = 0.2$, (c) $\beta = 0.4$, and (d) $\beta = 0.6$, respectively.	30
2.6	Plots of density versus density difference at time $t = 10^4 - 2\times10^4$ at $\eta = 0.05$, $t_0 = 0.1$, $a = 2.0$ for (a) $\beta = 0$, (b) $\beta = 0.2$, (c) $\beta = 0.4$, and (d) $\beta = 0.6$, respectively.	31
2.7	Spatiotemporal evolutions of density waves after time $t = 2 \times (10^4)s$ when $\eta = 0.3$, $a = 3.0$, and $t_0 = 0.1$ for (a) $\beta = 0$, (b) $\beta = 0.2$, (c) $\beta = 0.4$, and (d) $\beta = 0.6$, respectively.	33
2.8	Density profiles at time $t = 20000s$ when $\eta = 0.3$, $a = 3.0$, and $t_0 = 0.1$ for (a) $\beta = 0$, (b) $\beta = 0.2$, (c) $\beta = 0.4$, and (d) $\beta = 0.6$, respectively.	35

2.9 Plots of density versus density difference at time $t = 10^4 - 2 \times 10^4$ at $\eta = 0.3$, $t_0 = 0.1$, $a = 3.0$ for (a) $\beta = 0$, (b) $\beta = 0.2$, (c) $\beta = 0.4$, and (d) $\beta = 0.6$, respectively. 36

3.1 The schematic lattice model of unidirectional traffic flow on a two-lane highway with permissible lane changing 41
3.2 Phase diagrams with $\rho_0 = \rho_c = 0.25$ in (ρ, a) space for different values of parameter β with $\lambda = 0.2$, $t_0 = 1.2$ for (a) $\gamma = 0$ (b) $\gamma = 0.1$. 43
3.3 Spatio-temporal evolutions of density waves after $t = 10^4 s$ when $a = 1.0$, $\gamma = 0$ for (a) $\beta = 0$, (b) $\beta = 0.1$, (c) $\beta = 0.2$, and (d) $\beta = 0.3$, respectively. 47
3.4 Spatio-temporal evolutions of density waves after $t = 10^4 s$ when $a = 1.0$, $\gamma = 0.1$ for (a) $\beta = 0$, (b) $\beta = 0.1$, and (c) $\beta = 0.2$, respectively. 49
3.5 Profiles of the density wave at time $t = 10^4 s$ for different values of β when (a) $\gamma = 0$ (b) $\gamma = 0.1$. 50

4.1 The schematic 2D lattice model of unidirectional traffic flow with the junction on the highway. 56
4.2 Phase plot in the plane (d, ρ, a) by taking prior information (β) into account with consideration of junction point of road through the use of the control method. The plotted lines represent the stability curves for different values of parameter $\beta = 0, 0.3, 0.6,$ and 0.9 with $t_0 = 0.5$, $\rho_c = \rho_0 = 0.25$. 58
4.3 Phase plot in the plane (d, ρ, a) by taking prior information (β) into account with consideration of junction point through the use of the control method with a control signal. The plotted lines represent the stability curves with the control method for different values of parameter $\beta = 0, 0.3, 0.6,$ and 0.9, $t_0 = 0.5$, $\rho_c = \rho_0 = 0.25$, $\xi = 0.3$, and $\kappa = 0.1$. 62
4.4 Density profiles at time $t = 10300s$ with $d = 0$, $a = 0.9$ for (a) $\beta = 0$, (b) $\beta = 0.3$, (c) $\beta = 0.6$, and (d) $\beta = 0.9$, respectively, in positive y-direction $(r = 100)$. The inset profiles are drawn for density difference $(\rho(t) - \rho(t-1))$ versus density $(\rho(t))$. 63
4.5 Density profiles at time $t = 10300s$ with $d = 1.0$, $a = 0.9$ for (a) $\beta = 0$, (b) $\beta = 0.3$, (c) $\beta = 0.6$, and (d) $\beta = 0.9$, respectively, in positive x-direction $(j = 1)$. The inset profiles are drawn for density difference $(\rho(t) - \rho(t-1))$ versus density $(\rho(t))$. 65
4.6 Density profiles at time $t = 10300s$ with $d = 0.2$, $a = 0.9$ for (a) $\beta = 0$, (b) $\beta = 0.3$, (c) $\beta = 0.6$, and (d) $\beta = 0.9$, respectively, in positive y-direction $(r = 100)$. The inset profiles are drawn for density difference $(\rho(t) - \rho(t-1))$ versus density $(\rho(t))$. 66

4.7 Density profiles at time $t = 10300s$ with $d = 0.8$, $a = 0.9$ for (a) $\beta = 0$, (b) $\beta = 0.3$, (c) $\beta = 0.6$, and (d) $\beta = 0.9$, respectively, in positive x-direction ($j = 1$). The inset profiles are drawn for density difference ($\rho(t) - \rho(t-1)$) versus density ($\rho(t)$). 68
4.8 Density profiles at time $t = 10300s$ with $d = 0$, $a = 0.8$ for (a) $\beta = 0$, (b) $\beta = 0.3$, (c) $\beta = 0.6$, and (d) $\beta = 0.9$, respectively, in positive y-direction ($r = 100$). The inset profiles are drawn for density difference ($\rho(t)-\rho(t-1)$) versus density ($\rho(t)$). 69
4.9 Density profiles at time $t = 10300s$ with $d = 0.2$, $a = 0.8$ for (a) $\beta = 0$, (b) $\beta = 0.3$, (c) $\beta = 0.6$, and (d) $\beta = 0.9$, respectively, in positive y-direction ($r = 100$). The inset profiles are drawn for density difference ($\rho(t)-\rho(t-1)$) versus density ($\rho(t)$). 71

5.1 Variation of the optimal velocity versus density when uncertain factors happen. 76
5.2 Phase diagrams of (a) Density ($\rho_j(t)$) versus sensitivity (a) and (b) Density* ($\rho_j(t)^* = \chi\rho_j(t)$) versus sensitivity ($a$) for different values of χ, where $\chi =$ 1 to $\chi = 1.3$ by taking interval 0.1. 77
5.3 Spatio-temporal evolutions of density waves after $t = 9,800s$ with $\rho_0 = 0.2$, $a = 2.1$ for different values of χ. 80
5.4 Density profiles at time $t = 10000s$ for different values of χ corresponding to the panels of Fig. 5.3. 82
5.5 Instant flow versus Density with $a = 2.1$ for different values of χ corresponding to the panels of Fig. 5.3. 84

6.1 Distinct vehicles in the heterogeneous transportation system. 90
6.2 Variation of the optimal velocity versus density with $\rho_0 = \rho_c = 0.2$ for different values of fraction parameter corresponding to small (c_1) and large vehicles (c_2), where $A_1 = 1.08, A_2 = 7.14, v_{1,max} = 1.0, v_{2,max} = 2.0, W =$ 3.75. The optimal velocity curves at intervals of 0.1 for: (a) increasing c_1 from $c_1 = 0.1$ to $c_1 = 1.0$ and (b) increasing c_2 from $c_2 = 0.1$ to $c_2 = 1.0$. . 94
6.3 Phase diagrams of (a) Density ($\rho_j(t)$) versus sensitivity (a) and (b) Density* ($\rho_j(t)^* = B_l\rho_j(t)$) versus sensitivity ($a$) for different values of fraction parameter c when only two types of vehicles are considered as $c_1 = c$ and $c_2 = 1 - c$. 97
6.4 Density profiles with $a = 2.5$ at time $t = 25000$s for (a) $c = 0.1$, (b) $c = 0.2$, (c) $c = 0.3$, and (d) $c = 0.4$, respectively. 99
6.5 Instant flow ($J_j(t)$) versus density ($\rho_j(t)^*$) with $a = 2.5$ for (a) $c = 0.1$, (b) $c = 0.2$, (c) $c = 0.3$, and (d) $c = 0.4$, respectively. 101

6.6 Plots of Current versus density with $a = 2.5$ for (a) $c = 0.1$, (b) $c = 0.2$, (c) $c = 0.3$, and (d) $c = 0.4$, respectively. 103

List of Tables

Table No.	Title	Page No.
1.1	Variables in lattice model	13
2.1	The coefficients h_i of the model	27
2.2	The coefficients b_i of the model	27
3.1	The coefficients h_i of the model	45
3.2	The coefficients b_i of the model	46
5.1	Values of h_i coefficients	79
5.2	Values of b_i coefficients	79
6.1	Special cases related to new LHAO model	95
6.2	List of parameters	96
6.3	Values of h_i coefficients	98
6.4	Values of b_i coefficients	98

List of Abbreviations/Notations

OVM	Optimal velocity model
KdV	Korteweg-de Vries
mKdV	Modified Korteweg-de Vries
ITS	Intelligent Transportation System
LH	Lattice hydrodynamic
OCDE	Optimal current difference effect
UHDI	Uncertain historical density information
$\mathbf{a}$	Acceleration
V	Optimal velocity
a	Driver's sensitivity
j	Lattice site
v	Velocity
ρ	Density
ρ_0	Average density
ρ_c	Critical density
q	Flow
X	Space
T	Time
α	Amplitude of solitary wave
τ	Delay time
Δt	Time step
η	Passing coefficient
γ	Lane changing coefficient
λ	Reaction coefficient of OCDE
β	Coefficient of the predictive density variation
t_0	Predictive time
τ_0	Historical time
χ	Coefficient of UHDI
c	Proportion of small vehicles in mixed traffic
A_l	Area occupied by l^{th} type vehicle

Chapter 1

Introduction

The application of scientific and technological tenets to the planning, functionality, operation and administration of facilities in a transportation context is known as transportation engineering; moreover, it plays a vital role in providing convenient, efficient, rapid, safe, environmentally, and economically compatible movement of goods and people. Moreover, traffic flow has received significant attention in interdisciplinary sectors, such as mathematics, physics, and informatics. However, traffic networks are multi-component systems that include drivers, vehicles, road linkages, pedestrians, junctions (intersections), and their interactions. Traffic flow performance may be influenced by several factors, notably human behavior, environmental aspects, infrastructure, etc. The increase in population and economic expansion resulted in an increase in the number of vehicles. The great enough availability of transportation creates complications for vehicle interaction, leading to a slow down of traffic or a completely halted traffic, known as traffic congestion. Therefore, worldwide researchers are searching for solutions to the enduring problems associated with transportation, such as traffic jams, and improving safety. There are some of the enumerated negative effects of traffic congestion:

- Slower speeds of vehicles and an increase in vehicular queuing.
- The long queue increases travel time, which may lead to being late for a meeting, employment, or education, and may cause lost disciplinary action, revenue, or other losses.
- Frequent stopping or going and tight spacing increase the likelihood of vehicle collisions.
- Traffic jams may hinder emergency vehicles from reaching their destinations.
- Frustrated and stressed drivers encourage road rage and impact mental and physical health.
- Due to increased acceleration, brakes, and dense traffic, fuel is wasted, which raises greenhouse gas emissions and air pollution.

Transport engineering study began to take on a practical role from the time when re-

searchers and scientists started solving specific traffic problems. From a statistical mechanics and nonlinear dynamics viewpoint [3–7], the principles and various techniques of physics and mathematics have been applied in order to understand transportation systems better. A growing field of research called "traffic flow theory" examines the characteristics of traffic using mathematical and statistical concepts [2,8]. Mathematics developed itself as a reliable foundation for theoretically investigating transportation phenomena throughout this extremely dynamic time. Moreover, traffic researchers have applied the principles of fluid dynamics to investigate the behavior of vehicular flow, as it is same as fluid flow in a pipe [9,10]. Traffic flow can be described as one-dimensional compressible flow. Later pointed out by Daganzo [11], there are some dissimilarities between fluid flow and traffic flow. Firstly, fluid flow is isotropic, i.e., fluid particles respond according to stimulus from behind and front particles, but the drivers' reaction is only dependent upon the vehicles in front of them; therefore, vehicular flow is anisotropic. Secondly, just a few cars are affected by a traffic shock's breadth. Finally, in vehicular flow, the driver's personality is also a significant aspect that is irrelevant in the modeling of fluid flow.

Traffic flow mathematical models [12,13] are utilized to visualize and interpret vehicular flow on roadway networks. These models help to know the answers concerning the occurrence and intensity of traffic jams, the cause of vehicle queues' formation, the time taken to decrease congestion, etc. In addition, vehicles follow lane discipline behavior in many countries, but this behavior may be influenced due to availability of distinct vehicles with different speeds and sizes. Therefore, vehicular flow can be classified as either homogeneous or heterogeneous.

- In the homogeneous traffic flow, vehicles obey lane discipline by maintaining adequate distance. All vehicles are of the same characteristics. Moreover, the governing equations for all cars in the traffic flow are considered identical.
- The variety of vehicles with distinct features can be seen on roads, which is termed 'heterogeneity' in vehicles. These vehicles can be different by size, speed, motorized or non-motorized, two-wheeler, three-wheeler, etc. Commonly seen in the heterogeneous vehicular flow, vehicles do not follow the lane discipline. In addition, due to different sizes, more than one vehicle may move side-by-side on the road.

1.1 Traffic flow models

A variety of factors can influence traffic behavior, such as vehicle-vehicle interactions, distinct characteristics of human drivers (gender, psychology, age, and level of intoxication), state of infrastructure (roundabout, diversions, intersections, on-off ramps), vehicles' va-

rieties (small or large, slow or high speed) and effects of environmental (weather). As a result, the development of clusters and shock waves which propagates forward or/and backward depends on density. Consequently, mathematical models aid in the alleviation of traffic jams. For further clarification and understanding of traffic flow modeling, it will be necessary to explain its main aspects.

1.1.1 Components

The five essential components of traffic flow modeling are observation, principle, model formulation, discretization, and simulations. These components are explained as follows [14]:

1. The first stage is the creation of traffic flow models, which rely primarily on observations.
2. Observations are utilized to develop a conceptual (theoretical) structure in the second stage. The theoretical structure is a combination of assumptions (mostly related to behavioral) and statements (primarily qualitative).
3. The third stage involves the creation of traffic models using the theoretical structure. The collection of (typically continuous) equations constitutes the model.
4. In the fourth stage, discretization is needed since continuous models can't be implemented in computer simulations directly. Space, time, and/or other continuous variables are discretized based on the traffic model. Time is often split into discrete time steps in most simulation setups.
5. Finally, computer programming is used to implement the traffic flow model. Predictions or estimations of traffic state may be achieved using the simulation tool. For the purpose of validating, simulated results are compared to theoretical predictions (observations).

1.1.2 Classifications

The traffic flow models, generally according to 'level of detail' are classified as follows:

1.1.2.1 Microscopic models

In the microscopic approach, the motion of individual vehicles is modeled by incorporating their interactions with other vehicles within a system with the help of the typical function of position, velocity, and acceleration. In addition, ordinary differential equations are utilized to describe vehicular dynamics. The fundamental variables in the microscopic approach

are spacing (s^*), headway (h), and speed (u), and; the connection among these variables [2] can be expressed as $s^* = hu$.

Notations Description

The position and speed of n^{th} vehicle, respectively, are denoted by $x_n(t)$ and $u_n(t)$ at time t. The covered distance in a unit of time determines the vehicle's speed (u). Indexes $n-1$ and $n+1$, signifies the vehicles immediately behind and in front of n^{th} vehicle, respectively, as illustrated in Fig. 1.1. At time t, the distance between the bumpers of n^{th} and $n+1^{th}$ vehicles is described by distance headway $\Delta x_n(t)$ ($\Delta x_n(t) = x_{n+1}(t) - x_n(t)$). The difference between times (t_{n+1} and t_n) of two successive vehicles crossing a specific location (x) in space is defined by time headway and can be described as $\Delta t_n(x)$ ($\Delta t_n(x) = t_{n+1}(x) - t_n(x)$).

Car following models

The most popular branch of microscopic models is the car following models (CFMs), which are developed on the basis of a 'follow-the-leader' approach without overtaking on a uni-directional highway. The assumption is that each vehicle's motion depends on speed and distance difference from the front vehicle of it [15]. Newton's laws of motion are used in car-following theories [16–18]. In mechanics, acceleration is in terms of response with a certain sensitivity to the stimulus that the particle obtains in the form of force. This force occurs in some way due to interaction with other particles of the particle in the system. In the traffic stream, the driver accelerates or decelerates vehicle speed according to the surrounding situations. The speed of a vehicle, the distance headway, the speed differences in the following and leading vehicles (relative speed), etc., act as a stimulus to the road user. Hence, the stimulus is a function that depends upon more than one variable, which is represented as

$$\mathbf{a}_n(t) = G_{sti}(u_n(t), \Delta x_n(t), \Delta u_n(t)), \tag{1.1}$$

where G_{sti} depicts the stimulus function gained by the n^{th} ($n = 1, 2, 3, ...$) vehicle. In the above function, $\Delta x_n(t)$ defines distance headway; $\Delta u_n(t)$ represents relative speed. There are primarily two categories of theories for regulation. The first type is premised on the notion that each car must maintain the legally required distance from the vehicle in front of it, which is dependent upon the relative speeds of two consecutive vehicles [19]. The alternative regulation concept is that each vehicle has a legal speed that is determined by distance from the front vehicle of it.

In the sequences, Pipes [20] introduced the first safety distance model for collision avoid-

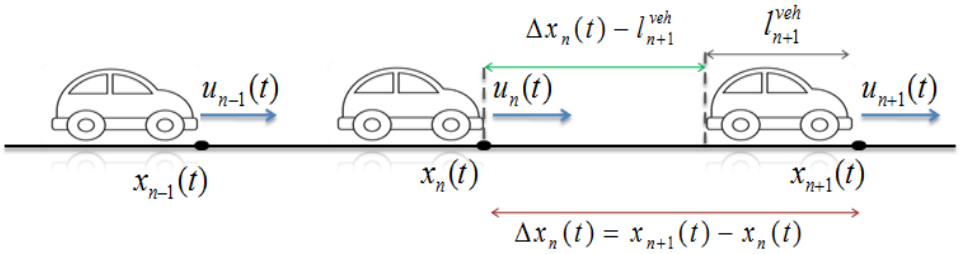

Figure 1.1: Illustrations of a simple microscopic approach in a one-dimensional system.

ance, and the formulation of CFM is given as

$$x_{n+1} = x_n + (D + T'u_n) + l_{n+1}^{veh}, \tag{1.2}$$

$(D + T'u_n(t))$ is the postulated legal separation between vehicles at position n and $n+1$; l_{n+1}^{veh} is length of $n+1^{th}$ vehicle. In addition, some models were developed based on the "stimulus-response" (follow the leader) approach from a different perspective at general motors research laboratories, which are known as the GHR models [21–25].

Further, the most useful car-following models are the optimal velocity models (OVM) [26–28]. In these models, the vehicle's length is neglected for convenience, and traffic is considered under homogeneous conditions. According to the theory behind this approach, each driver endeavors to reach an optimal velocity (V) relying on distance to ahead vehicle. The acceleration of n^{th} vehicle is determined by the discrepancy between optimal velocity (V) and actual velocity $(u_n(t))$ at time t. The formulation of the OV model represented by Bando et al. [28] with regards to the stimulus-response approach is

$$\mathbf{a}_n = a[V(\Delta x_n) - u_n]. \tag{1.3}$$

Here, a indicates the sensitivity coefficient of driver. The OV function, having maximum speed (v_{max}) with safety distance (h_c), is as

$$V(\Delta x_n) = \frac{v_{max}}{2}[\tanh(\Delta x_n - h_c) + \tanh(h_c)]. \tag{1.4}$$

Further, many new car-following models [29–33] for homogeneous traffic were developed by incorporating realistic traffic features in accordance with the theory of OV model. In an actual traffic environment, drivers and vehicles can differ due to a variety of factors, such as differences in gender, age, vehicle type, and so forth. Furthermore, in light of the heterogeneity in driver and vehicle type, researchers proposed a number of car-following

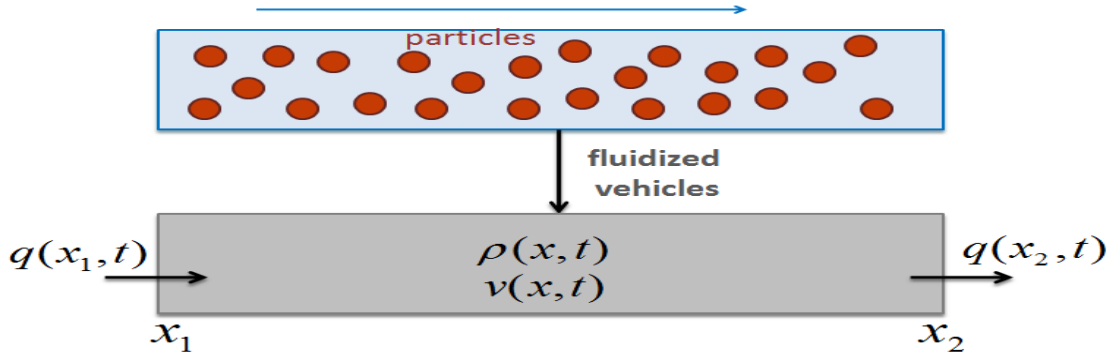

Figure 1.2: Illustrations of a simple macroscopic approach in a one-dimensional system [1].

models [34–38]. All the models mentioned above describe the traffic for a lane-based system, but vehicles do not follow the lane in some countries. Therefore, many extended microscopic models were proposed based on a non-lane-based system [39–41] to represent the realistic heterogeneity among the vehicles.

1.1.2.2 Macroscopic models

The observed dense traffic flow from a distance seems to be a fluid stream, where each vehicle represents a fluid molecule. Traffic is treated as a one-dimensional compressible fluid; hence, the hydrodynamic theory of fluids is used to develop a macroscopic explanation of traffic. The illustration of the macroscopic model is displayed in Fig. 1.2. In this theory, individual vehicle behavior is overlooked to concentrate on vehicles' aggregate behavior. The aggregate variables are defined, such as density $\rho(x,t)$, average speed or velocity $v(x,t)$, and flow $q(x,t)$ [1]. There is a fundamental relationship between micro and macro variables, which is displayed in Fig. 1.3. It is shown that all macro variables (ρ, v, q) are fundamentally related to each other by $q = \rho v$ [2]. Further, macroscopic models can be categorized based on first- and second-order models.

First-order continuum model

One of the most popular continuum models is the Lighthill-Whitham-Richard (LWR) model, introduced by Lighthill, Whitham [42] and Richards [43], also called the 'simple continuum model.' Without entrances or exits on the segment of the road, the number of vehicles remains conserved. Following the conservation law, the continuity equation is

$$\partial_t \rho(x,t) + \partial_x(q(x,t)) = 0, \tag{1.5}$$

where the symbol ∂ denotes the partial derivative; $\partial_t = \partial/\partial t$ and $\partial_x = \partial/\partial x$. It was proposed that the mean velocity is a function that depends on density under equilibrium

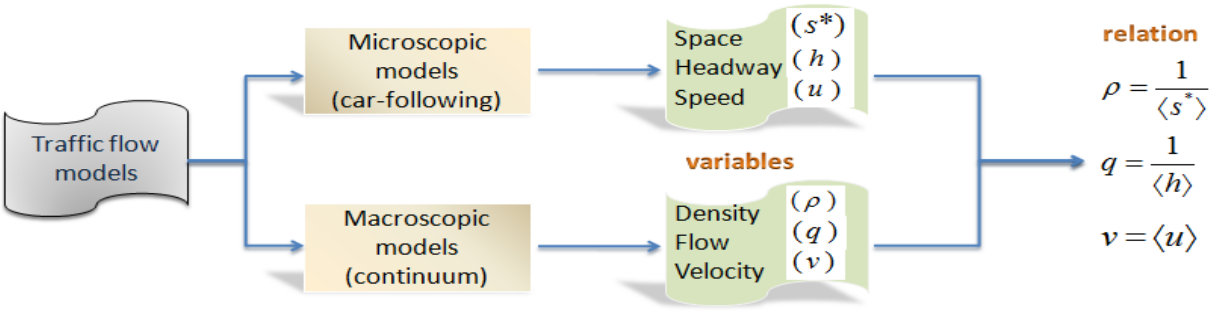

Figure 1.3: Categories of traffic flow models and their connection [2]; $\langle\ \rangle$ denotes the mean value.

conditions, i.e., $v(x,t) = v_e(\rho(x,t))$, which leads to

$$\partial_t \rho(x,t) + \partial_x(\rho(x,t) v_e(\rho(x,t))) = 0, \tag{1.6}$$

where $v_e(.)$ represents the equilibrium velocity function. Due to the use of an instantaneous speed density relationship, the simple continuum model was inadequate to describe a few well-known traffic phenomena, including stop-go waves, hysteresis, and platoon dispersion. Furthermore, since no stability condition can be obtained from the model, so fails to demonstrate the amplification of minor disturbances in heavy traffic. Consequently, higher-order continuum models for non-equilibrium states came into existence.

Higher-order continuum model

In order to address the limitations of the LWR model, a higher-order continuum model, known as the Payne-Whitham (PW) model, was developed by Payne [44]. The new model equation (momentum equation) was introduced in addition to the continuity equation. Various high-order models that fall under the categories of density-gradient (DG) [44–47] and speed-gradient (SG) [48–51] models were presented.

The DG model can be expressed in general form as below

$$\partial_t v + v\partial_x v = -\frac{c^2(\rho)}{\rho}\partial_x \rho + \frac{v_e(\rho) - v}{\tau}, \tag{1.7}$$

where, $c(\rho)$ represents sonic speed; τ denotes reaction time. In Equation 1.7, the left side denotes acceleration. On the right side, the first term is anticipation term, which indicates how drivers respond to the traffic situations ahead of them. The term $\partial_x \rho$ represents the tendency of drivers. The second term signifies the relaxation of velocity (v) towards density-dependent equilibrium velocity ($v_e(\rho)$).

However, as noted by Daganzo [11], the characteristic speed in Payne's model [44] always exceeds the macroscopic flow velocity. This implies that the traffic conditions that exist behind a flow of traffic will have an impact on its future conditions. Vehicles are anisotropic particles and only respond to their leader, but Payne's model violated this principle. After that, with some improvements over Payne's model, various models [45,47,52–54] were presented, but they fail to address the issue related to characteristic speed. Hence, there was the need to develop a new non-equilibrium model.

To overcome the flaws of previous models, a new SG model [49] was presented as

$$\partial_t v + v\partial_x v = c_0\partial_x v + \frac{v_e(\rho) - v}{\tau}, \tag{1.8}$$

where, c_0 is the propagating speed. In the above equation, the anticipation term is the speed gradient term in lieu of the density gradient term. This replacement fixes the problem with a characteristic speed that existed in the previous models. As a result, the new model can accurately reflect the anisotropic feature.

Several modified and extended versions of macroscopic models were developed by taking into account various traffic scenarios [55–65]. In reality, various kinds of vehicles are available on the road. These vehicles impact the traffic flow directly or indirectly through their different characteristics. Afterward, to study the heterogeneous phenomena, some macroscopic models [66–70] were extended by considering into account the heterogeneity effect. Moreover, the non-lane-based phenomena occur due to distinct types of vehicles when vehicles do not move on a particular lane according to lane discipline. Vehicles adjust their speed to use lateral gaps between theirs and update their position. Therefore, a new factor, 'area occupancy,' based on the lateral gap phenomenon, was considered in Refs. [71,72]. Later on, the second-order macroscopic model [73] was extended using area occupancy instead of density for traffic concentration. Further, a review of macroscopic models was also presented [74].

1.2 Formation of traffic jams

The flow-density empirical results indicate that vehicular traffic exhibit two distinct dynamical phases: free flow and congested. Freely flowing traffic is defined as traffic in which each driver can travel as he desires and is uninfluenced by the presence of other vehicles. Additionally, when the density rises in this instance, traffic flow does too. A congested phase of traffic is one in which the vehicle's velocity remains lower than the desired velocity. Moreover, in a congested state, an increased density results in a reduction in traffic

flow.

Traffic congestion is an annoyance in daily life. Every vehicle tries to move as fast as it can, which can result in the occurrence of traffic jams. Moreover, an experiment conducted in a lab demonstrated that when average vehicle density rises above a particular threshold, the emergence of traffic congestion develops spontaneously [75–77]. Throughout the experiment, the circular road was considered in a homogeneous lane condition. In the initial stage, all vehicles are considered homogeneous and move at the same speed. For a while, the free flow was maintained. The small fluctuations appeared in the homogeneous flow after some time. The disruption of free flow made it impossible for the vehicles to continue moving uniformly. Then the disturbance started to grow larger, resulting in a jam cluster that propagated in the backward direction of the moving vehicles. The jam cluster propagates like a solitary wave, retaining its velocity and size. According to theoretical and empirical evidence, traffic jams manifest as density waves [76,78,79]. Nonlinear equations have been proposed to describe traffic jams as density waves. To explain the density waves, Burger's as well as the Korteweg-de Vries (KdV), and the modified Korteweg-de Vries (mKdV) equations are all utilized.

The single-pulse density wave was discovered by Kerner and Konhäuser [80] in computational solutions of the hydrodynamic model. Linear stability analysis was used to analyze the traffic model. Later on, nonlinear analysis was carried out to analyze the traffic jam [79]. KdV equation was obtained from the hydrodynamic model by Kurtze and Hong [79] through nonlinear analysis. The derived KdV equation is a dispersive and nonlinear partial differential equation. It describes the large waves propagating with small amplitude but finite in a dispersive medium. The well-known KdV equation in simple form is given by:

$$\partial_T S + 2S\partial_X S - \partial_X^3 S = 0. \tag{1.9}$$

Here S is the function of X and T where the variable X is for space and T is for time. The temporal evolution of a wave that is propagating in one direction is described by the term $\partial_T S$. Moreover, the nonlinear term $S\partial_X S$ depicts the wave's steepening, and the term $\partial_X^3 S$ reflects linear dispersion, which describes wave spreading. The solution of the KdV equation is called "'solitary wave" or "soliton" and is given as [81]:

$$S(X,T) = \alpha \ \mathrm{sech}^2\Big(\sqrt{\frac{\alpha}{12}}\big(X - \frac{\alpha T}{3}\big)\Big), \tag{1.10}$$

where α denotes the amplitude of a solitary wave. Furthermore, Komatsu and Sasa [82] obtained the mKdV equation and demonstrated that the traffic jam could be described in

the pattern of the kink-antikink density wave. The mKdV equation is

$$\partial_T S + \partial_X S^3 - \partial_X^3 S = 0, \tag{1.11}$$

and its solution is described as [1,81]:

$$S(X,T) = \sqrt{\mu}\tanh\Big(\sqrt{\frac{\mu}{2}}(X-\mu T)\Big). \tag{1.12}$$

1.3 Lattice Hydrodynamic (LH) Model

Nagatani [83] pioneered the lattice hydrodynamic approach to traffic dynamics modeling by combining the concepts of micro and macro models. LH model includes continuity and evolution equations for the unidirectional homogeneous traffic flow. This approach has the capability of expressing various phases of traffic conditions. The model results depict traffic congestion in kink-antikink density waves around the critical point and explain collective traffic patterns. In this approach, space is subdivided into lattice sites. (see Fig. 1.4). The governing equations are derived based on continuum models at each lattice site.

Investigating homogeneous characteristics of traffic on one-lane highway, a unidirectional road of length L is considered without entrance and/or exits. Further, the road is discretized into N equally spaced lattice sites. The continuity equation analyzes the aggregate behavior of vehicular flow, and it relates the traffic's local density $\rho(x,t)$ to the velocity $v(x,t)$ is given as

$$\partial_t \rho(x,t) + \partial_x(\rho(x,t)v(x,t)) = 0. \tag{1.13}$$

The continuity equation specifies the number of vehicles that are constantly conserved. The velocity v obeys the evolution equation with similarities to the Navier-Stokes equation but considers some distinct features. The simplified version of continuum model is presented by Nagatani [83] as

$$\partial_t(\rho(x,t)v(x,t)) = a\rho_0 V(\rho(x+\delta,t)) - a\rho(x,t)v(x,t), \tag{1.14}$$

where, the local density is represented by $\rho(x+\delta,t)$ at position $x+\delta$ at time t. The average density is defined as ρ_0. δ stands for average headway, which is inversely proportional to the average density, i.e., $\delta = 1/\rho_0$. The notion is that a driver modifies his vehicle velocity in accordance with front density ($\rho(x+\delta,t)$) or headway ($h(x,t)$). The headway and ahead density are interconnected as a relation of $\rho(x+\delta,t) = 1/h(x,t)$. a is the coefficient for the

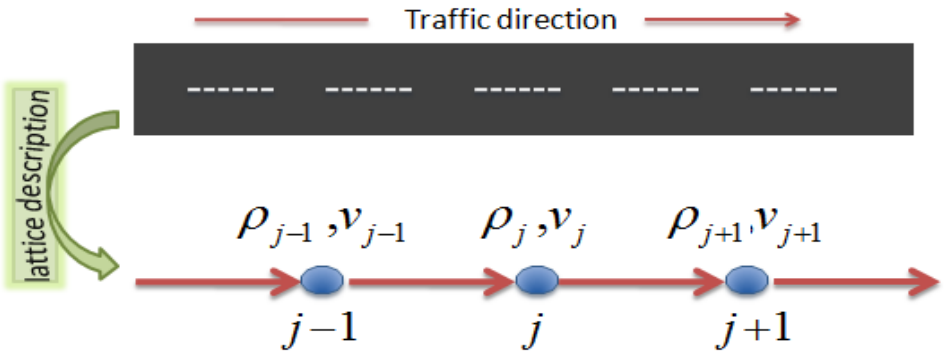

Figure 1.4: The schematic illustration of lattice hydrodynamic model.

driver's sensitivity. $\rho_0 V(\rho(x+\delta,t))$ signifies the optimal flow and $\rho(x,t)v(x,t)$ represents the actual flow. It can be seen that the vehicular flow is evaluated by the local density at position x as well as at position $x+\delta$.

Further, space variable (x) is taken as dimensionless with consideration of $x^* = x/\delta$; hereafter, x^* is thus denoted by x. Continuity equation is then improved as

$$\partial_t \rho + \rho_0 \partial_x(\rho v) = 0, \tag{1.15}$$

as well as the evolution equation is [83]

$$\partial_t(\rho v) = a[\rho_0 V(\rho(x+1)) - \rho v]. \tag{1.16}$$

Here, the Eqs. (1.15) and (1.16) are adopted as Model M_1. Based on the above two equations, Nagatani [83] introduced one class of models named as "Lattice Hydrodynamic" model. In this approach, the continuity and evolution equations are considered in the lattice version and described at each lattice site. The subscript j is used for the j^{th} site. The first lattice version model (Model M_2) is given by Nagatani [83] as

$$\partial_t \rho_j + \rho_0(\rho_j v_j - \rho_{j-1} v_{j-1}) = 0, \tag{1.17}$$

$$\partial_t(\rho_j v_j) = a[\rho_0 V(\rho_{j+1}) - \rho_j v_j], \tag{1.18}$$

where, v_j and ρ_j on j^{th} site, respectively, denote velocity and local density (also mentioned in Table 1.1). The evolution equation (Eq. (1.18)) describes the rate of change of flow as the difference between the optimal and actual flow. $V(.)$ is the optimal velocity function, having maximum velocity (v_{max}) with critical density (ρ_c) and adopted the same as given

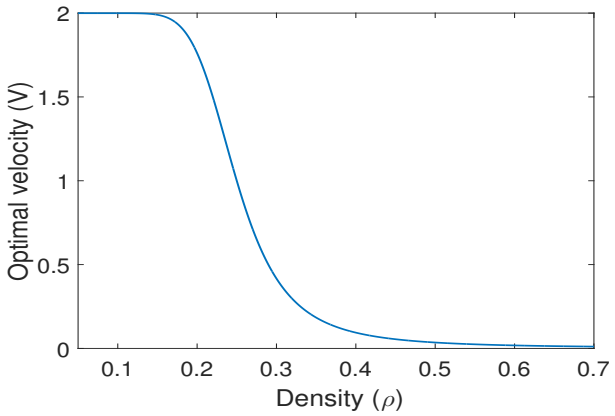

Figure 1.5: Diagram of Density (ρ) versus Optimal velocity (V).

in [28]:

$$V(\rho_j) = \frac{v_{max}}{2}\Big[\tanh\Big(\frac{1}{\rho_j} - \frac{1}{\rho_c}\Big) + \tanh\Big(\frac{1}{\rho_c}\Big)\Big], \tag{1.19}$$

where the critical density (ρ_c) is inversely proportional to the safety distance. Moreover, Fig. 1.5 shows the plot for density versus the optimal velocity, which has two properties such as (1) monotonically decreasing function as $V'(\rho_j) \leq 0$, (2) existing upper bound and inflection point at $\rho_j = \rho_c$.

By eliminating velocity (v) from the equations in Model M_1 and Model M_2, the achieved evolution density equations for both models are given by

$$\left.\begin{array}{ll} \partial_t^2\rho + a\partial_t\rho + a\rho_0^2\partial_x V(\rho(x+1)) = 0, & \text{Model } M_1 \\ \partial_t^2\rho_j + a\partial_t\rho_j + a\rho_0^2(V(\rho_{j+1}) - V(\rho_j)) = 0. & \text{Model } M_2 \end{array}\right\} \tag{1.20}$$

The objective is to determine the stability criterion for both models (M_1 and M_2), which is accomplished via a study of linear stability. At first, on each lattice site's traffic is assumed to have a constant density ρ_0, resulting in identical optimal velocity $V(\rho_0)$. This leads to the hypothesis that the uniform steady-state solution is represented by $\rho_j(t) = \rho_0$ and $v_j(t) = V(\rho_0)$. A small deviation ($y_j(t)$) is given to constant density, i.e., $\rho_j(t) = \rho_0 + y_j(t)$ and then; regarding Fourier modes, it is expanded. The phase plane (ρ, a) is then split into two stable and unstable zones using the stability criteria.

Further, nonlinear stability analysis is conducted to learn more about the characteristics of traffic congestion. The modified Korteweg-de Vries (mKdV) equation is obtained near the critical point using the reductive perturbation method. The traffic jams are described

Table 1.1: Variables in lattice model

Parameter	Unit
sensitivity(a)	s^{-1}
velocity (v)	site/s
density (ρ)	veh/site

by the mKdV equation's solution expressed as perspective of kink antikink solitons. The phase plane (ρ, a) is partitioned into metastable, unstable, and stable zones by the coexisting curves found using nonlinear analysis.

After that, computer simulations are performed using some numerical techniques, and then the simulation results are compared to theoretical (analytical) results. The assumptions are deemed acceptable when numerical findings concur with theoretical ones.

The lattice approach's primary benefit is that the models are amenable to mathematical analysis, and density waves can be shown in terms of kink-antikink soliton representing the phase transitions from free flow to congested phase or vice versa according to traffic situations. The traffic flow dynamic is a nonlinear and complex phenomenon that instantly alters when vehicles enter the congestion or exit. Moreover, it is observed that when congestion occurs downstream, it affects the upstream traffic, resulting in slowing down the upstream traffic flow. Congestion can be suppressed if an idea about the traffic conditions ahead receives in advance, which can also help in optimizing the flow. To solve issues related to congestion, Intelligent Transportation System (ITS) plays a vital role in traffic circumferences.

1.3.1 Role of ITS

Over the past two decades, traffic flow modeling has advanced at a furious speed. In various applications, the traffic flow models are often integrated with the combination of measurable data on the present traffic situation and quick computing methods. As a result of this combination, now it's possible to generate reliable and helpful short-term forecasts (predictions or prior information) regarding the traffic situation's progression [14]. During this time, Intelligent Transportation System (ITS) has become more famous because of their advanced applications [84]. In vehicular networks system, ITS aims to enhance transportation efficiency by reducing congestion. It provides users the prior knowledge regarding traffic conditions, that includes; which routes are suitable, local convenience, environmental impacts, and so on, which diminishes commuters' traveling time while improving their comfort and safety. The predictions in actual traffic are especially beneficial

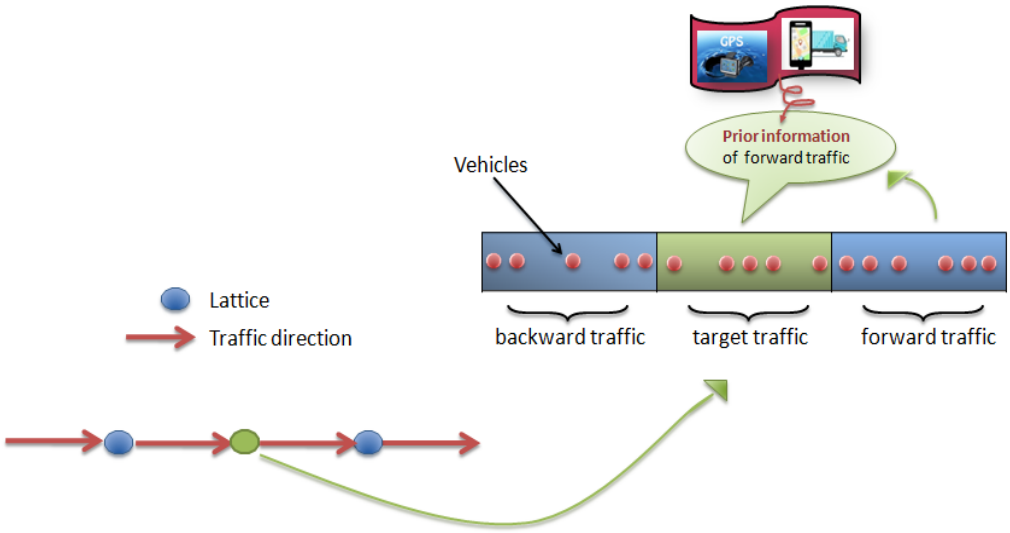

Figure 1.6: Illustration of receiving information on ahead traffic through ITS.

in unusual cases such as severe weather, traffic accidents, road constructions, etc.

The forecasting regarding the state of traffic flow relying on information technology (IT) is highly trustworthy. In actual vehicular flow, the response of the driver is impacted by the traffic ahead in the next moment. Drivers alter their maneuvers after learning about the conditions downstream. Drivers are able to modify their velocity as a result of the prior information (predictive effect) of the downstream. In order to explain the importance of the prior information, a new one-dimensional LH model was proposed [85] and the schematic diagram of LH model is shown in Fig. 1.6. The continuity equation was unaltered (Eq. (1.21)) while the new evolution equation was presented (Eq. (1.22)) as

$$\partial_t \rho_j(t) + \rho_0(\rho_j(t)v_j(t) - \rho_{j-1}(t)v_{j-1}(t)) = 0, \tag{1.21}$$

$$\partial_t(\rho_j(t)v_j(t)) = a\rho_0 V\big(\rho_{j+1}(t) + \beta(\rho_{j+1}(t+t_0) - \rho_{j+1}(t))\big) - a\rho_j(t)v_j(t). \tag{1.22}$$

Here, t_0 is the predictive time, and the predictive density is defined as $\rho_{j+1}(t+t_0)$ at time $t+t_0$ on site $j+1$. In Eq. (1.22), the term including $(\rho_{j+1}(t+t_0) - \rho_{j+1}(t))$ is known as the expected density variation or predictive density, representing the density difference between the next and the present moment on site $j+1$. The parameter $\beta(\beta \geq 0)$ is the coefficient of predictive density. The results proved that the traffic flow stability increases after getting an accurate estimation about downstream traffic conditions.

1.3.2 Extensions of LH model

The lattice hydrodynamic model has gained great popularity for its simplicity. Afterward, various extensions and improvements based upon lattice model were made. Moreover, LH

models can be categorized as either homogeneous or heterogeneous.

1.3.2.1 Homogeneous lattice models

In the homogeneous traffic flow models, various important factors related to drivers, environment, vehicles, etc., have been investigated to show actual traffic phenomena. Some of these factors are listed as optimal current difference effect [86–88], backward-looking effect [89–92], anticipation effect [93–95], so on [96–100]. In addition, overtaking (passing) is possible when the following vehicle's speed is more as compared to the leading vehicle or when leading vehicle decelerates its speed. In this case, the following vehicle may overtake the ahead vehicle to avoid the collision, which is related to an actual traffic situation. Considering the effect of passing, many extended versions of lattice models were presented [101–106].

However, the aforementioned lattice models only represent some traffic phenomena for a single lane. In an actual traffic environment, multi-lane roads are also accessible and are proven to be suited. Therefore, Nagatani [107] further extended his original lattice model for a two-lane system incorporating the lane-changing behavior. Following that, various essential aspects [108–121] were taken into account in the lattice model for two- or multi-lane roads having rule of lane change. Moreover, the LH models were expanded for curved roads [122–126] for one and two-lane traffic dynamics by taking into account the influence of road design because roads are not always straight and might be curved or have slopes. Furthermore, Nagatani [127] proposed two dimensional (2D) LH model that considered into account two different vehicle kinds: eastbound (moves in positive x direction only) and northbound (moves in positive y direction only). Afterward, the two-dimensional lattice hydrodynamic models [128–131] were presented with the consideration of realistic factors.

1.3.2.2 Heterogeneous lattice models

In vehicular dynamics, various categories of vehicles exist, such as motor-two-wheeler, motor-three-wheeler, car, bus, truck, etc. Every vehicle behaves differently in the same traffic situations because of their distinct characteristics. Therefore, heterogeneity among vehicles can be seen. Further, the lattice model was extended from homogeneous to heterogeneous [132] to analyze the impact of heterogeneity on traffic dynamics. But the heterogeneous lattice model was based on a lane-based criterion. However, when there are varieties of vehicles available on roads, it is obvious that vehicles occupy less or more space according to their size and utilize the lateral gap between theirs by adjusting their speed, known as the area occupancy effect. Recently, a new area occupancy lattice model [133]

has been presented for a disordered traffic system.

1.4 Thesis contribution

The aim of the thesis is to propose new models which help to minimize traffic congestion and optimize traffic flow. The thesis' primary contribution is the modification, improvement, and evaluation of LH model in light of real and existing homogeneous or heterogeneous traffic phenomena. The affects of the prior information (predictive effect) from different perspectives have been examined. The extended or new models have been analyzed theoretically with the use of linear and nonlinear analysis. Further, to confirm the theoretical conclusions, numerical simulations are employed. In addition, the contribution of the thesis is mainly based on the following concepts as

- **Predictive effect:** Intelligent Transportation Systems (ITS) plays a vital role in creating efficient operational strategies for the traffic system to address some of the traffic issues. ITS provides prior information, which may be widely used in providing information about ahead traffic conditions and controlling traffic flow. Based on the concept of prior information (predictive effect) and its effects on traffic dynamics, the homogeneous lattice hydrodynamic models are proposed for (i) a one-lane system when overtaking is permitted (**Chapter 2**), (ii) a two-lane system with the lane change occurring rule (**Chapter 3**) and (iii) a two-dimensional road with the junction (**Chapter 4**).

- **Uncertainty:** When uncertainty occurs while receiving information regarding ahead traffic conditions, there may be a chance of information interruption. Moreover, historical information based on previous traveling time, previous density, or other historical sources can also affect driving performance. Therefore, the influence of uncertainty on downstream historical information is considered while developing a new lattice model (**Chapter 5**).

- **Heterogeneity:** In heterogeneous disordered traffic, every vehicle has a different size and speed, and the area occupied by vehicles depends on their size. Vehicles use lateral gaps to occupy an available space on the road by adjusting their speed. Moreover, they may react differently to identical traffic conditions. The said characteristics may affect the overall movement of vehicular flow. Based on the heterogeneity among vehicles, a novel lattice model, including the area occupancy effect, is proposed for a non-lane-based traffic system (**Chapter 6**).

- **Analyses:** The models are analyzed through stability analysis as well as numerical

techniques. The theoretical analysis is used to determine how various factors affect traffic flow stability. Linear and nonlinear stability analyses are conducted for the same. Theoretical investigations are then verified via numerical simulations. The results are shown in terms of phase plots and graphs. For simulations, the programming is done using MATLAB software.

Finally, **Chapter 7** summarizes the results of this thesis. In the present thesis, the lattice model has been used to examine several issues in the traffic environment. Therefore, in light of the importance of the lattice technique, the potential future scope is also provided.

Chapter 2

Influence of predictive effect in overtaking on traffic dynamics

In the past few decades, traffic jams have become a serious issue with the rapid increase of vehicles on the road. Traffic jams, especially in developing countries, lead to enormous delays, increased fuel consumption, and monetary losses, which affect the overall movement of traffic. Somewhere, traffic jam not only increases environmental pollution but also imposes safety dangers. It becomes necessary to resolve the issues related transportation system. Therefore, many mathematical models have been proposed to develop an optimal road network with a maximum traffic flow, provide a safe atmosphere for passengers, and minimize traffic jams. Broadly, the traffic flow models can be categorized into microscopic models such as car-following models [28,134–144], and macroscopic models such as continuum models [42,43,49,64,145] based on the level of details. In the microscopic models, the behavior of each and every vehicle is explored, describing the speed and position of the vehicle separately. In contrast, macroscopic models are based on the assumption that a traffic stream on a single lane can be considered a continuum of moving particles in which the individual vehicles are not detailed; rather, aggregated variables are described for each road stretch.

Another model class relying on the lattice hydrodynamic method has recently gained popularity. As discussed in the previous chapter, Nagatani [83] introduced the first simplest lattice hydrodynamic (LH) model for a single unidirectional highway, which incorporates the ideas of both car-following and continuum models. This model is used to investigate the jamming transitions in terms of kink density wave. The modified Korteweg-de Vries (mKdV) equation is derived near the critical point. After that, many extendable versions of the traditional lattice model have been presented, including a number of essential traffic features such as the optimal flow difference effect [86,87,98], backward-looking effect [89–92], multi-phase optimal velocity function's impacts [100,105,146], traffic jerk effect [147], etc.

In many countries, the traffic is ordered, i.e., one vehicle follows another vehicle. The speed

The content of this chapter has been published in The European Physical Journal B, 93: 1-10, (2020).

of the vehicles mainly depends on the vehicles ahead (leading vehicles). Sometimes, the leading vehicles travel faster than the following vehicles, and the following vehicles may not decelerate. But in actual traffic, it is impossible that the leading vehicles will achieve their optimal velocity every time. In many cases, the leading vehicles may decelerate, resulting in a reduction in the speed of the following vehicles. In this situation, traffic congestion may occur. Therefore, sometimes overtaking/passing may help reduce congestion and optimize the traffic flow. To describe this phenomenon, Nagatani [101] extended his basic model by considering the passing effect. Passing is influenced due to a variety of parameters which includes the speed difference between overtaking and overtaken vehicles, weather forecast, road geometry, human factors, etc. In this context, a few researchers [102–106,126] investigated lattice models describing the passing effect on the traffic system.

In a real traffic environment, the speed of vehicles usually depends upon the speed of the vehicles ahead in the next moment. Drivers modify their driving skills and adjust their speed by accelerating or decelerating according to the prior information of downstream traffic conditions; this prior information is called the predictive effect. In order to explain the importance of the predictive effect, Wang et al. [85] presented LH model which concluded that the traffic flow stability increases after getting an accurate estimation about downstream traffic conditions. Overtaking and the predictive effect are interconnected as the faster-moving vehicles get prior information about the downstream conditions that help them decide whether to accelerate or decelerate and also help them overtake the slower-moving vehicles. But the impact of passing with predictive effect has not been explored yet. However, the togetherness of these effects (the predictive and the passing effects) can help to reduce traffic jams and enhance traffic flow stability. In light of this, a new model is developed that takes into consideration the predictive effect with passing, and we investigate its effect on traffic dynamics theoretically and numerically.

The chapter is structured into five sections: a more realistic lattice model is proposed by taking the predictive effect with passing in Section 2.1. The theoretical investigation of the model is carried out in Section 2.2 and Section 2.3 through linear and nonlinear stability analysis, respectively. In order to validate the theoretical findings, numerical simulations are performed in Section 2.4, and finally, in Section 2.5, a conclusion is drawn.

2.1 Proposed LH model

The first and most basic (as discussed in Chapter 1) lattice hydrodynamic model was put out by Nagatani [83] for unidirectional single-lane highway and is

$$\partial_t \rho_j + \rho_0(\rho_j v_j - \rho_{j-1} v_{j-1}) = 0, \tag{2.1}$$

$$\partial_t(\rho_j v_j) = a[\rho_0 V(\rho_{j+1}) - \rho_j v_j], \tag{2.2}$$

where ρ_0 stands for the average density; a is the sensitivity of the drivers. v_j and ρ_j signifies the velocity and local density at j^{th} site, respectively. $V(.)$ is called the optimal velocity function.

In real traffic systems, vehicles are moving at different speeds. Some vehicles accelerate faster than other vehicles on the road. When there is less space than is safe space between the faster moving (following vehicles) and slower moving vehicles (leading vehicle), they always try to avoid collision. Faster-moving vehicles also try to achieve their optimal velocity by overtaking the slower-moving vehicle. Therefore, overtaking/passing is one of the important traffic characteristics in the traffic network. By keeping in mind, after that, Nagatani [101] extended his basic lattice model by considering the effect of passing into account. Overtaking occurs when the traffic current at j^{th} site exceeds that at $j + 1^{th}$ site, and it is equivalent to the optimal current differential between sites j and $j + 1$. Therefore, to explain overtaking phenomenon, the continuity equation remains unaltered in this model, while the evolution equation is extended to include the passing influence as

$$\partial_t(\rho_j v_j) = a[\rho_0 V(\rho_{j+1}) - \rho_j v_j] + a\eta\rho_0[V(\rho_{j+1}) - V(\rho_{j+2})], \tag{2.3}$$

where, passing constant is defined by η.

In actual traffic, after getting information about the estimated behavior of surrounding vehicles from the information technology, drivers react according to the downstream flow in the next moment. It is known as the predictive effect. Therefore, to explain the nature of the predictive effect in the traffic stream, the evolution equation [85] is given as follows

$$\partial_t(\rho_j v_j) = a\rho_0 V\big(\rho_{j+1}(t) + \beta(\rho_{j+1}(t + t_0) - \rho_{j+1}(t))\big) - a\rho_j(t)v_j(t). \tag{2.4}$$

Here, t_0 defines predictive time and $\rho_{j+1}(t+t_0)$ signifies the predictive density at $j + 1^{th}$ site. β is coefficient for density variation. The optimal velocity depends on the density of the instant downstream site at time t and the predictive density at direct downstream site on time $t + t_0$. Whenever the density on immediate downstream site at next moment reduces, traffic conditions on downstream are therefore improved. This results in an increase in the optimal velocity. In accordance with the optimal velocity function, when downstream

conditions become better, the upstream driver should speed up his vehicle for smoothness of traffic flow, which influences future traffic conditions in traffic dynamics.

The important aspect of the predictive effect with passing has yet to be explored. Therefore, the evolution equation is extended to study the impact of the impact of the predictive effect with passing on traffic dynamics as follows

$$\begin{aligned}\partial_t(\rho_j v_j) &= a\rho_0 V\big(\rho_{j+1}(t)+\beta(\rho_{j+1}(t+t_0)-\rho_{j+1}(t))\big)-a\rho_j(t)v_j(t)\\ &+a\eta\rho_0\big[V\big(\rho_{j+1}(t)+\beta(\rho_{j+1}(t+t_0)-\rho_{j+1}(t))\big)-V\big(\rho_{j+2}(t)+\beta(\rho_{j+2}(t+t_0)-\rho_{j+2}(t))\big)\big].\end{aligned} \tag{2.5}$$

Using Taylor series expansion to expand the term $V\big(\rho_{j+1}(t)+\beta(\rho_{j+1}(t+t_0)-\rho_{j+1}(t))\big)$ of Eq. (2.5) and ignore the higher order terms, we get

$$V\big(\rho_{j+1}(t)+\beta(\rho_{j+1}(t+t_0)-\rho_{j+1}(t))\big)=V(\rho_{j+1}(t))+V'(\rho_{j+1}(t))t_0\beta\partial_t\rho_{j+1}(t). \tag{2.6}$$

After eliminating the speed v_j in Eqs. (2.1) and (2.5) by using Eq. (2.6), the density evolution equation with overtaking effect is obtained as

$$\begin{aligned}\partial_t^2\rho_j &+ a\rho_0^2[V(\rho_{j+1})-V(\rho_j)]+at_0\beta\rho_0^2[V'(\rho_{j+1})\partial_t\rho_{j+1}-V'(\rho_j)\partial_t\rho_j]\\ &+at_0\beta\eta\rho_0^2\big[2V'(\rho_{j+1})\partial_t\rho_{j+1}-V'(\rho_{j+2})\partial_t\rho_{j+2}-V'(\rho_j)\partial_t\rho_j\big]\\ &+a\partial_t\rho_j+a\eta\rho_0^2[2V(\rho_{j+1})-V(\rho_{j+2})-V(\rho_j)]=0.\end{aligned} \tag{2.7}$$

In the above equation, for $\eta=0$, the model reduces to the one discussed in ref. [85]. In addition, for $\beta=0$ or $t_0=0$, the model coincides with Nagatani's model [101]. Further, for $\beta=0$ or $t_0=0$, the proposed model with $\eta=0$ reduces to basic model [83].
The following optimal velocity function is adopted as follows [83]:

$$V(\rho_j)=\frac{v_{max}}{2}\Big[\tanh\Big(\frac{1}{\rho_j}-\frac{1}{\rho_c}\Big)+\tanh\Big(\frac{1}{\rho_c}\Big)\Big], \tag{2.8}$$

where v_{max} and ρ_c represent the maximal velocity and critical density, respectively. This optimal velocity function has an inflection point at $\rho_j=\rho_c$, and it is a monotonically decreasing function having an upper bound.

2.2 Linear stability analysis

In the case of overtaking permitted with the help of predictive effect, traffic may influence. Therefore, linear stability analysis is applied to examine the proposed model. Initially, the

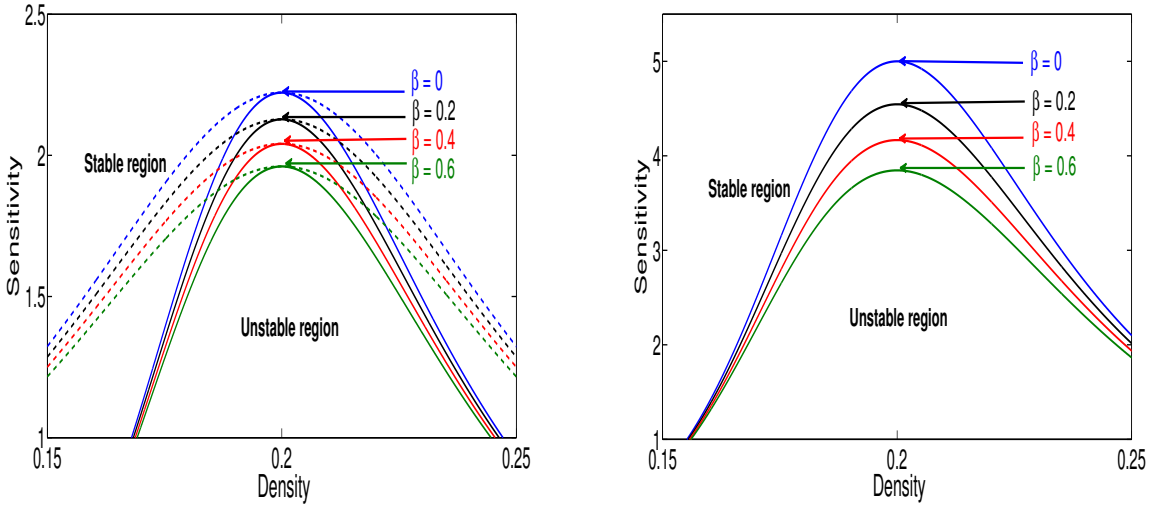

Figure 2.1: Phase diagram in parameter space (ρ, a) for different values of β with $t_0 = 0.1$ when (a) $\eta = 0.05$, and (b) $\eta = 0.3$. The solid lines in (a) and (b) show neutral stability curves, whereas the dashed lines in (a) represent the coexisting stability curves. The coexisting curves do not exist for $\eta = 0.3$ in (b).

uniform-steady state of traffic flow is considered. For this, it is supposed that the vehicles move with fixed density ρ_0 and constant optimal velocity $V(\rho_0)$. Thus, the solution for Eq. (2.7) is

$$\rho_j(t) = \rho_0, \quad v_j(t) = V(\rho_0). \tag{2.9}$$

A small perturbation in terms of $y_j(t)$ to the above uniform density is given, which leads to

$$\rho_j(t) = \rho_0 + y_j(t). \tag{2.10}$$

Through placing the Eq. (2.10) into (2.7), and linearizing it, we obtain

$$\begin{aligned}\partial_t^2 y_j + a\rho^2 V'(\rho_0)[y_{j+1} - y_j] + at_0\beta\rho^2 V'(\rho_0)[\partial_t y_{j+1} - \partial_t y_j] + a\partial_t y_j \\ + at_0\beta\eta\rho_0^2 V'(\rho_0)[(2\partial_t y_{j+1} - \partial_t y_{j+2} - \partial_t y_j)] + a\eta\rho_0^2 V'(\rho_0)[2y_{j+1} - y_{j+2} - y_j] = 0.\end{aligned} \tag{2.11}$$

Further, the perturbation term is assumed as $y_j = \exp(ikj + \omega t)$ and put into Eq. (2.11) which results

$$\begin{aligned}\omega^2 + a\big[t_0\beta\rho_0^2 V'(\rho_0)(e^{ik} - 1) + 1 + t_0\beta\eta\rho_0^2 V'(\rho_0)(2e^{ik} - e^{2ik} - 1)\big]\omega \\ + a{\rho_0}^2 V'(\rho_0)(e^{ik} - 1) + a\eta\rho_0^2 V'(\rho_0)(2e^{ik} - e^{2ik} - 1) = 0.\end{aligned} \tag{2.12}$$

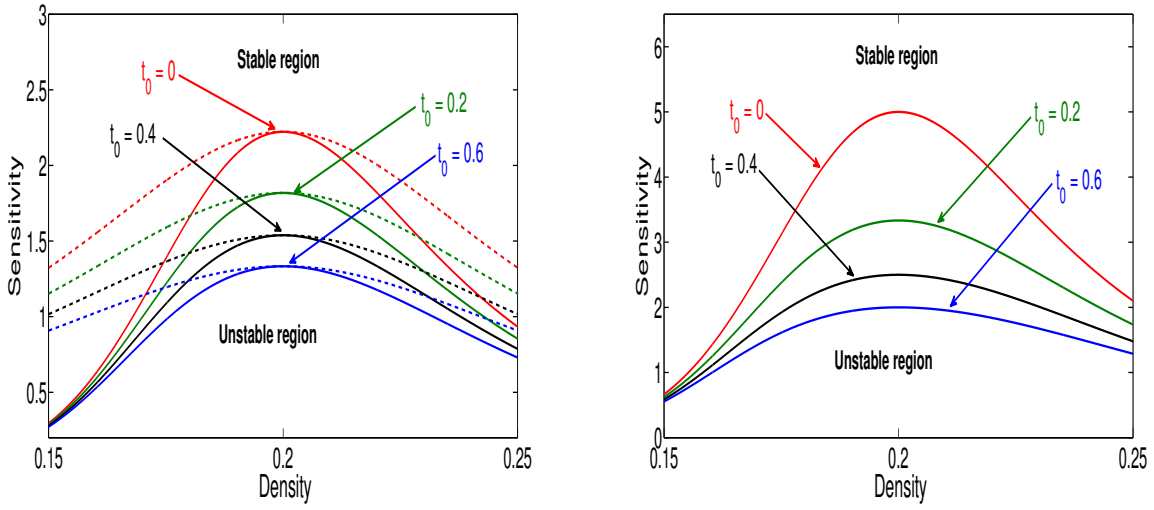

Figure 2.2: Phase diagram in parameter space (ρ, a) for different values of t_0 with $\beta = 0.5$ when (a) $\eta = 0.05$, and (b) $\eta = 0.3$. The solid lines in (a) and (b) show neutral stability curves, whereas the dashed lines in (a) represent the coexisting stability curves. The coexisting curves do not exist for $\eta = 0.3$ in (b).

The linear and quadratic terms of the coefficient (ik), after substituting $\omega = \omega_1(ik) + \omega_2(ik)^2$..... into (2.12), are obtained as

$$\omega_1 = -{\rho_0}^2 V'(\rho_0). \tag{2.13}$$

$$\omega_2 = -\frac{{\omega_1}^2}{a} - \frac{{\rho_0}^2 V'(\rho_0)}{2} - t_0\beta\omega_1{\rho_0}^2 V'(\rho_0) + \eta{\rho_0}^2 V'(\rho_0). \tag{2.14}$$

When $\omega_2 < 0$, the uniform steady-state flow develops into an unstable state. Conversely, if $\omega_2 > 0$, the homogeneous traffic flow becomes stable against a long wavelength perturbation. Therefore, the neutral stable condition is obtained by

$$a = \frac{-2{\rho_0}^2 V'(\rho_0)}{1 - 2t_0\beta\rho_0^2 V'(\rho_0) - 2\eta}. \tag{2.15}$$

Hence, the stability criterion for the study state is given

$$a > \frac{-2{\rho_0}^2 V'(\rho_0)}{1 - 2t_0\beta\rho_0^2 V'(\rho_0) - 2\eta}. \tag{2.16}$$

Clearly, the result is influenced by the parameters β, t_0, and η. It is clear from Eq. (2.16) that the influence parameters β and t_0 play an important role in the stability of traffic flow when passing is considered. The neutral stability curves in Fig. 2.1 and Fig. 2.2 are represented by solid lines in the phase space (ρ, a) for different values of β and

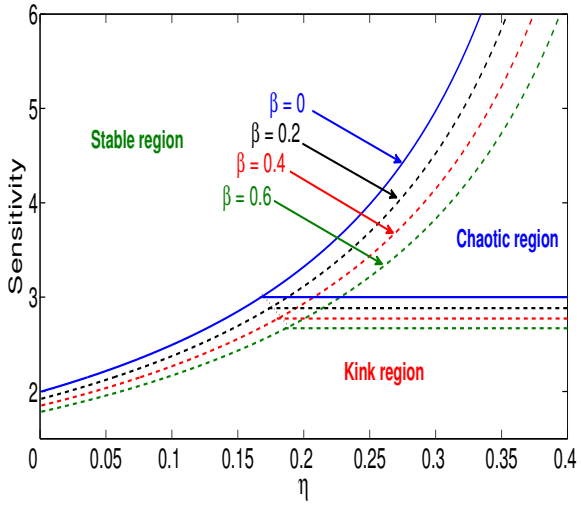

Figure 2.3: Phase diagram in (η, a) space

t_0, respectively, corresponding to $\eta = 0.05$ and $\eta = 0.3$. The position of the apex of these curves lower as β and t_0 grow means traffic flow stability significantly increases. Hence, traffic congestion is suppressed efficiently. In an actual traffic network under a jam situation, the faster moving vehicles try to overtake the slower ones. Moreover, Fig. 2.1 and Fig. 2.2 show that the stable region increases for a smaller value of passing instead of a higher value of passing.

2.3 Nonlinear stability analysis

The long-wavelength expansion methodology is adopted to look into the effects of overtaking depending upon the predictive effect on the evolution features of traffic congestion. Close to the critical point, the mKdV equation is derived. We import the slow variables X and T for a small positive scaling parameter $\epsilon(0 < \epsilon \ll 1)$. Let us consider the density is

$$\rho_j(t) = \rho_c + \epsilon S(X,T); \quad \text{where, } X = \epsilon(j + pt), \quad T = \epsilon^3 t, \tag{2.17}$$

here the constant term p needs to be determined. Now, by using Taylor series expansion in Eq. (2.7) with the help of Eq. (2.17) and after expanding it up to fifth-order of ϵ, we obtain the following nonlinear equation

$$\epsilon^2 h_1 \partial_X S + \epsilon^3 h_2 \partial_X^2 S + \epsilon^4 (\partial_T S + h_3 \partial_X^3 S + h_4 \partial_X S^3) + \epsilon^5 (h_5 \partial_T \partial_X S + h_6 \partial_X^4 S + h_7 \partial_X^2 S^3) = 0. \tag{2.18}$$

The coefficients $h_i (i = 1, 2, ..., 7)$ are displayed in Table 2.1, where $V' = \frac{\partial V(\rho)}{\partial \rho}\Big|_{\rho=\rho_c}$ and

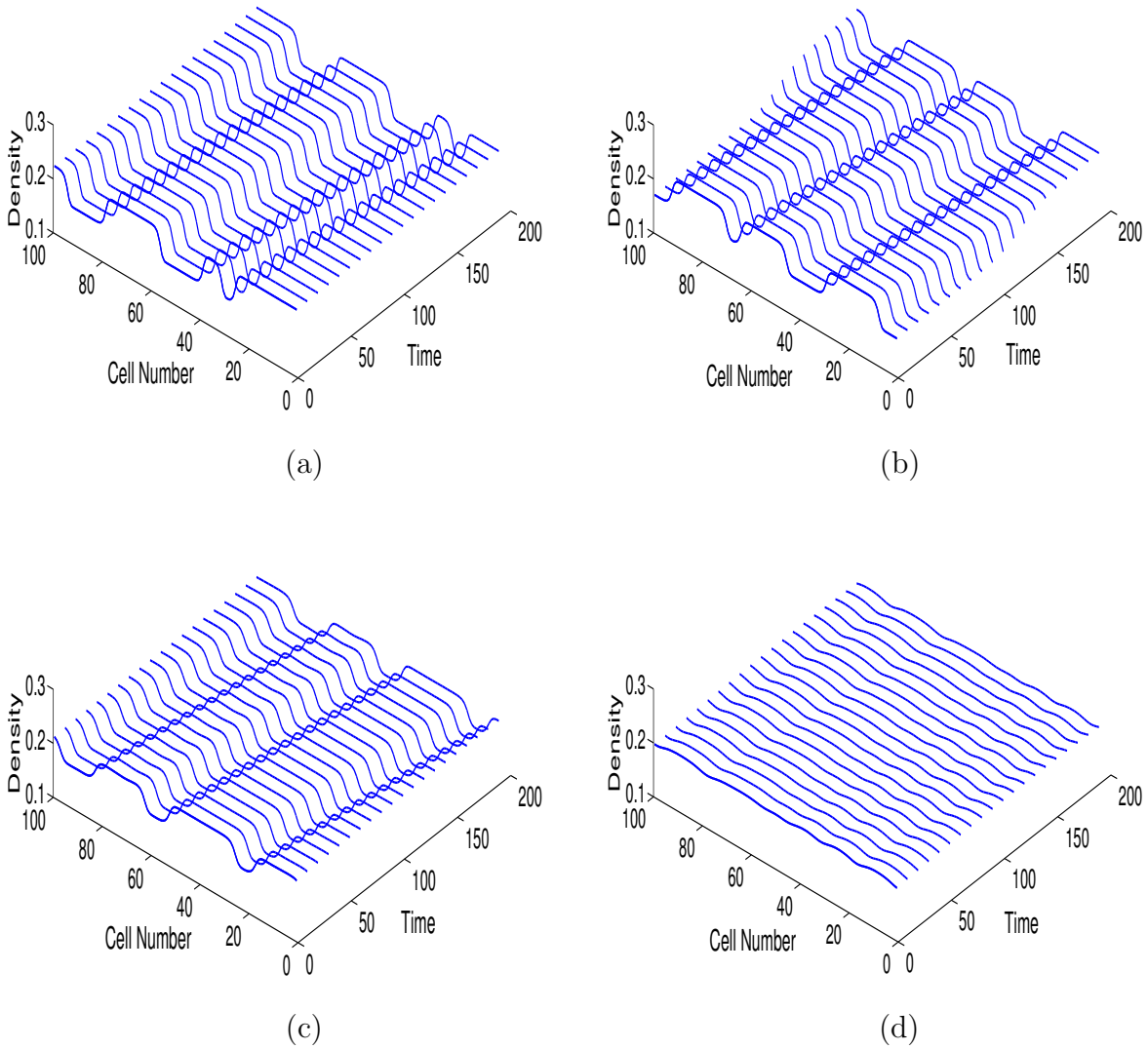

Figure 2.4: Spatiotemporal evolutions of density waves after time $t = 2 \times (10^4)s$ when $\eta = 0.05$, $a = 2.0$, and $t_0 = 0.1$ for (a) $\beta = 0$, (b) $\beta = 0.2$, (c) $\beta = 0.4$, and (d) $\beta = 0.6$, respectively.

Table 2.1: The coefficients h_i of the model

coefficients	**values**
h_1	$p + {\rho_0}^2 V'$
h_2	$\frac{p^2}{a} + \frac{\rho_0^2 V'}{2}\big[1 + 2pt_0\beta - 2\eta\big]$
h_3	$\frac{\rho_0^2 V'}{6}\big[1 - 6\eta + 3pt_0\beta(1-2\eta)\big]$
h_4	$\frac{\rho_0^2 V'''}{6}$
h_5	$\frac{2p}{a} + t_0\beta\rho_0^2 V'$
h_6	$\frac{\rho_0^2 V'}{24}\big[1 - 14\eta + 4pt_0\beta(1-6\eta)\big]$
h_7	$\frac{\rho_0^2 V'''}{12}\big[1 + 2pt_0\beta - 2\eta\big]$

Table 2.2: The coefficients b_i of the model

coefficients	**values**
b_1	$-\frac{\rho_0^2 V'}{6}\big[1 - 6\eta + 3pt_0\beta(1-2\eta)\big]$
b_2	$\frac{\rho_0^2 V'''}{6}$
b_3	$-\frac{\rho_0^2 V'}{2}\big[1 + 2pt_0\beta - 2\eta\big]$
b_4	$\frac{\rho_0^2 V'}{24}\big[1 - 14\eta + 4pt_0\beta(1-6\eta)\big] + \frac{2p}{a_c}\big[1 - \frac{a_c t_0\beta}{2}\big]b_1$
b_5	$\frac{\rho_0^2 V'''}{12}\big[1 + 2pt_0\beta - 2\eta\big] - \frac{2p}{a_c}\big[1 - \frac{a_c t_0\beta}{2}\big]b_2$

$V''' = \frac{\partial^3 V(\rho)}{\partial \rho^3}\Big|_{\rho=\rho_c}$. Close to the critical point (ρ_c, a_c), we define $a_c = a(1+\epsilon^2)$. By comparing the coefficient of ϵ^2 in Eq. (2.18), we obtain $p = -{\rho_0}^2 V'$ and then eliminate the cubic term of ϵ, Eq. (2.18) becomes:

$$\epsilon^4(\partial_T S - b_1\partial_X^3 S + b_2\partial_X S^3) + \epsilon^5(b_3\partial_X^2 S + b_4\partial_X^4 S + b_5\partial_X^2 S^3) = 0, \tag{2.19}$$

where, the coefficients b_i are given in Table 2.2. In order to convert Eq. (2.19) into standard mKdV equation, we adopt the following transformation $T' = b_1 T$ and $S = \sqrt{\frac{b_1}{b_2}} S'$ i.e.

$$T' = \Big(\frac{1 + 3pt_0\beta(1-2\eta) - 6\eta}{6} \times (-\rho_0^2 V')\Big)T, \tag{2.20}$$

$$S = \Big(-\frac{1 + 3pt_0\beta(1-2\eta) - 6\eta}{V'''} V'\Big)^{\frac{1}{2}} S', \tag{2.21}$$

with $b_1 > 0$ will lead to the condition for existence as

$$1 + 3pt_0\beta - 6pt_0\eta\beta - 6\eta > 0. \tag{2.22}$$

By applying the above transformation in Eq. (2.19), one can get the resulting equation given as

$$\partial_{T'} S^{'} - \partial_X^3 S^{'} + \partial_X S^{'3} + \epsilon M[S'] = 0, \tag{2.23}$$

where $M[S^{'}] = \frac{1}{b_1}[b_3\partial_X^2 S^{'} + b_4\partial_X^4 S^{'} + \frac{b_1 b_5}{b_2}\partial_X^2 S^{'3}]$. After ignoring the $O(\epsilon)$ from Eq. (2.23), the solution of the standard mKdV equation in terms of kink antikink wave is given as

$$S_0^{'}(X, T^{'}) = \sqrt{\mu}\tanh\Big(\sqrt{\frac{\mu}{2}}(X - \mu T^{'})\Big), \tag{2.24}$$

where, μ is the propagation velocity for the kink antikink solution. To determine the value of μ, the following condition is solved

$$(S_0^{'}, M[S_0^{'}]) \equiv \int_{-\infty}^{\infty} dX S_0^{'} M[S_0^{'}] = 0 \ \text{ where } M[S_0^{'}] = M[S'], \tag{2.25}$$

and we have

$$\mu = \frac{5b_2 b_3}{2b_2 b_4 - 3b_1 b_5}. \tag{2.26}$$

Hence, the kink antikink solution is given as

$$\rho_j = \rho_c + \epsilon\sqrt{\frac{b_1\mu}{b_2}}\tanh\Big(\sqrt{\frac{\mu}{2}}(X - \mu b_1 T)\Big), \tag{2.27}$$

with $\epsilon^2 = \left(\frac{a_c}{a} - 1\right)$ and the amplitude ('denoted by α') of the derived solution is $\sqrt{\frac{b_1 \epsilon^2 \mu}{b_2}}$.

If condition (2.22) is fulfilled only then the aforementioned kink antikink solution exists that is as

$$0 \leq \eta < f(t_0, \beta), \tag{2.28}$$

where

$$f(t_0, \beta) = \frac{1 + 3t_0\beta}{6(1 + t_0\beta)}. \tag{2.29}$$

The mKdV equation (2.23) exists only for $0 \leq \eta < f(t_0, \beta)$ and it can not be derived from the above nonlinear analysis for $\eta \geq f(t_0, \beta)$. The kink antikink soliton solution represents the coexisting phase, including freely moving as well as jammed phase in the phase space (ρ, a) described by $\rho_j = \rho_c \pm \alpha$ for $\eta < f(t_0, \beta)$.

Fig. 2.1(a) and Fig. 2.2(a) show the neutral stability curves (solid curves) and the coexisting curves (dashed curves) obtained from linear and nonlinear stability analysis, respectively, for different values of β and t_0 at $\eta = 0.05$, which splits the phase plane into metastable, unstable and stable regions. A disturbance won't affect the traffic flow in the stable region, while, in other regions, it will lead to congested traffic flow. The coexisting and the neutral curves both lower down, corresponding to increasing in value of parameter β, resulting in a higher rate of stability of traffic flow. Moreover, in Fig. 2.1(b) and Fig. 2.2(b), the coexisting curves do not exist at $\eta = 0.3$ for any value of β and t_0 as the condition $\eta < f(t_0, \beta)$ is not satisfied. The curve $a = \frac{2}{1+2t_0\beta-2\eta}$ is obtained with the help of linear stability analysis, which represents the phase boundaries between the stable region and kink region for $\eta < f(t_0, \beta)$ while for $\eta \geq f(t_0, \beta)$, it represents the phase boundaries between the stable region and chaotic region. Fig. 2.3 shows that there exist only two regions, namely 'stable region and kink region,' in the phase diagram for $\eta < f(t_0, \beta)$. But when the value of the passing constant exceeds its limit, i.e., at $\eta \geq f(t_0, \beta)$, the unstable region is further divided into two regions kink region and the chaotic region. Moreover, the kink region reduces with an increase in the value of β. In the unstable region, the line $a = \frac{2}{1+2t_0\beta-2f(t_0,\beta)}$ represents the boundary between kink region and chaotic region. When the passing rate is high $\eta \geq f(t_0, \beta)$, the predictive effect also plays a significant role. The free flow region has enhanced when β value rises, while the kink and chaotic regions are diminished.

2.4 Numerical simulations

To check the capability of the proposed model in describing the influence of the predictive effect with passing and to test the validity of linear as well as nonlinear stability analysis,

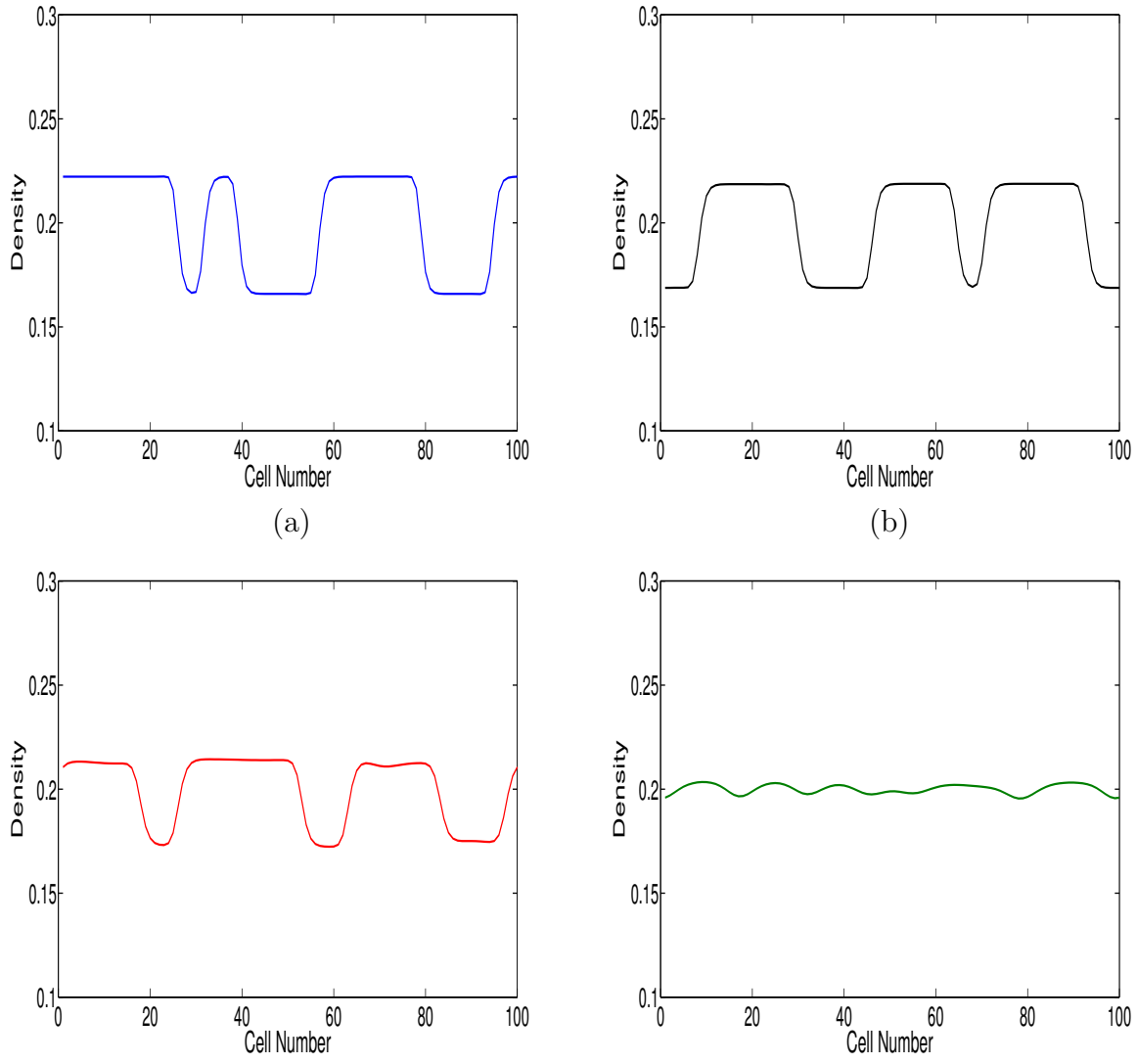

Figure 2.5: Density profiles at time $t = 20000s$ when $\eta = 0.05$, $a = 2.0$, and $t_0 = 0.1$ for (a) $\beta = 0$, (b) $\beta = 0.2$, (c) $\beta = 0.4$, and (d) $\beta = 0.6$, respectively.

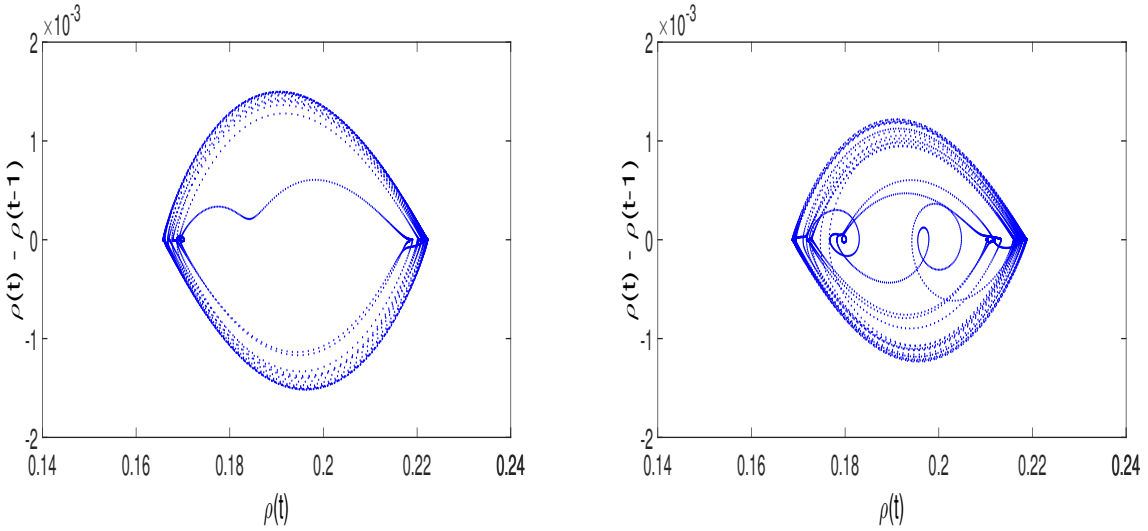

Figure 2.6: Plots of density versus density difference at time $t = 10^4 - 2 \times 10^4$ at $\eta = 0.05$, $t_0 = 0.1$, $a = 2.0$ for (a) $\beta = 0$, (b) $\beta = 0.2$, (c) $\beta = 0.4$, and (d) $\beta = 0.6$, respectively.

numerical simulations are performed under periodic boundary conditions. Therefore, the Eq. (2.7) is written in discrete form as

$$\begin{aligned}\rho_j(t+2\Delta t) &= 2\rho_j(t+\Delta t) - \rho_j(t) - a\rho_0^2\Delta t^2\big[V(\rho_{j+1}(t)) - V(\rho_j(t))\big] \\ &- a\rho_0^2\beta t_0\Delta t\Big[V'(\rho_{j+1}(t))[\rho_{j+1}(t+\Delta t) - \rho_{j+1}(t)] - V'(\rho_j(t))[\rho_j(t+\Delta t) - \rho_j(t)]\Big] \\ &- a\rho_0^2\eta\Delta t^2[2V(\rho_{j+1}(t)) - 2V(\rho_{j+2}(t)) - V(\rho_j(t))] - a\Delta t[\rho_j(t+\Delta t) - \rho_j(t)] \\ &- a\rho_0^2\beta t_0\eta\Delta t\Big[2V'(\rho_{j+1}(t))[\rho_{j+1}(t+\Delta t) - \rho_{j+1}(t)] \\ &- V'(\rho_{j+2}(t))[\rho_{j+2}(t+\Delta t) - \rho_{j+2}(t)] - V'(\rho_j(t))[\rho_j(t+\Delta t) - \rho_j(t)]\Big], \end{aligned} \tag{2.30}$$

where Δt is for the forward differences. We are taking $\Delta t = 0.07$ during the simulation. We define the initial conditions as follows

$$\rho_j(1) = \rho_j(0) = \begin{cases} \rho_0; & j \neq \frac{M}{2}, \frac{M}{2} - 1 \\ \rho_0 + \Delta\rho; & j = \frac{M}{2} - 1 \\ \rho_0 - \Delta\rho; & j = \frac{M}{2} \end{cases}, \tag{2.31}$$

where $M = 100$ represents the total number of lattice sites and the remaining parameters are chosen as $\rho_0 = \rho_c = 0.2$, $t_0 = 0.1$, $\Delta\rho = 0.05$, and $v_{max} = 2.0$.

As discussed in the previous section, the kink soliton solution of the mKdV equation exists only for $0 \leq \eta < f(t_0, \beta)$. Therefore, two cases are presented to analyze the effects of passing and also discuss the results for two different ranges of η as follows:

Case 1: When the value of passing constant is smaller i.e., $\eta < f(t_0, \beta)$

Fig. 2.4 shows the temporal and spatial evolution of density waves, which describes the impact of parameter β representing the influence of predictive effect for a lower rate of passing $\eta = 0.05$ after $t = 2 \times 10^4$ time steps. It is clear from Fig. 2.4(a)-(c) that the kink antikink soliton solution occurs, which propagates backward direction corresponding to the small initial disturbance. Due to this, the uniform flow evolves into the congested flow as the stability condition (2.16) is not satisfied. It is observed that the amplitude of density waves decreases as β increases, but the traffic congestion is not completely disappeared in Fig. 2.4(a)-(c). In the stable region, the initial disturbance completely disappears, and traffic flow reaches a uniform state at $\beta = 0.6$ as shown in Fig. 2.4(d).

Fig. 2.5 is the clear picture of density profiles at time $t = 20000$s corresponding to the panel of Fig. 2.4. The free flow region turns wide, and the fluctuation of the density waves gradually decreases with the increase in β, which indicates that the predictive effect enhances the stability of traffic flow. For $\beta = 0.6$, the initial disturbance in the traffic

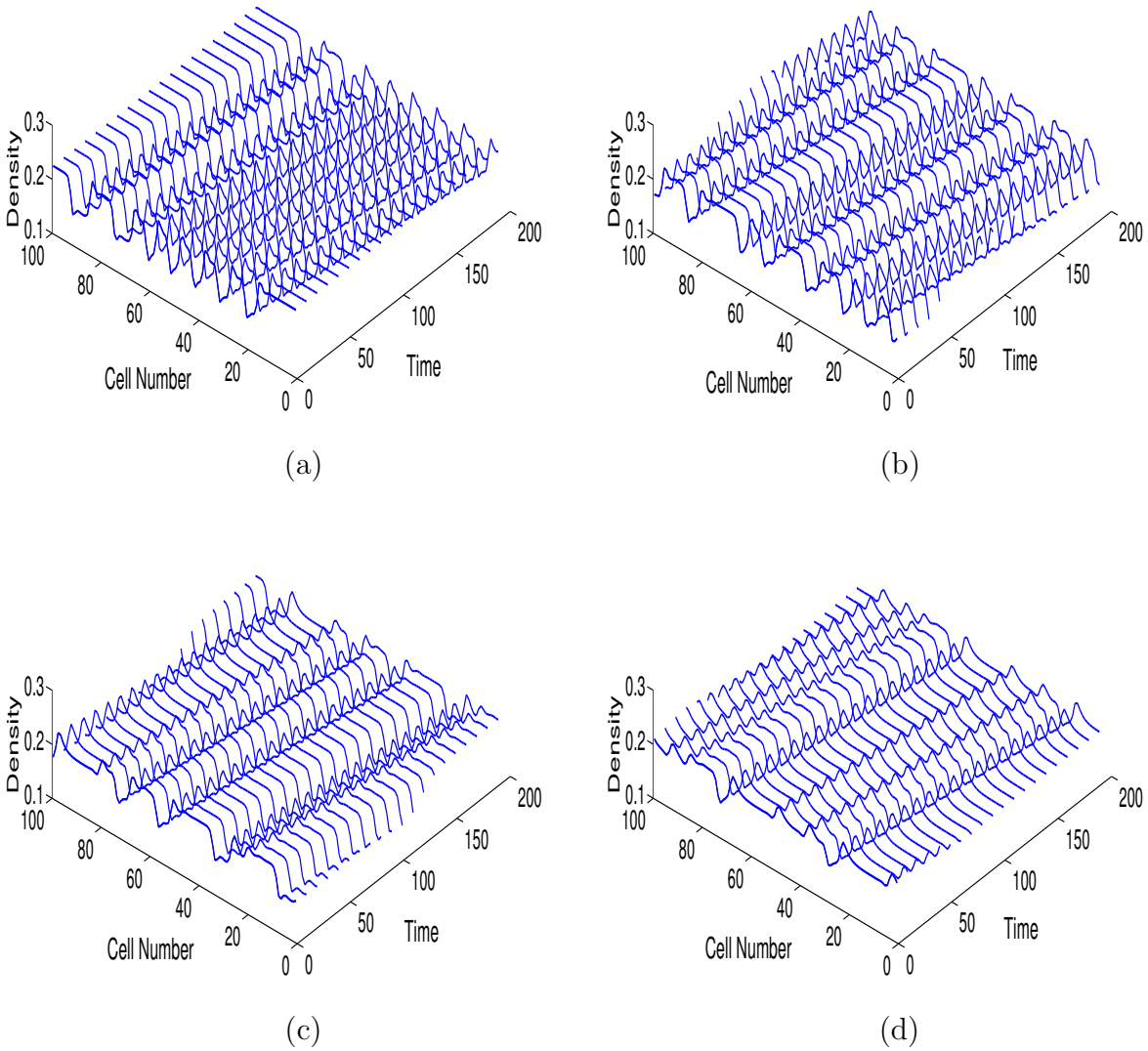

Figure 2.7: Spatiotemporal evolutions of density waves after time $t = 2 \times (10^4)s$ when $\eta = 0.3$, $a = 3.0$, and $t_0 = 0.1$ for (a) $\beta = 0$, (b) $\beta = 0.2$, (c) $\beta = 0.4$, and (d) $\beta = 0.6$, respectively.

system will be absorbed, which means the traffic jam disappears, and the homogeneous traffic flow finally evolves into a stable uniform flow. Numerical results are consistent with the analytical findings for $\eta < f(t_0, \beta)$. Therefore, it is reasonable to conclude that the predictive effect improves the stability of traffic flow for a lower rate of passing.

The phase plot is drawn to verify the periodic behavior of traffic flow concerning $\rho(t) - \rho(t-1)$ versus $\rho(t)$ in Fig. 2.6 when the value of passing constant is smaller. The results are shown for $t = 10^4 - 2 \times 10^4$ in Fig. 2.6 with the same parameters analogous to Fig. 2.4. The closed loop is the set of spread points in the phase plane. The closed loop pattern exhibits the periodic nature for all values of β. The nonlinear stability analysis is used to compute the free flow and the jammed state, respectively, described by the left and the right endpoints in the closed loop. It is found that to increase the value of β, the area of the loop significantly reduces and transforms into a solitary point at $\beta = 0.6$ for a smaller rate of passing.

Case 2: When the value of passing constant is larger i.e., $\eta \geq f(t_0, \beta)$

Here, we further analyze the impact of the predictive effect on the traffic flow dynamics at a higher rate of passing $\eta = 0.3$. It is clear from the results that the patterns of density profiles are different for smaller values as compared to the higher values of β. Fig. 2.7 displays the temporal and spatial evolution of density waves after $t = 2 \times 10^4$ time steps for different values of β at a higher rate of passing. It is observed that the fluctuation of density waves lowers down with the increase in the values of β. In Fig. 2.7(a)-(b), the traffic is in the kink region as $a < \frac{2}{1+2t_0\beta-2f(t_0,\beta)}$ and in Fig. 2.7(c)-(d) the traffic remain in the chaotic region which displays the density waves propagates in a backward direction. On the phase plane, one can conclude that kink, as well as chaotic region, exist in the unstable region, which verifies the analytical results shown in Fig. 2.3.

Fig. 2.8 shows the density profiles at time $t = 20000$s corresponding to the panel of Fig. 2.7. On comparing Fig. 2.8(a)-(b) with Fig. 2.5(a)-(b), it is observed that the profiles of kink jam for a higher value of passing are different from those obtained for a smaller value of passing. In Fig. 2.8(a)-(b), the density profile exhibit bando wave till $a < a_c$, i.e., when the traffic remains in the kink region. After that, when the traffic enters a chaotic region, the profiles of the density wave become irregular in Fig. 2.8(c)-(d). Noticeably, the density wave amplitude decreases as β increases. Moreover, increase in β, the kink region converts into the chaotic region. It is found that numerical results are consistent with the analytical results obtained in the section 2.3 if a is less than a_c the traffic remains in the kink region while for a is greater than a_c, the traffic enters into the chaotic region.

Fig. 2.9 displays the phase plots of density versus density difference for time $t = 10^4 - 2 \times 10^4$

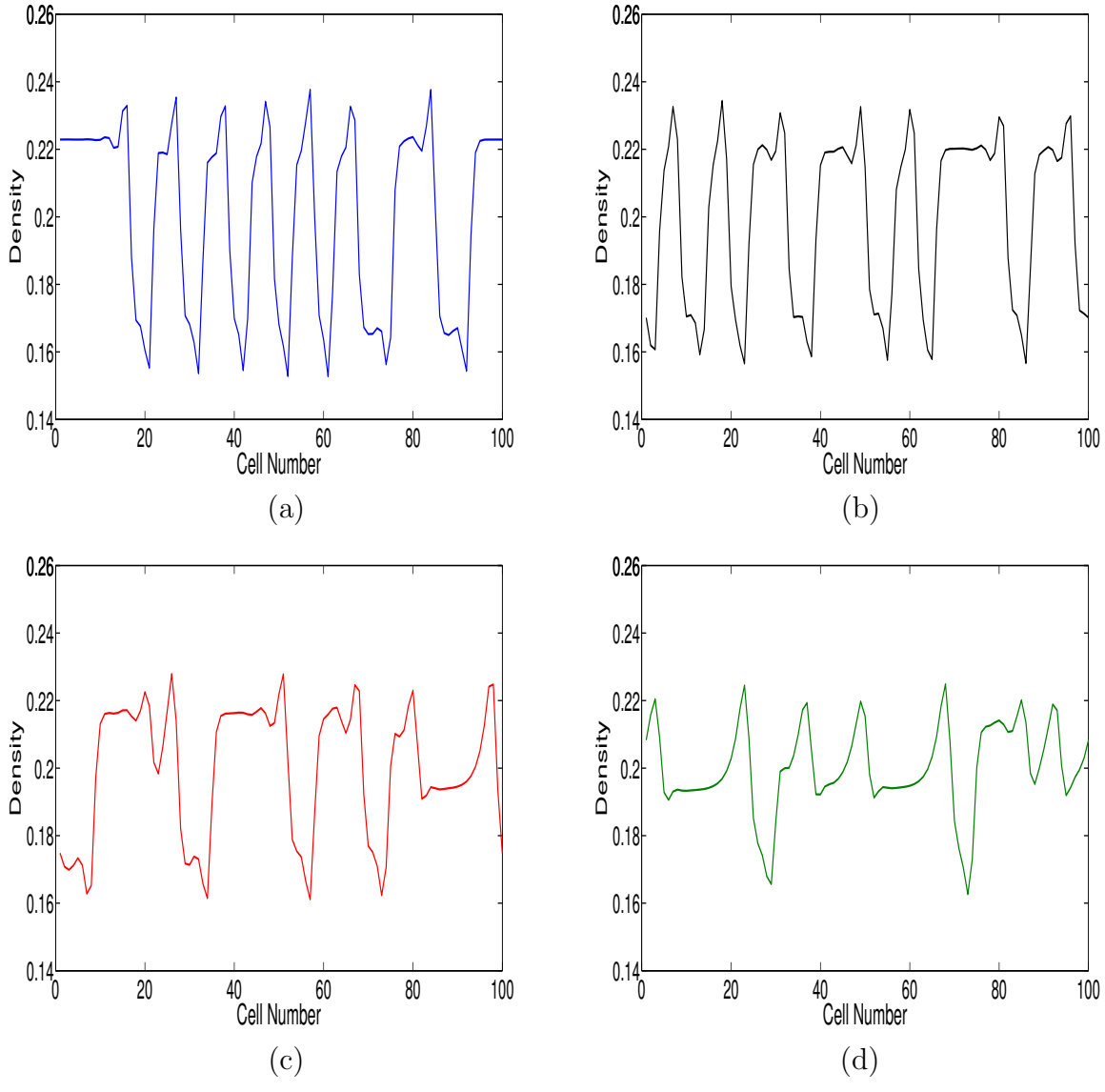

Figure 2.8: Density profiles at time $t = 20000s$ when $\eta = 0.3$, $a = 3.0$, and $t_0 = 0.1$ for (a) $\beta = 0$, (b) $\beta = 0.2$, (c) $\beta = 0.4$, and (d) $\beta = 0.6$, respectively.

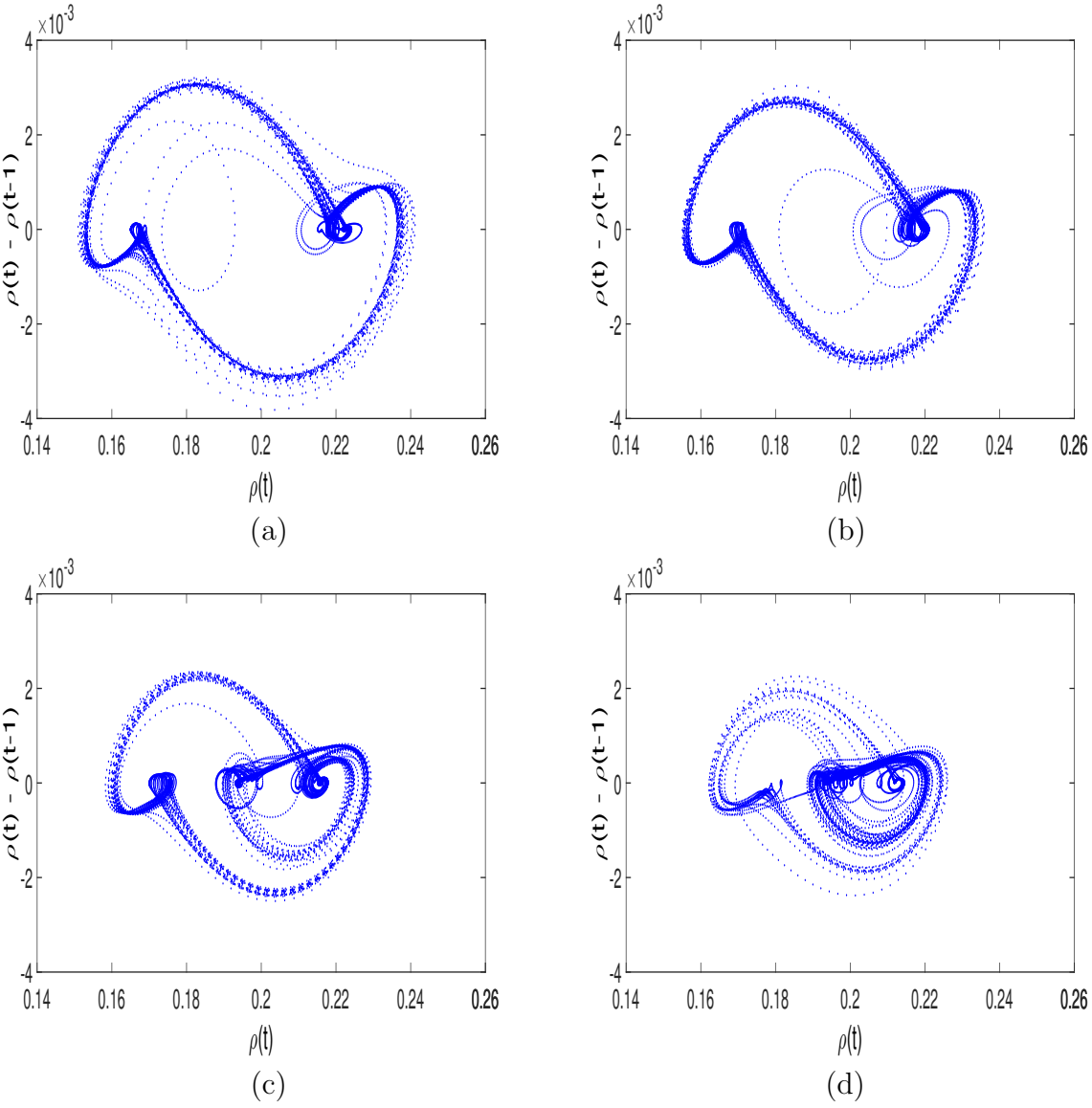

Figure 2.9: Plots of density versus density difference at time $t = 10^4 - 2 \times 10^4$ at $\eta = 0.3$, $t_0 = 0.1$, $a = 3.0$ for (a) $\beta = 0$, (b) $\beta = 0.2$, (c) $\beta = 0.4$, and (d) $\beta = 0.6$, respectively.

when the value of the passing constant is larger. For smaller values of β, the closed loop is shown in Fig. 2.9(a)-(b) formed by the set of dispersed points, which shows the periodic behavior of traffic when traffic is in the kink region. In Fig. 2.9(c)-(d), the irregular pattern exhibits dispersed points around a closed loop for the high value of β, which corresponds to the irregular behavior of traffic. The chaotic phase shows the behavioral characteristics of the disorder.

The results show that the predictive effect plays an important role in enhancing the stability of traffic flow for all possible values of the passing constant and conclude that when the value of β is increasing, the loop diminishes in size even at a larger value of passing.

2.5 Conclusion

In the present chapter, a new lattice hydrodynamic model of traffic flow is proposed to explore the influence of predictive effect when passing is permissible. The predictive effect is investigated theoretically with the help of linear and nonlinear stability analysis. It is found that when vehicles are permitted to overtake, in this situation, the predictive effect is important in enhancing traffic flow stability. Moreover, the phase diagram in the parameter space (η, a) is presented by using theoretical results, which show the different regions of flow as stable region, kink region, and chaotic region. The impact of important parameters (β is the coefficient for predictive effect and η is the passing constant) in the form of the neutral stability lines and the coexisting stability lines are plotted. To describe the traffic congestion near the critical point, the mKdV equation is derived and obtained condition for which the kink solution of the mKdV equation exists. Simulations are carried out to test the reliability of theoretical results and are consistent with the theoretical results. From the theoretical and numerical results, it is concluded:

- The predictive effect significantly increases traffic flow's stability; when overtaking occurs between vehicles.
- Phase boundaries are described for a higher and smaller value of η in the plane (η, a).
- For a smaller rate of passing constant, there are only two regions that exist: stable and kink. In this case, the traffic jam comes out in terms of kink waves.
- For a higher rate of passing, one more region exists, known as the chaotic region, which shows an irregular pattern of traffic jams.
- Finally, it is concluded that when drivers have prior information about the ahead traffic situations helps to reduce traffic congestion, no matter whether overtaking occurs less or more.

Chapter 3

Two-Lane traffic based on predictive effect

Nowadays, with the increase of vehicles on roads, traffic congestion has become a more serious topic for scientists and researchers. Energy waste, environmental pollution, and even traffic accidents are caused by congestion. Many micro-macro traffic flow models [30,49,57,59,62,134,140,148–151], in the context of reducing traffic jams, have been studied in the last few decades and also explain the collective properties of traffic flow.

To investigate the traffic characteristics, Nagatani [83] proposed the first simplest hydrodynamic model with a lattice version to analyze the density waves and the phase transition in congested traffic flow, as discussed in Chapter 1. Further, various researchers have developed a series of extended homogeneous lattice models to more precisely reflect real traffic consisting of different factors and traffic conditions such as density difference effect [96], driver's behavior [123], honk effect [152], historic effect [97,98], etc.

However, all the above lattice models are only suited to describe the traffic flow on a single lane. But in real traffic, most road networks are made up of multi-lane highways, which are considered more suitable. On the two-lane highway, in the case of a traffic jam ahead, drivers may change lanes to avoid congestion. To fulfill this requirement, Nagatani [107] presented a two-lane lattice hydrodynamic model by extending the basic one-lane lattice model, which reflects the lane-changing rule. Thereafter, many two-lane lattice models have been presented [108,112–115,153–157] with the lane changing behavior. All the models mentioned above conclude that traffic flow stability enhances if lane changing is allowed. Later, with the rapid advancement of information technology (IT) and sensor technology, drivers can obtain an accurate estimation of real-time traffic conditions. Using such information, drivers take suitable measures to adjust their driving behavior in advance. Therefore, some lattice hydrodynamic models accounting for the effect of anticipation from different perspectives have been presented [93–95,109,117,118].

In real vehicular flow on roadways, the driver's behavior is influenced by the vehicles ahead in the next moment. After getting information about downstream conditions, drivers modify their driving skills. Thus, the front vehicles' prior information (predictive effect) helps

The content of this chapter has been published in Physica A: Statistical Mechanics and its Applications, 539: 122913, (2020).

drivers adjust their velocity accordingly. Therefore, the predictive effect plays an important role in explaining this phenomenon. Based on the mentioned phenomenon, the predictive effect of expected traffic variation [85] is incorporated in a single-lane lattice model. Further, as explained in Chapter 2, Kaur and Sharma [158] explored the behavior of the predictive effect with passing, and concluded that the predictive effect and passing are interconnected as whenever fast-speed vehicles obtain the prior information about downstream traffic conditions, then this information helps to overtake the slow speed vehicles according to the situation. Furthermore, the predictive effect has not yet been explored in a two-lane lattice model. Therefore, we propose a lattice model by incorporating the predictive and optimal current difference effects (OCDE) for a two-lane traffic system. We theoretically investigate its effect on traffic dynamics and examine these results by considering a hypothetical test case.

This Chapter is structured as follows: A new lattice model is proposed in Section 3.1 considering the influence of the predictive effect and OCDE for a two-lane highway. The theoretical investigation of the proposed model is carried out in Section 3.2 and 3.3. More specifically, Section 3.2 deals with linear stability analysis, while nonlinear stability analysis is performed in Section 3.3. Section 3.4 provides numerical simulations to validate the theoretical findings. Finally, a conclusion with the possible future scope is drawn in Section 3.5.

3.1 Lattice model

In the literature on traffic flow, it is found that multi-lane models are more consistent instead of one-lane models. In this regret, Nagatani [83] further extended his basic one-lane lattice model for a two-lane system by incorporating the effect of lane changing in the continuity equation. Fig. 3.1 represents the schematic model of unidirectional traffic flow on a two-lane highway with permissible lane changing. The lane change will occur in two possibilities:

- Firstly, when the density on the second lane at j^{th} site is lower than that at site $j-1$ on the first lane, then the lane change will occur from the first lane to the second lane at the following rate $\gamma|\rho_0^2 V^{'}(\rho_0)|(\rho_{1,j-1}(t)-\rho_{2,j}(t))$. γ is the dimensionless coefficient, and $|\rho_0^2 V^{'}(\rho_0)|$ is a constant that is introduced to ensure that it is dimensionless.

- Secondly, when the density at site $j+1$ on the first lane is lower than that at j^{th} site on the second lane, the lane change will occur at the rate as follows: $\gamma|\rho_0^2 V^{'}(\rho_0)|(\rho_{2,j}(t)-\rho_{1,j+1}(t))$ from second lane to first lane.

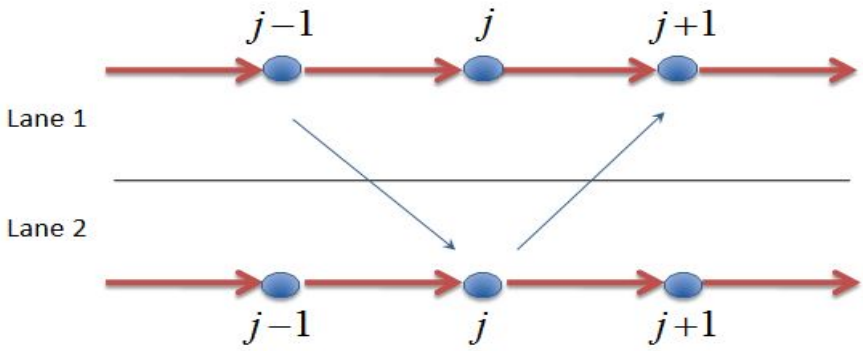

Figure 3.1: The schematic lattice model of unidirectional traffic flow on a two-lane highway with permissible lane changing

Here, $\rho_{1,j}(t)(\rho_{2,j}(t))$ represents the density on the first (second) lane. Therefore, the continuity equation for a two-lane highway was formulated by Nagatani [107] as

$$\partial_t \rho_j(t) + \rho_0(\rho_j(t)v_j(t) - \rho_{j-1}(t)v_{j-1}(t)) = \gamma|\rho_0^2 V^{'}(\rho_0)|(\rho_{j-1}(t) - 2\rho_j(t) + \rho_{j+1}(t)), \quad (3.1)$$

where $\rho_j = \frac{\rho_{1,j}+\rho_{2,j}}{2}$, $\rho_j v_j = \frac{\rho_{1,j}v_{1,j}+\rho_{2,j}v_{2,j}}{2}$ and $V(\rho_j) = \frac{V(\rho_{1,j})+V(\rho_{2,j})}{2}$. Later, the two-lane lattice model was extended by Peng [153] to consider the impacts of optimal current difference effect (OCDE). Then, the continuity equation remains intact, while the evolution equation is extended as follows

$$\partial_t(\rho_j(t)v_j(t)) = a[\rho_0 V(\rho_{j+1}(t)) - \rho_j(t)v_j(t)] + a\rho_0\lambda(V(\rho_{j+2}(t)) - V(\rho_{j+1}(t))), \quad (3.2)$$

where λ represents the reactive coefficient of optimal current difference, and second term denotes the OCDE.

However, as far as the author's knowledge is concerned, the predictive effect is not considered in the two-lane lattice model. Therefore, a more realistic traffic flow model is proposed to capture the predictive effect consisting of OCDE for a two-lane system. The continuity equation remains unaltered while the evolution equation is extended as follows

$$\begin{aligned}\partial_t(\rho_j(t)v_j(t)) = a[\rho_0 V\big(\rho_{j+1}(t) + \beta(\rho_{j+1}(t+t_0) - \rho_{j+1}(t))\big) - \rho_j(t)v_j(t)] \\ + a\rho_0\lambda(V(\rho_{j+2}(t)) - V(\rho_{j+1}(t))),\end{aligned} \quad (3.3)$$

where t_0 represents the predictive time and $\rho_{j+1}(t+t_0)$ denotes the predictive density at site $j+1$. The parameter $\beta(0 \leq \beta \leq 1)$ is the coefficient of the predictive density variation.

$V\big(\rho_{j+1}(t) + \beta(\rho_{j+1}(t+t_0) - \rho_{j+1}(t))\big)$ can be approximated by Taylor series expansion,

containing variable $\rho_{j+1}(t+t_0)$ of Eq. (3.3) and neglecting nonlinear terms, we get

$$V\big(\rho_{j+1}(t)+\beta(\rho_{j+1}(t+t_0)-\rho_{j+1}(t))\big)=V(\rho_{j+1}(t))+V'(\rho_{j+1})\beta t_0\partial_t\rho_{j+1}(t). \tag{3.4}$$

By using Eqs. (3.1), (3.3) and (3.4), the density equation is obtained as

$$\begin{aligned}\partial_t^2\rho_j+a\rho_0^2[V(\rho_{j+1})-V(\rho_j)]+a\rho_0^2\beta t_0[V'(\rho_{j+1})\partial_t\rho_{j+1}-V'(\rho_j)\partial_t\rho_j]+a\partial_t\rho_j\\ -a\gamma|\rho_0^2V'(\rho_0)|(\rho_{j-1}-2\rho_j+\rho_{j+1})+a\rho_0^2\lambda[V(\rho_{j+2})-2V(\rho_{j+1})+V(\rho_j)]\\ -\gamma|\rho_0^2V'(\rho_0)|(\partial_t\rho_{j-1}-2\partial_t\rho_j+\partial_t\rho_{j+1})=0.\end{aligned} \tag{3.5}$$

In addition, the optimal velocity function adopted by Nagatani [107] is used, which is given as

$$V(\rho_j)=\frac{v_{max}}{2}\Big[\tanh\Big(\frac{1}{\rho_j}-\frac{1}{\rho_c}\Big)+\tanh\Big(\frac{1}{\rho_c}\Big)\Big], \tag{3.6}$$

where $v_{max}=2.0$ represents the maximal velocity. This function has a turning point at $\rho_j=\rho_c$. The proposed model is general and covers the following four existing models.

- $\lambda=0$, $\gamma=0$, the model reduces to the one discussed in ref. [85].
- $\beta=0$ or $t_0=0$, the model coincides with Peng's model [153].
- $\beta=0$ or $t_0=0$ with $\lambda=0$, the model reduces to Nagatani's two-lane model [107].
- $\beta=0$ or $t_0=0$ with $\lambda=0$, $\gamma=0$, the model covers Nagatani's basic model [83].

3.2 Linear stability analysis

For investigation of predictive effect on the traffic flow's jamming transition, linear stability analysis is performed. Initially, the traffic is considered to move with a constant density ρ_0, resulting in identical optimal velocity $V(\rho_0)$. Then, the steady-state solution on the two-lane highway for Eq. (3.5) is

$$\rho_j(t)=\rho_0,\quad v_j(t)=V(\rho_0). \tag{3.7}$$

$y_j(t)$ is supposed to be a small fluctuation to the uniform density on site j,

$$\rho_j(t)=\rho_0+y_j(t). \tag{3.8}$$

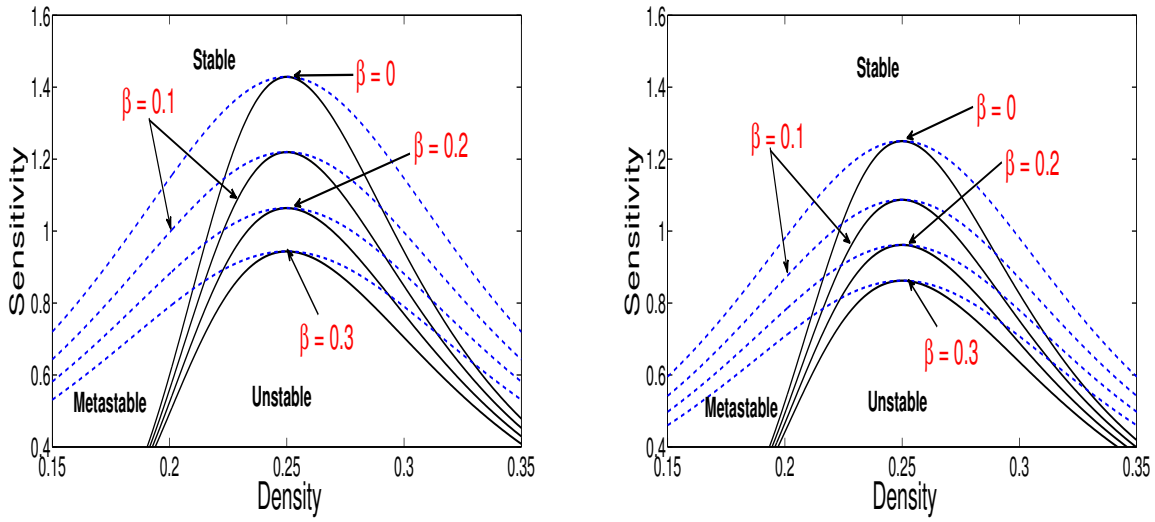

(a) (b)

Figure 3.2: Phase diagrams with $\rho_0 = \rho_c = 0.25$ in (ρ, a) space for different values of parameter β with $\lambda = 0.2$, $t_0 = 1.2$ for (a) $\gamma = 0$ (b) $\gamma = 0.1$.

Substituting Eq. (3.8) into (3.5), we get

$$\begin{aligned}\partial_t^2 y_j(t) + a\rho_0^2 V'(\rho_0)[y_{j+1}(t) - y_j(t)] + a\beta t_0 \rho_0^2 V'(\rho_0)[\partial_t y_{j+1}(t) - \partial_t y_j(t)] + a\partial_t y_j(t) \\ - a\gamma|\rho_0{}^2 V'(\rho_0)|[y_{j-1}(t) - 2y_j(t) + y_{j+1}(t)] + a\lambda\rho_0{}^2 V'(\rho_0)[y_{j+2}(t) - 2y_{j+1}(t) + y_j(t)] \\ - \gamma|\rho_0{}^2 V'(\rho_0)|[\partial_t y_{j-1}(t) - 2\partial_t y_j(t) + \partial_t y_{j+1}(t)] = 0.\end{aligned} \tag{3.9}$$

Putting $y_j(t) = \exp(ikj + \omega t)$ into Eq. (3.9), we obtain

$$\begin{aligned}\omega^2 + \left[a\beta t_0 \rho_0^2 V'(\rho_0)(e^{ik} - 1) + a - \gamma|\rho_0{}^2 V'(\rho_0)|(e^{-ik} - 2 + e^{ik})\right]\omega + a\rho_0{}^2 V'(\rho_0)(e^{ik} - 1) \\ - a\gamma|\rho_0{}^2 V'(\rho_0)|(e^{-ik} - 2 + e^{ik}) + a\lambda\rho_0^2 V'(\rho_0)(e^{2ik} - 2e^{ik} + 1) = 0.\end{aligned} \tag{3.10}$$

Set $\omega = \omega_1(ik) + \omega_2(ik)^2 .....$ into (3.10) and we obtain the long wave expansion of ω. By neglecting higher-order terms, we get the following equations

$$\omega_1 = -\rho_0{}^2 V'(\rho_0). \tag{3.11}$$

$$\omega_2 = -\frac{\omega_1{}^2}{a} - \frac{\rho_0{}^2 V'(\rho_0)}{2} - \beta t_0 \omega_1(\rho_0{}^2 V'(\rho_0)) - \lambda(\rho_0{}^2 V'(\rho_0)) + \gamma|\rho_0{}^2 V'(\rho_0)|. \tag{3.12}$$

If the inequality $\omega_2 < 0$, the steady state flow develops into the unstable state in long wavelength waves; conversely, it becomes stable if $\omega_2 > 0$. Thus, the stable critical condition is

obtained by $\omega_2 = 0$.

$$a = \frac{-2{\rho_0}^2 V'(\rho_0)}{1 - 2\beta t_0 \rho_0^2 V'(\rho_0) + 2(\lambda + \gamma)}. \tag{3.13}$$

Hence, the linear stability condition for the homogeneous traffic flow can be obtained by $\omega_2 > 0$, i.e.,

$$a > \frac{-2{\rho_0}^2 V'(\rho_0)}{1 - 2\beta t_0 \rho_0^2 V'(\rho_0) + 2(\lambda + \gamma)}. \tag{3.14}$$

The result is influenced by the parameters β, γ. Eq. (3.14) clearly shows that as the parameter β increases, the unstable region reduces by taking lane-changing parameter γ on the two-lane highway. Fig. 3.2(a) and 3.2(b) shows the neutral curves (solid black lines) in the phase space (ρ, a) for different values of β ($\beta = 0,\ 0.1,\ 0.2$ and 0.3, respectively) by taking the values of $t_0 = 1.2$ and $\lambda = 0.2$ when $\gamma = 0$ and $\gamma = 0.1$, respectively. The position of the apex of the neutral curves decreases due to the increasing values of β as well as lane changing parameter γ, which indicates that the stability of traffic flow significantly increased. It is found that the stable region becomes larger in a two-lane traffic system as compared to the one discussed in ref. [85] when lane changing is allowed.

3.3 Nonlinear stability analysis

We investigate the influence of predictive effect to describe the traffic jam around the critical point (ρ_c, a_c) by using the reduced perturbation method. The mKdV equation is obtained. First of all, the space variable X and time variable T for a small positive scaling parameter $\epsilon (0 < \epsilon \ll 1)$ are defined as follows

$$X = \epsilon(j + pt), \quad T = \epsilon^3 t, \tag{3.15}$$

where p is a constant term that needs to be determined. Let the density is

$$\rho_j(t) = \rho_c + \epsilon S(X, T). \tag{3.16}$$

Substituting (3.15) and (3.16) into Eq. (3.5) and Taylor series expansion is used to expand (3.5) up to fifth order of ϵ, the following nonlinear equation is obtained

$$\epsilon^2 h_1 \partial_X S + \epsilon^3 h_2 \partial_X^2 S + \epsilon^4 (\partial_T S + h_3 \partial_X^3 S + h_4 \partial_X S^3) + \epsilon^5 (h_5 \partial_T \partial_X S + h_6 \partial_X^4 S + h_7 \partial_X^2 S^3) = 0. \tag{3.17}$$

The coefficients h_i are shown in Table 3.1, where $V' = \frac{\partial V(\rho)}{\partial \rho}\Big|_{\rho=\rho_c}$ and $V''' = \frac{\partial^3 V(\rho)}{\partial \rho^3}\Big|_{\rho=\rho_c}$.

Table 3.1: The coefficients h_i of the model

coefficients	**values**
h_1	$p + {\rho_0}^2 V'$
h_2	$\frac{p^2}{a} + \frac{\rho_0^2 V'}{2}\big[1 + 2\lambda + 2p\beta t_0 + 2\gamma\big]$
h_3	$\frac{\rho_0^2 V'}{6}\big[1 + 6\lambda + 3p\beta t_0 + \frac{6p\gamma}{a}\big]$
h_4	$\frac{\rho_0^2 V'''}{6}$
h_5	$\frac{2p}{a} + \beta t_0 \rho_0^2 V'$
h_6	$\frac{{\rho_0}^2 V'}{24}\big[1 + 14\lambda + 4p\beta t_0 + 2\gamma\big]$
h_7	$\frac{{\rho_0}^2 V'''}{12}\big[1 + 2\lambda + 2p\beta t_0\big]$

Near the critical point (ρ_c, a_c), we consider $a_c = a(1+\epsilon^2)$. By substituting $p = -{\rho_0}^2 V'$, the quadratic and the cubic terms of ϵ are eliminated, then we gain the following equation

$$\epsilon^4(\partial_T S - b_1\partial_X^3 S + b_2\partial_X S^3) + \epsilon^5(b_3\partial_X^2 S + b_4\partial_X^4 S + b_5\partial_X^2 S^3) = 0, \tag{3.18}$$

where, the coefficients b_i are exhibited in Table 3.2. The following transformation is used: $T = \frac{1}{b_1}T'$ and $S = \sqrt{\frac{b_1}{b_2}}S'$ to convert Eq. (3.18) into standard mKdV equation. So, the resulting Eq. (3.18) can be written as

$$\partial_{T'} S' - \partial_X^3 S' + \partial_X {S'}^3 + \frac{\epsilon}{b_1}\Big[b_3\partial_X^2 S' + b_4\partial_X^4 S' + \frac{b_1 b_5}{b_2}\partial_X^2 {S'}^3\Big] = 0. \tag{3.19}$$

After ignoring the correction term $O(\epsilon)$ in Eq. (3.19), one can get the kink antikink solution of the standard mKdV equation given as

$$S_0'(X, T') = \sqrt{\mu}\,\tanh\Big(\sqrt{\frac{\mu}{2}}(X - \mu T')\Big). \tag{3.20}$$

Here, μ represents the propagation velocity for the kink antikink density wave and can be computed by solving the following condition

$$(S_0', M[S_0']) \equiv \int_{-\infty}^{\infty} dX S_0' M[S_0'] = 0, \tag{3.21}$$

Table 3.2: The coefficients b_i of the model

coefficients	**values**
b_1	$-\frac{\rho_0^2 V'}{6}\big[1+6\lambda+3p\beta t_0+\frac{6p\gamma}{a_c}\big]$
b_2	$\frac{\rho_0^2 V'''}{6}$
b_3	$-\frac{\rho_0^2 V'}{2}\big[1+2\lambda+2p\beta t_0+2\gamma\big]$
b_4	$\frac{{\rho_0}^2 V'}{24}\big[1+14\lambda+4p\beta t_0+2\gamma\big]+\frac{2p}{a_c}\big[1-\frac{a_c\beta t_0}{2}\big]b_1$
b_5	$\frac{\rho_0^2 V'''}{12}\big[1+2\lambda+2p\beta t_0\big]-\frac{2p}{a_c}\big[1-\frac{a_c\beta t_0}{2}\big]b_2$

where $M[S_0'] = \frac{1}{b_1}[b_3\partial_X^2 S' + b_4\partial_X^4 S' + \frac{b_1 b_5}{b_2}\partial_X^2 S'^3]$. By solving (3.21), the suitable choice of μ is obtained as

$$\mu = \frac{5b_2 b_3}{2b_2 b_4 - 3b_1 b_5}. \tag{3.22}$$

Hence, the kink-antikink solution is obtained

$$\rho_j = \rho_c + \epsilon\sqrt{\frac{b_1\mu}{b_2}}\tanh\Big(\sqrt{\frac{\mu}{2}}(X-\mu b_1 T)\Big), \tag{3.23}$$

where $\epsilon^2 = \Big(\frac{a_c}{a}-1\Big)$ and the amplitude α of the derived solution is $\sqrt{\frac{b_1\epsilon^2\mu}{b_2}}$.

The kink-antikink soliton solution of Eq. (3.23) represents the coexisting phase, including both the freely moving phase and the congested phase, which can be described by $\rho_j = \rho_c - \alpha$ and $\rho_j = \rho_c + \alpha$, respectively, in the phase space (ρ, a). Fig. 3.2 shows the neutral stability curves (solid curves) and the coexisting curves (dotted curves) obtained from the linear and nonlinear analysis, respectively, split the phase plane into three regions: the stable region (above the coexisting curves), the metastable region (between the coexisting and the neutral stability curves) and the unstable region (below the neutral curves). It is seen that when lane changing is allowed, i.e., with an increased value of γ, the neutral and the coexisting curves both lower down, corresponding to the parameter β, resulting in a higher rate of stability of traffic flow.

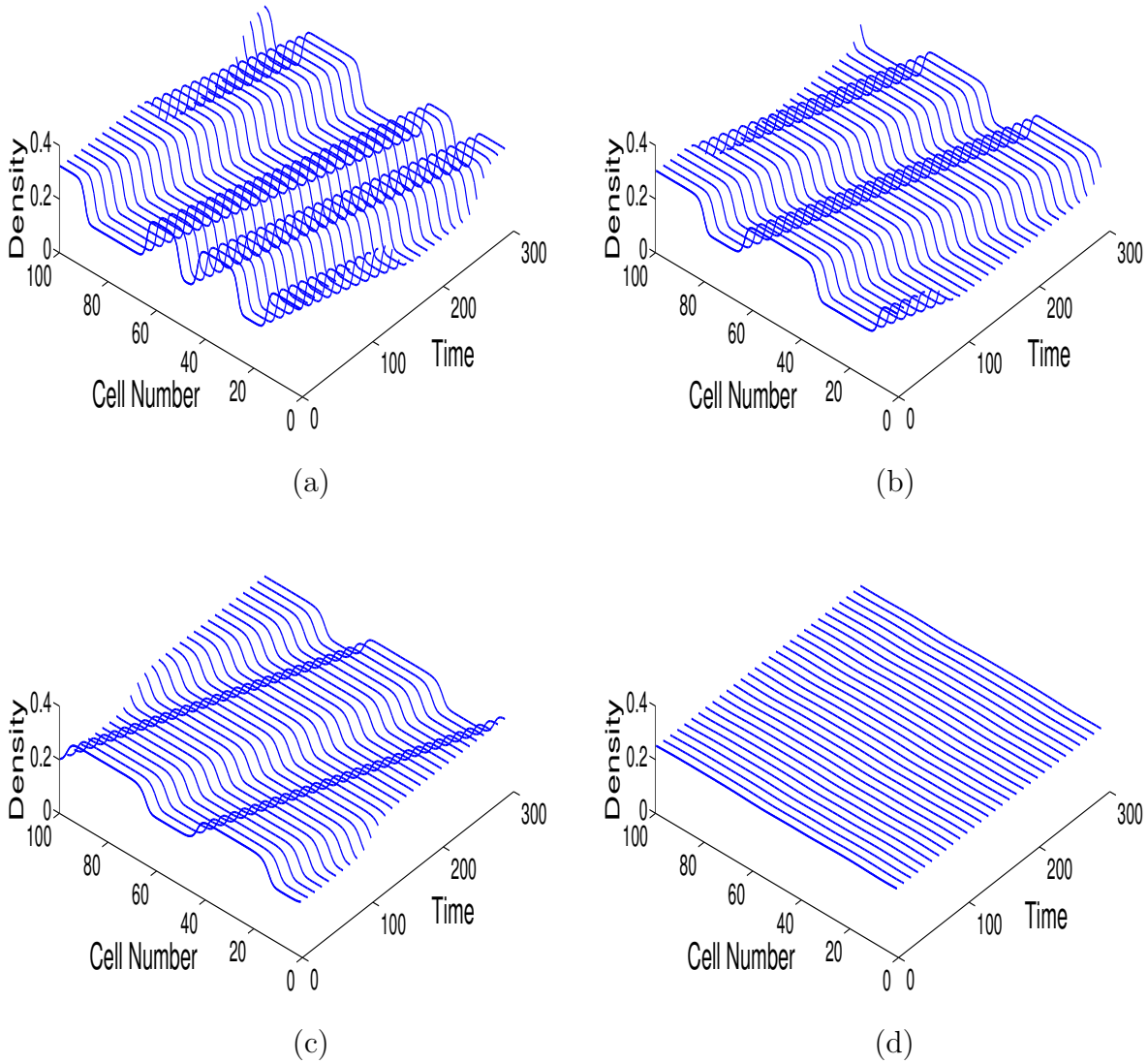

Figure 3.3: Spatio-temporal evolutions of density waves after $t = 10^4 s$ when $a = 1.0$, $\gamma = 0$ for (a) $\beta = 0$, (b) $\beta = 0.1$, (c) $\beta = 0.2$, and (d) $\beta = 0.3$, respectively.

3.4 Simulation

In the previous two sections, the influence of the predictive effect on the two-lane traffic stream has been investigated theoretically by linear and nonlinear analysis. In this section, numerical simulations are performed to examine the theoretical analysis. For numerical computation, Eq. (3.5) is written in discrete form as

$$\begin{aligned}\rho_j(t+2\Delta t) &= 2\rho_j(t+\Delta t) - \rho_j(t) - a\rho_0^2\Delta t^2\big[V(\rho_{j+1}(t)) - V(\rho_j(t))\big] - a\Delta t[\rho_j(t+\Delta t) - \rho_j(t)] \\ &- a\rho_0^2\beta t_0\Delta t\Big[V'(\rho_{j+1}(t))[\rho_{j+1}(t+\Delta t) - \rho_{j+1}(t)] - V'(\rho_j(t))[\rho_j(t+\Delta t) - \rho_j(t)]\Big] \\ &+ a\Delta t^2\gamma|\rho_0^2V'(\rho_0)|(\rho_{j-1}(t) - 2\rho_j(t) + \rho_{j+1}(t)) - a\rho_0^2\Delta t^2\lambda[V(\rho_{j+2}(t)) - 2V(\rho_{j+1}(t)) + V(\rho_j(t))] \\ &+ \Delta t\gamma|\rho_0^2V'(\rho_0)|\big[\rho_{j-1}(t+\Delta t) - 2\rho_j(t+\Delta t) + \rho_{j+1}(t+\Delta t) - (\rho_{j-1}(t) - 2\rho_j(t) + \rho_{j+1}(t))\big].\end{aligned} \tag{3.24}$$

Here, Δt is the time step, and the value of Δt is taken as 0.15 during the simulation. The periodic boundary conditions are applied. A step function describes the initial conditions for each lattice:

$$\rho_j(0) = \rho_0 = 0.25. \qquad j \in [1, N], \tag{3.25}$$

$$\rho_j(1) = \begin{cases} \rho_0; & j \neq \frac{N}{2}, \frac{N}{2} - 1 \\ \rho_0 + \Delta\rho; & j = \frac{N}{2} - 1 \\ \rho_0 - \Delta\rho; & j = \frac{N}{2} \end{cases}, \tag{3.26}$$

where, $\Delta\rho = 0.05$ is the initial disturbance. N defines the total number of sites ($N = 100$), and the other parameters are selected as $a = 1.0$, $\rho_0 = \rho_c = 0.25$, $t_0 = 1.2$.

In the following simulation, we change the value of β to analyze its influence on the stability of traffic flow in a two-lane traffic system. Fig. 3.3(a)-(d) displays the temporal and spatial evolution of density waves after $t = 10^4$ time steps for different values of β ($\beta = 0,\ 0.1,\ 0.2$ and 0.3, respectively) when lane changing is not allowed i.e., $\gamma = 0$. According to Fig. 3.3(a)-(c), it is found that the kink-antikink soliton solution occurs, and their amplitude decreases as β increases. It shows that the traffic congestion has not completely disappeared. Fig. 3.3(d) depicts that as soon as $\beta = 0.3$, i.e., the disturbance completely vanishes, and the traffic flow reaches a uniform state over the whole space. It indicates that the stable region increases whenever β increases.

Fig. 3.4(a)-(c) gives the simulation results for different values of β ($\beta = 0,\ 0.1$ and 0.2, respectively) when lane changing is permitted i.e., $\gamma = 0.1$. It is observed that the initial disturbance is continuously amplified over time in patterns Fig. 3.4(a)-(b) while

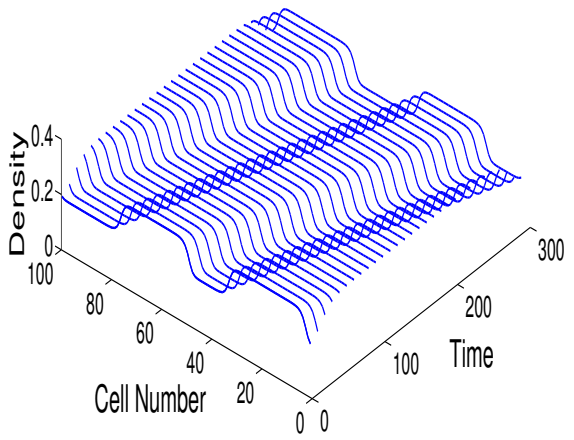

(a)

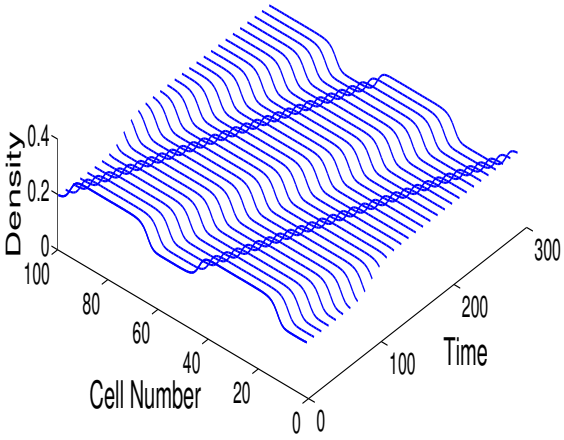

(b)

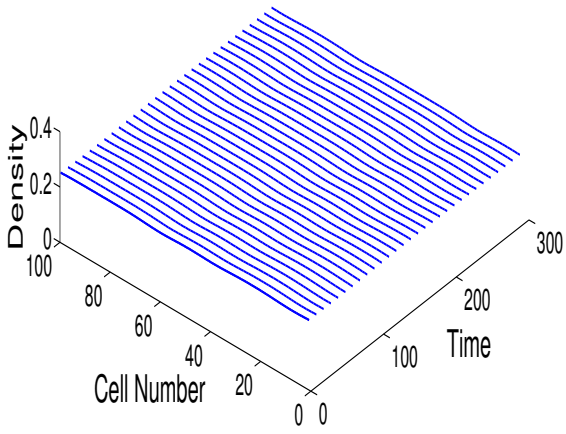

(c)

Figure 3.4: Spatio-temporal evolutions of density waves after $t = 10^4 s$ when $a = 1.0$, $\gamma = 0.1$ for (a) $\beta = 0$, (b) $\beta = 0.1$, and (c) $\beta = 0.2$, respectively.

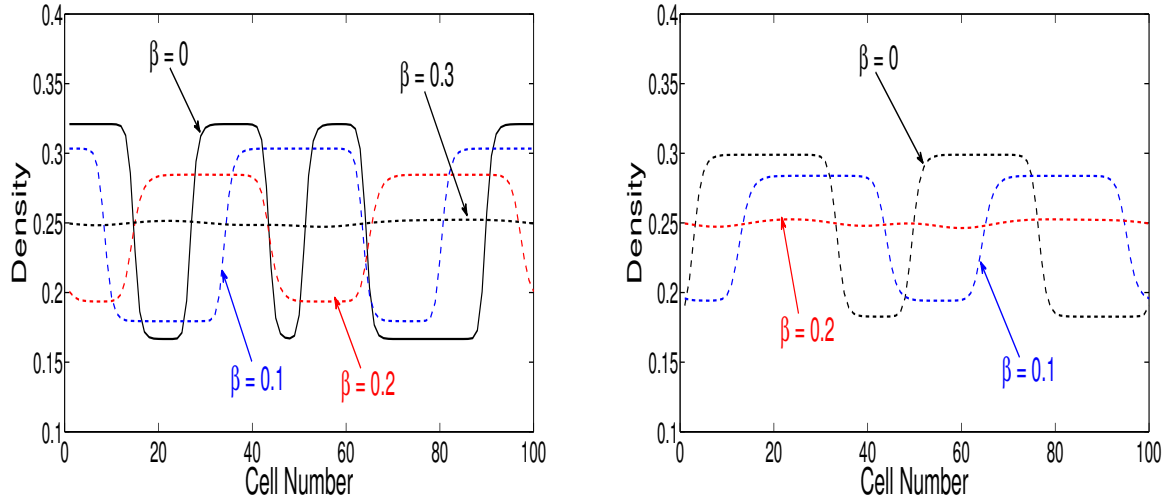

Figure 3.5: Profiles of the density wave at time $t = 10^4 s$ for different values of β when (a) $\gamma = 0$ (b) $\gamma = 0.1$.

the disturbance in pattern Fig. 3.4(c) will dissolve quickly with the high value of β when $\gamma = 0.1$. The traffic flow becomes stable over the entire space. Therefore, one can conclude that the traffic jam can be suppressed effectively by considering the predictive effect of two-lane into account.

Fig. 3.5(a) and 3.5(b) is the clear pictures of the density profiles for different values of β at fixed time $t = 10^4 s$ analogous to the panels of Fig. 3.3 and Fig. 3.4, respectively. It shows that the fluctuation of density waves gradually decreases with β increasing in the two-lane vehicular system. The disturbance in the traffic system will be absorbed, and the homogeneous traffic finally evolves into a stable uniform flow for the high value of β under the conditions of lane changing. It is observed that the predictive effect, as well as the lane-changing effect, improve the stability of traffic flow in a two-lane system. Therefore, from the analytical analysis and simulation results, we can conclude that traffic jams can be efficiently suppressed by taking the predictive effect in a two-lane traffic system. Since the stability condition is satisfied.

3.5 Conclusion and future scope

- In this chapter, a new lattice model is proposed to explore the influence of predictive effect concerning the OCDE for a two-lane traffic system, which is closely associated with the actual traffic conditions.

- The predictive effect is investigated analytically in traffic flow through linear as well as nonlinear stability analysis. Through nonlinear stability analysis, we obtained the mKdV equation to describe the traffic congestion around the critical point.
- Besides, the phase diagrams are obtained in the density-sensitivity space to exhibit the influence of different values of parameter β and γ in two-lane system.
- It is observed that parameter β plays an important role in stabilizing the traffic flow on the two-lane highway with the consideration of OCDE when lane changing is permitted. It is also concluded that the predictive effect can suppress the traffic jam under the conditions of lane changing.
- It can be seen that the high value of parameter β is prompt to increase the stability of traffic flow in the two-lane system when lane changing is allowed. We found that simulation results are consistent with the analytical results and finally, it can be concluded that our assumption is reasonable and the predictive effect impact significantly the traffic dynamics for two-lane traffic network.
- Even though the new lattice model is appropriate to explain the influence of the predictive effect in a two-lane homogeneous vehicular flow yet, it can be further extended to explore the critical phenomenon lies in actual traffic systems, for example, honk effect [152], backward-looking effect [89,90], etc.
- The newly proposed model can be further utilized to investigate the impacts of crucial aspects of transportation, such as fuel and energy consumption, etc.

Chapter 4

Impact of prior information on two-dimensional vehicular system

A million vehicles exist in transportation systems that interact with one another and influence the traffic flow, which is causing the nonlinear vehicular flow to become extremely complex and dense. Various elements, including human behavior, road geometry, environmental factors, etc., may slow vehicle movement, which may form traffic congestion. Moreover, one of the issues to increase congestion may be the design of roads. Improper geometric configuration can increase the collisions between road users and result in a decline in protection and increase travel time. Traffic jams may be decreased by introducing an intersection point on a one-way road. The intersection of roads usually involves the splitting or joining of roads, diverging, etc. Moreover, a lot of attention is being given to the road's intersection in the transportation system, where one-way roads are separated into two-way or more-way roads.

In the vehicular system, the proceeding vehicles follow the leading vehicles and maintain their distance to avoid collisions. There are various models to study traffic flow properties, which help to minimize congestion and maximize road traffic flow. There are various types of roads that exist in real traffic environments, such as one-way roads, two-way roads, higher dimensional roads, shared lane (junction, roundabout) roads, etc. Using the lattice approach, Nagatani [83] investigated the homogeneous traffic characteristics on a one-way (single) unidirectional highway (as mentioned in Chapter 1). Further, some improvements over Nagatani's basic model have been made, such as two-lane system [155,156,159], driver's behavior effect [112,120,123,160], the influence of multi-phase OV function [100,105,146], so on.

One-lane or multi-lane roads may be connected with other roads through nodes (junctions). In that situation, drivers change their path according to their destination using the turning point. Therefore, to capture the movements from one route to other routes in the traffic system, Biham et al. [161] presented a new two-dimensional (2D) cellular automaton (CA) model by considering the two types of cars (East-bound and North-bound). In this model,

The content of this chapter has been published in The European Physical Journal B, 94: 1-12, (2021).

east-bound cars move in x positive direction, and north-bound cars move in y positive direction. It was found that transitions occur from the free-moving phase to the congested phase with an increase in the density of the car. The extendable version of two dimensional CA model was proposed by Nagatani [162] with consideration of two-level crossing. Later on, two dimensional CA model was presented by Chung et al. [163] to describe a traffic jam with faulty traffic lights. Results showed that faulty traffic lights speed up the overall traffic at the low density of cars. Further, the traditional lattice hydrodynamic model was extended by Nagatani [127] for a 2D traffic system in which the movement of traffic flows in the two directions (x and y) was studied. It was found that phase transitions occur among the freely moving, coexisting, and congested phases below a critical point, depending on the fraction of traffic currents. After that, optimal current difference effect [128,129], honk effect [130], driver's memory effect [131], passing effect [164] and shared lane marking effect [165] were considered in 2D lattice model.

Moreover, accurate estimates and timely traffic flow information are needed for individual travelers, government departments, and industry sectors. The prior information (predictive effect) aids road users in making better transport decisions, reducing traffic congestion, lower carbon emissions, and improving traffic flow. The objective of the prior information is to provide maximum traffic flow. It is based on historical and real-time traffic data gathered from various sensor sources, such as inductive loops, crowdsourcing, social media, smartphone Global Positioning System (GPS), etc. Drivers change their vehicle's speed to optimize the flow after receiving accurate information about traffic conditions ahead. In this light, a new lattice model is proposed in Chapter 2 based on the connection between overtaking and the predictive effect. It is concluded that the predictive effect is beneficial in suppressing traffic jams when passing is allowed. Furthermore, in Chapter 3, Kaur and Sharma [166] presented a two-lane lattice model with consideration of the predictive effect in which concluded that the predictive effect could suppress the traffic jam under the conditions of lane changing. In addition, the prior information can also help drivers choose the right path for their destination at the junction point in a 2D traffic network, where one-way roads convert into two-way roads. At the junction on the road, the upstream lane diverts into many downstream lanes. If the downstream conditions are known based on the prior information, the flow can maximize in the respective lane. As far as the author's knowledge, the prior information has not yet been explored in a 2D lattice model with a junction road. Therefore, we propose a 2D lattice model to study the impact of the prior information for the junction road.

This Chapter is organized as follows; In Section 4.1, a 2D lattice hydrodynamic model is proposed using prior information with junction road. The control method analysis is

executed to research how the prior information affects the stability of vehicular flow without and with control signal in Sections 4.2 and 4.3, respectively. In Section 4.4, the numerical simulation is carried out to validate the findings of theoretical analysis, and a conclusion is drawn in Section 4.5.

4.1 Two dimensional (2D) lattice model with junction road

The basic one-dimensional (1D) lattice hydrodynamic (LH) model was introduced by Nagatani [83]. Further, the traditional 1D lattice model was expanded into a 2D lattice model by capturing the movement of traffic flow in two different directions (x and y). Nagatani [127] developed the first 2D lattice model for traffic systems.

In a traffic network, roads may be connected, and a traffic flow from upstream lanes may be diverted to various downstream lanes through a junction point. Drivers continuously analyze the road condition ahead. After receiving information from the intelligent transportation system (ITS) about the estimated behavior of surrounding traffic, they try to adjust their vehicle's speed. They also choose their path according to their destination. Sometimes, drivers can increase their vehicle's speed, where the traffic flow is maximum, to achieve the destination, and it is then possible if they have some prior information about the downstream conditions of traffic. This prior information is called predictive effect [85]. To analyze the physical impacts of the predictive effect with the junction point on the traffic network, we propose a 2D lattice model. As shown in Figure 4.1, the model contains three road sections that reflect the real traffic characteristics, and they are described as follows:

Road section 1: For section 1, the continuity equation and the evolution equation of the proposed model by taking the prior information in the 2D lattice model are given below

$$\partial_t \rho_{r,j}(t) + \rho_0 (q_{r,j}(t) - q_{r-1,j}(t)) = 0, \tag{4.1}$$

$$\partial_t q_{r,j}(t) = a\big[\rho_0 V(\rho_{r+1,j}(t) + \beta(\rho_{r+1,j}(t+t_0) - \rho_{r+1,j}(t)))\big] - a q_{r,j}(t), \tag{4.2}$$

$$(r = 1,\ 2,\ 3, ...,\ L-1;\ j = 1).$$

where, the local density and the local flux are described by $\rho_{r,j}(t)$ and $q_{r,j}(t)$, respectively, on site (r, j) at time t; the variable a is defined as sensitivity of drivers; ρ_0 stands for the average density; $V(.)$ is the optimal velocity function. Here, t_0 is defined as the predictive

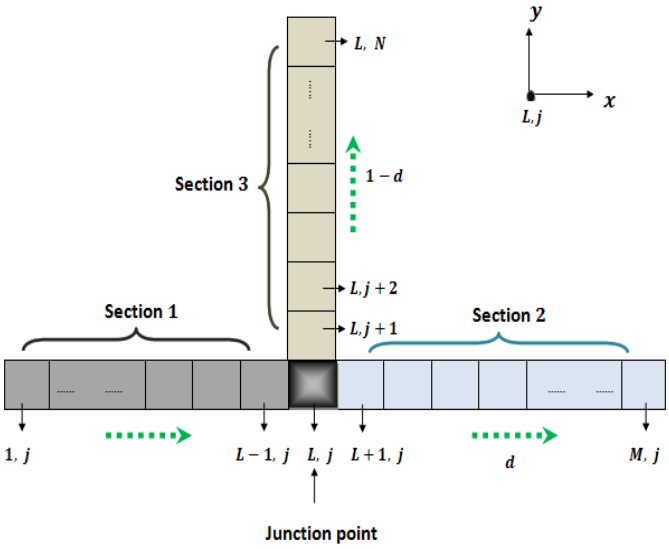

Figure 4.1: The schematic 2D lattice model of unidirectional traffic flow with the junction on the highway.

time. $\rho_{r+1,j}(t+t_0)$ depicts the predictive density at $(r+1,j)$ site at time $t+t_0$. The parameter $\beta(\beta \geq 0)$ denotes the coefficient for the predictive density variation. Using Taylor series approximation and retaining the first-order terms, the simplified version of the evolution equation (4.2) is

$$\partial_t q_{r,j}(t) = a\rho_0 V(\rho_{r+1,j}(t)) + a\beta t_0 \rho_0 \partial_t \rho_{r+1,j}(t) V'(\rho_{r+1,j}(t)) - a q_{r,j}(t). \tag{4.3}$$

Road section 2 **and road section** 3: In our proposed model, after crossing the junction point, some proportion of traffic from upstream sites may go straight (road section 2) or may turn left (road section 3). The intensity of traffic flow on road section 2 and 3 can differ from the intensity of traffic flow on road section 1. The traffic from section 1 will enter either the positive x-direction (section 2) or the positive y-direction (section 2). In order to incorporate and explain this phenomenon, let us consider a fraction parameter d, which signifies the proportion of traffic either in the positive x-direction or in the positive y-direction. The traffic conditions ahead in the next moment affect vehicular flow. If the downstream conditions are better in that direction, then the flow will also be maximum. After getting the prior information from ITS about ahead traffic conditions, drivers adjust their speed which helps to maximize the flow. To capture the above phenomenon, the

following model equations are used

$$\partial_t \rho^x_{r,j}(t) + d\rho_0(q^x_{r,j}(t) - q^x_{r-1,j}(t)) = 0, \tag{4.4}$$

$$\partial_t q^x_{r,j}(t) = ad\rho_0 V(\rho_{r+1,j}(t)) + ad\beta t_0 \rho_0 \partial_t \rho_{r+1,j}(t) V'(\rho_{r+1,j}(t)) - a q^x_{r,j}(t), \tag{4.5}$$

$$(r = L+1,\ L+2,\ L+3, ..., M;\ j = 1).$$

$$\partial_t \rho^y_{r,j}(t) + (1-d)\rho_0(q^y_{r,j}(t) - q^y_{r,j-1}(t)) = 0, \tag{4.6}$$

$$\partial_t q^y_{r,j}(t) = a(1-d)\rho_0 V(\rho_{r,j+1}(t)) + a(1-d)\beta t_0 \rho_0 \partial_t \rho_{r,j+1}(t) V'(\rho_{r,j+1}(t)) - a q^y_{r,j}(t), \tag{4.7}$$

$$(r = L;\ j = 2,\ 3,\ 4, ..., N).$$

Here, $\rho^x_{r,j}(t)$ ($\rho^y_{r,j}(t)$) and $q^x_{r,j}(t)$ ($q^y_{r,j}(t)$) represent the density and the flux in the x-direction (y-direction), respectively. Fraction parameter d ($(1-d)$) represents the traffic intensity in x-direction (y-direction). Eqs. (4.4) and (4.5) (Eqs. (4.6) and (4.7)) represent the continuity equation and the evolution equation, respectively, for the x-direction (y-direction).

Junction point: There is a linkage among the road section 1, section 2, and section 3. At the link point, the traffic flow will be affected by the flow in x-direction as well as in y-direction. On the other hand, if the drivers obtain information about the downstream situations, then it will be easy for them to choose the direction and modify the lane by going straight or turning left. The following two equations are used to explain the behavior of traffic at the junction point:

$$\partial_t \rho_{r,j}(t) + \rho_0(q_{r,j}(t) - q_{r-1,j}(t)) = 0, \tag{4.8}$$

$$\begin{aligned}\partial_t q_{r,j}(t) = {} & ad\rho_0 V(\rho_{r+1,j}(t)) + a(1-d)\rho_0 V(\rho_{r,j+1}(t)) + ad\beta t_0 \rho_0 \partial_t \rho_{r+1,j}(t) V'(\rho_{r+1,j}(t)) \\ & + a(1-d)\beta t_0 \rho_0 \partial_t \rho_{r,j+1}(t) V'(\rho_{r,j+1}(t)) - a q_{r,j}(t),\end{aligned} \tag{4.9}$$

where, the junction point is at $(r, j) = (L, 1)$.

Here, $V(.)$ is used for the optimal velocity function, and it is given as

$$V(\rho_{r,j}(t)) = \frac{v_{max}}{2}\Big[\tanh\Big(\frac{1}{\rho_{r,j}(t)} - \frac{1}{\rho_c}\Big) + \tanh\Big(\frac{1}{\rho_c}\Big)\Big], \tag{4.10}$$

v_{max} signifies maximal velocity and it is taken as 2.0; ρ_c indicates critical density.

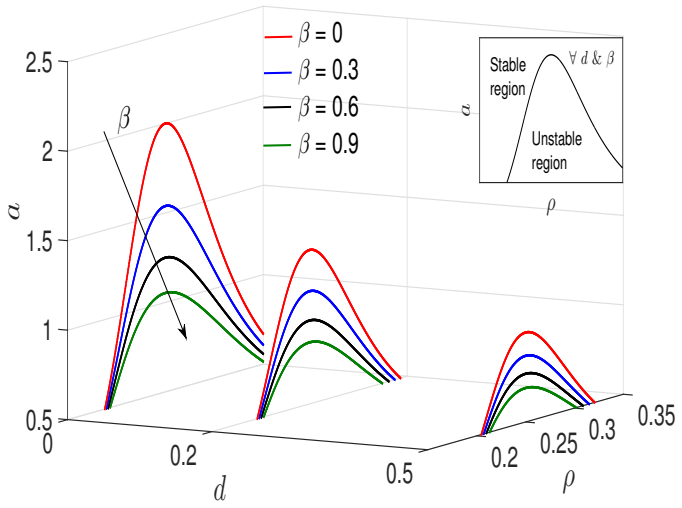

Figure 4.2: Phase plot in the plane (d, ρ, a) by taking prior information (β) into account with consideration of junction point of road through the use of the control method. The plotted lines represent the stability curves for different values of parameter $\beta = 0, 0.3, 0.6,$ and 0.9 with $t_0 = 0.5,\ \rho_c = \rho_0 = 0.25$.

4.2 Linear stability analysis

The stability condition is obtained by analyzing the model through control method. In a traffic flow system, it is assumed that the desired traffic density and flux have a steady-state solution, which is given below

$$[\rho_{r,j}, q_{r,j}]^T = [\rho_0, q_0]^T, \tag{4.11}$$

Then, around the steady-state for model equations of road sections 1, 2, and 3, we take an error system of the traffic flow network. The transforming equations of all road sections can be rewritten in the following way:

$$\partial_t \delta\rho_{r+1,j}(t) + d\rho_0(\delta q_{r+1,j}(t) - \delta q^x_{r,j}(t)) = 0, \tag{4.12}$$

$$\partial_t \delta\rho_{r,j+1}(t) + (1-d)\rho_0(\delta q_{r,j+1}(t) - \delta q^y_{r,j}(t)) = 0, \tag{4.13}$$

$$\begin{aligned}\partial_t \delta q_{r,j}(t) =& ad\rho_0 \delta\rho_{r+1,j}(t)\Lambda_{r+1,j} + a(1-d)\rho_0\delta\rho_{r,j+1}(t)\Lambda_{r,j+1} \\ &+ ad\rho_0\beta t_0 \partial_t\delta\rho_{r+1,j}(t)\Lambda_{r+1,j} + a(1-d)\rho_0\beta t_0\partial_t\delta\rho_{r,j+1}(t)\Lambda_{r,j+1} - a\delta q_{r,j}(t),\end{aligned} \tag{4.14}$$

where $q_{r,j}(t) = q^x_{r,j}(t) + q^y_{r,j}(t)$. Here, $\delta\rho_{r+1,j}(t) = \rho_{r+1,j}(t) - \rho_0$, $\delta q_{r+1,j}(t) = q_{r+1,j}(t) - q_0$, $\Lambda_{r+1,j} = \frac{\partial V(\rho_{r+1,j}(t))}{\partial \rho_{r+1,j}(t)}|_{\rho_{r+1,j}(t)=p_0}$, $\Lambda_{r,j+1} = \frac{\partial V(\rho_{r,j+1}(t))}{\partial \rho_{r,j+1}(t)}|_{\rho_{r,j+1}(t)=p_0}$, and $\Lambda_{r+1,j} = \Lambda = \Lambda_{r,j+1}$.

Apply the Laplace Transform on Eqs. (4.12) to (4.14), we get the following equations

$$sP_{r+1,j}(s) + d\rho_0(Q_{r+1,j}(s) - Q^x_{r,j}(s)) = 0, \tag{4.15}$$

$$sP_{r,j+1}(s) + (1-d)\rho_0(Q_{r,j+1}(s) - Q^y_{r,j}(s)) = 0, \tag{4.16}$$

$$\begin{aligned} sQ_{r,j}(s) =& ad\rho_0 P_{r+1,j}(s)\Lambda + a(1-d)\rho_0 P_{r,j+1}(s)\Lambda + ad\rho_0\beta t_0 sP_{r+1,j}(s)\Lambda \\ &+ a(1-d)\rho_0\beta t_0 sP_{r,j+1}(s)\Lambda - aQ_{r,j}(s). \end{aligned} \tag{4.17}$$

Where $L(\rho_{r+1,j}(t)) = P_{r+1,j}(s)$, $L(q_{r+1,j}(t)) = Q_{r+1,j}(s)$, $L(.)$ represents the Laplace Transformation where $s = i\omega$ denotes the complex variable.
Abolishing the densities $P_{r+1,j}(s)$ and $P_{r,j+1}(s)$ from Eqs. (4.15) to (4.17), Eq. (4.18) appears for the flux:

$$Q_{r,j}(s) = \frac{-a\rho_0^2\Lambda(1+s\beta t_0)}{D(s)}[d^2 Q_{r+1,j}(s) + (1-d)^2 Q_{r,j+1}(s)], \tag{4.18}$$

where $D(s) = s^2 + as - a\rho_0^2\Lambda(1+\beta t_0 s)(d^2 + (1-d)^2)$ is the characteristic polynomial. The transfer function matrix is given as follows

$$G(s) = \frac{-a\rho_0^2\Lambda(1+s\beta t_0)}{D(s)}[d^2 \quad (1-d)^2]. \tag{4.19}$$

According to the control method's stability rule, a traffic jam can never occur in the traffic system if the two conditions mentioned below are met:

1. The characteristic polynomial $D(s)$ is stable.

2. The H_∞ norm of the transfer function $G(s)$ is less than or equal to 1, i.e.,

$$||G(s)||_\infty = \sup_{w\in[0,+\infty)} |G(i\omega)| \leq 1.$$

Based on the criterion of Hurwitz stability, the first condition is satisfied if $D(s)$ has all the coefficients of the same sign. It is clear that the characteristics polynomial is stable according to the Hurwitz stability rule. Now, considering $||G(s)||_\infty \leq 1$ in order to fulfill the second condition, that is

$$\begin{aligned} |G(i\omega)|^2 =& |G(i\omega)G(-i\omega)| \\ =& \frac{(a\rho_0^2\Lambda)^2(1+\beta^2 t_0^2\omega^2)(d^2+(1-d)^2)^2}{[\omega^2 + a\rho_0^2\Lambda(d^2+(1-d)^2)]^2 + [a - a\rho_0^2\Lambda\beta t_0(d^2+(1-d)^2)]^2\omega^2} \\ &\leq 1, \quad \omega \in [0,+\infty). \end{aligned} \tag{4.20}$$

The sufficient condition for stability is rewritten as

$$\omega^2[\omega^2 + a^2(1 - 2\rho_0^2\Lambda\beta t_0(d^2 + (1-d)^2)) + 2a\rho_0^2\Lambda(d^2 + (1-d)^2)] \geq 0, \quad \omega \in [0, +\infty). \tag{4.21}$$

The following criterion should be fulfilled in order to ensure that Eq. (4.21) holds

$$a^2(1 - 2\rho_0^2\Lambda\beta t_0(d^2 + (1-d)^2)) + 2a\rho_0^2\Lambda(d^2 + (1-d)^2) \geq 0. \tag{4.22}$$

Therefore, the stability condition is achieved with the consideration of predictive effect with junction point:

$$a \geq \frac{-2\rho_0^2\Lambda(d^2 + (1-d)^2)}{(1 - 2\rho_0^2\Lambda\beta t_0(d^2 + (1-d)^2))}. \tag{4.23}$$

Fig. 4.2 displays the phase plot in the plane (d, ρ, a), which represents the relationship between the prior information (β) and the fraction parameter (d). Clearly from Eq. (4.23), the stability condition is influenced by β, t_0, and d. Here, the predictive time t_0 is considered constant and is taken as $t_0 = 0.5$. The area below the neutral stability curves is unstable, whereas the area above the neutral stability curves is stable. The prior information plays a significant role in the traffic flow stability by taking junction point into account, as shown in Fig. 4.2. The plotted lines depict the stability curves for distinct values of β in plane (d, ρ, a). When $d = 0$, that means all vehicles turn left at the junction point, and no vehicles move straight. For $d = 0$, we get stability curves for distinct values of $\beta(\beta = 0,\ 0.3,\ 0.6,\ 0.9)$. The peak of curves obtained from various values of β decreases as β increases. For $d \neq 0$ and $d \neq 1$, i.e., cars enter downstream lanes in different directions with different probabilities. It is seen that when the prior information is taken, i.e., with an increased value of β, the curves lower down, corresponding to the different values of d, resulting in a high rate of stability of traffic flow. It is found from Fig. 4.2 that the stable area is enhanced whenever β and d increases ($0 \leq d \leq 0.5$), which depicts that the predictive effect has a positive impact on traffic dynamics with consideration of junction road in 2D traffic network. The results demonstrate that the prior information is beneficial to diminish traffic congestion in the 2D lattice model with a junction point.

4.3 Stability analysis with control signal

In this section, the control signal is incorporated into 2D lattice model by considering the effect of the prior information with junction on the road. Let us apply a control signal

term to model equations; we get

$$\partial_t \rho_{r+1,j}(t) + d\rho_0(q_{r+1,j}(t) - q^x_{r,j}(t)) = 0, \tag{4.24}$$

$$\partial_t \rho_{r,j+1}(t) + (1-d)\rho_0(q_{r,j+1}(t) - q^y_{r,j}(t)) = 0, \tag{4.25}$$

$$\begin{aligned}\partial_t q_{r,j}(t) =& ad\rho_0 V(\rho_{r+1,j}(t)) + a(1-d)\rho_0 V(\rho_{r,j+1}(t)) + ad\beta t_0 \rho_0 \partial_t \rho_{r+1,j}(t) V'(\rho_{r+1,j}(t)) \\ &+ a(1-d)\beta t_0 \rho_0 \partial_t \rho_{r,j+1}(t) V'(\rho_{r,j+1}(t)) - a q_{r,j}(t) + U_{r,j}(t),\end{aligned} \tag{4.26}$$

where the control signal $U_{r,j}(t)$ represents the flow difference between the target lattice site and its following lattice site, is

$$U_{r,j}(t) = \xi d(q_{r+1,j}(t) - q^x_{r,j}(t)) + \kappa(1-d)(q_{r,j+1}(t) - q^y_{r,j}(t)). \tag{4.27}$$

Here ξ denotes the feedback gain of the flux difference between (r, j) and $(r+1, j)$ lattice sites at time t, and κ is another feedback gain of the flux difference between (r, j) and $(r, j+1)$ lattice sites at time t. It is assumed that the desired traffic density and flux have a steady state solution which is the same as given in Eq. (4.11). Thus, the traffic dynamics model can be formulated around a steady state with a control signal defined by Eq. (4.27) as

$$\partial_t \delta\rho_{r+1,j}(t) + d\rho_0(\delta q_{r+1,j}(t) - \delta q^x_{r,j}(t)) = 0, \tag{4.28}$$

$$\partial_t \delta\rho_{r,j+1}(t) + (1-d)\rho_0(\delta q_{r,j+1}(t) - \delta q^y_{r,j}(t)) = 0, \tag{4.29}$$

$$\begin{aligned}\partial_t \delta q_{r,j}(t) =& ad\rho_0 \delta\rho_{r+1,j}(t)\Lambda_{r+1,j} + a(1-d)\rho_0 \delta\rho_{r,j+1}(t)\Lambda_{r,j+1} + ad\rho_0\beta t_0 \partial_t \delta\rho_{r+1,j}(t)\Lambda_{i+1,j} \\ &+ a(1-d)\rho_0\beta t_0 \partial_t \delta\rho_{r,j+1}(t)\Lambda_{r,j+1} - a\delta q_{r,j}(t) + \xi d(\delta q_{r+1,j} - \delta q^x_{r,j}) \\ &+ \kappa(1-d)(\delta q_{r,j+1} - \delta q^y_{r,j}).\end{aligned} \tag{4.30}$$

After applying the Laplace Transform, we obtain

$$sP_{r+1,j}(s) + d\rho_0(Q_{r+1,j}(s) - Q^x_{r,j}(s)) = 0, \tag{4.31}$$

$$sP_{r,j+1}(s) + (1-d)\rho_0(Q_{r,j+1}(s) - Q^y_{r,j}(s)) = 0, \tag{4.32}$$

$$\begin{aligned}sQ_{r,j}(s) =& ad\rho_0 P_{r+1,j}(s)\Lambda + a(1-d)\rho_0 P_{r,j+1}(s)\Lambda + ad\rho_0\beta t_0 sP_{r+1,j}(s)\Lambda \\ &+ a(1-d)\rho_0\beta t_0 sP_{r,j+1}(s)\Lambda - aQ_{r,j}(s) + \xi d(Q_{r+1,j}(s) - Q^x_{r,j}(s)) \\ &+ \kappa(1-d)(Q_{r,j+1}(s) - Q^y_{r,j}(s)).\end{aligned} \tag{4.33}$$

Where $L(\rho_{r+1,j}(t)) = P_{r+1,j}(s)$, $L(q_{r+1,j}(t)) = Q_{r+1,j}(s)$, $L(.)$ denotes the Laplace Transformation where $s = i\omega$ indicates the complex variable.
After abolishing the densities $P_{r+1,j}(s)$ and $P_{r,j+1}(s)$ from Eqs. (4.31) to (4.33), the fol-

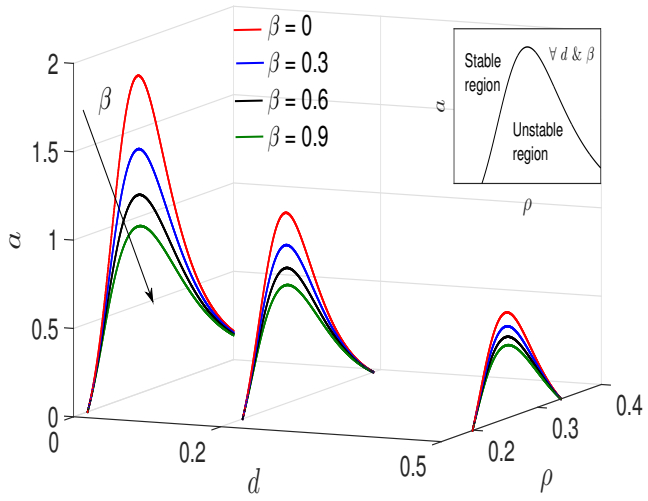

Figure 4.3: Phase plot in the plane (d, ρ, a) by taking prior information (β) into account with consideration of junction point through the use of the control method with a control signal. The plotted lines represent the stability curves with the control method for different values of parameter $\beta = 0, 0.3, 0.6,$ and 0.9, $t_0 = 0.5$, $\rho_c = \rho_0 = 0.25$, $\xi = 0.3$, and $\kappa = 0.1$.

lowing equation appears for the flux:

$$\begin{aligned} Q_{r,j}(s) =& \frac{1}{D^*(s)}[(\xi ds - a\rho_0^2\Lambda(1+s\beta t_0)d^2)Q_{r+1,j}(s) \\ &+ (\kappa(1-d)s - a\rho_0^2\Lambda(1+s\beta t_0)(1-d)^2)Q_{r,j+1}(s)], \end{aligned} \tag{4.34}$$

where $D^*(s) = s^2 + as - a\rho_0^2\Lambda(1+\beta t_0 s)(d^2+(1-d)^2) + (\xi d + \kappa(1-d))s$ is the characteristic polynomial. The transfer function matrix is given as follows:

$$G^*(s) = \frac{1}{D^*(s)}[(\xi ds - a\rho_0^2\Lambda(1+s\beta t_0)d^2) \quad (\kappa(1-d)s - a\rho_0^2\Lambda(1+s\beta t_0)(1-d)^2)]. \tag{4.35}$$

According to the control method's stability rule, a traffic jam can never occur in the traffic system if the two conditions are satisfied: (i) The characteristic polynomial $D^*(s)$ is stable, and (ii) The H_∞ norm of the transfer function $G^*(s)$ is less than or equal to 1. Based on the criterion of Hurwitz stability and known conditions, $D^*(s)$ is stable. Then, considering $||G^*(s)||_\infty \leq 1$ and can be written in the following equation

$$|G^*(i\omega)|^2 = |G^*(i\omega)G^*(-i\omega)| \leq 1, \qquad \omega \in [0, +\infty). \tag{4.36}$$

The sufficient condition for stability is rewritten as

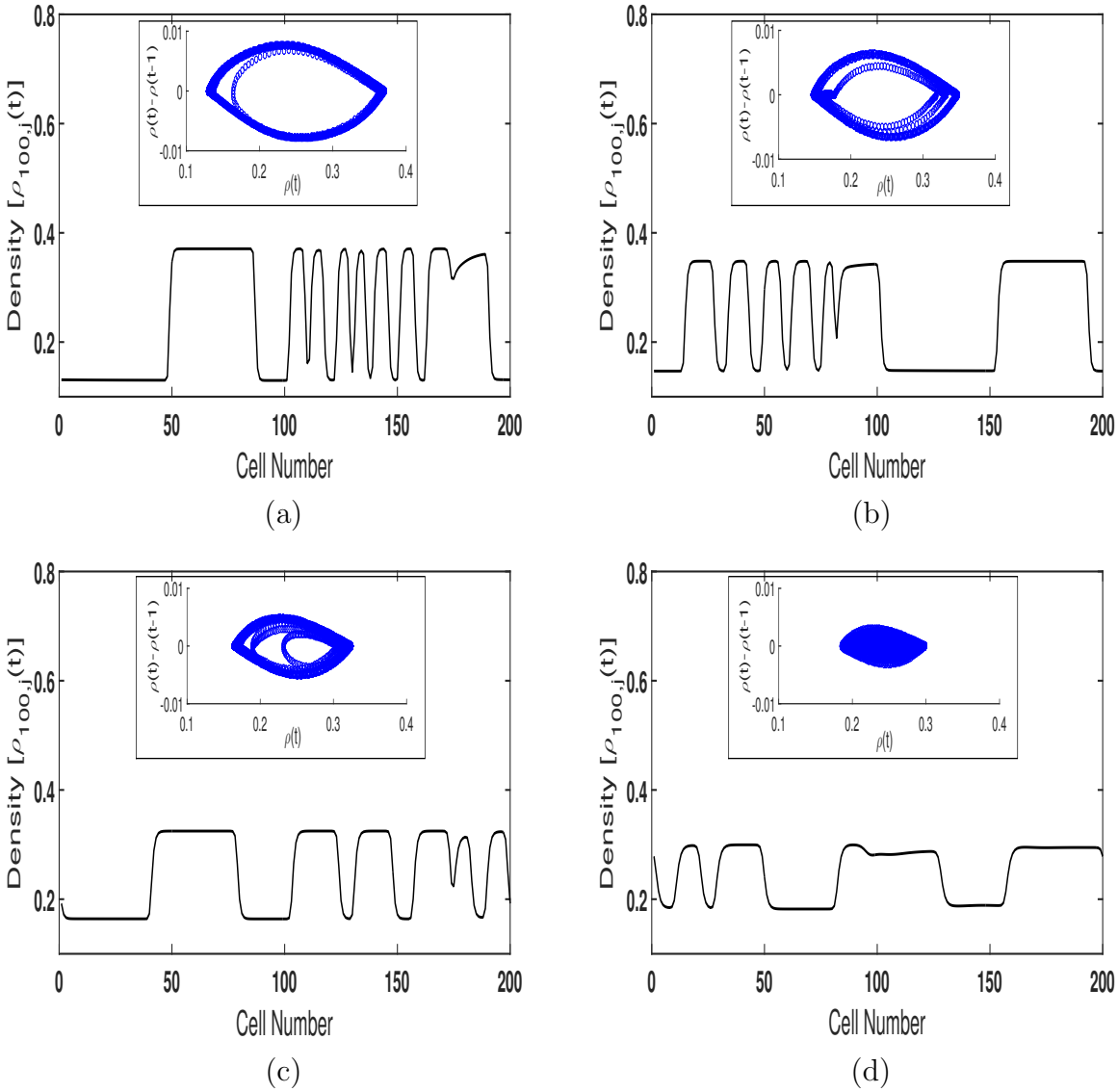

Figure 4.4: Density profiles at time $t = 10300s$ with $d = 0$, $a = 0.9$ for (a) $\beta = 0$, (b) $\beta = 0.3$, (c) $\beta = 0.6$, and (d) $\beta = 0.9$, respectively, in positive y-direction ($r = 100$). The inset profiles are drawn for density difference ($\rho(t) - \rho(t-1)$) versus density ($\rho(t)$).

$$\omega^2[\omega^2 + a^2(1 - 2\rho_0^2\Lambda\beta t_0(d^2 + (1-d)^2)) + 2a(\rho_0^2\Lambda(d^2 + (1-d)^2) + \xi d + \kappa(1-d))] \geq 0, \quad \omega \in [0, +\infty). \tag{4.37}$$

The following criterion should be fulfilled in order to ensure that Eq. (4.37) holds

$$a^2(1 - 2\rho_0^2\Lambda\beta t_0(d^2 + (1-d)^2)) + 2a(\rho_0^2\Lambda(d^2 + (1-d)^2) + \xi d + \kappa(1-d)) \geq 0. \tag{4.38}$$

Therefore, the stability condition is achieved with the consideration of predictive effect for junction in 2D model with control signal is:

$$a \geq \frac{-2\rho_0^2\Lambda(d^2 + (1-d)^2) - 2(\xi d + \kappa(1-d))}{(1 - 2\rho_0^2\Lambda\beta t_0(d^2 + (1-d)^2))}. \tag{4.39}$$

Fig. 4.3 depicts the phase plot in the plane (d, ρ, a) for 2D lattice model with consideration of the prior information for the junction road by using stability analysis with the control signal. The prior information plays an important role in the traffic flow stability with the junction, as shown in Fig. 4.3. The plotted lines show the stability curves for distinct values of β in plane (d, ρ, a) with $t_0 = 0.5$, $\xi = 0.3$, and $\kappa = 0.1$. We can see from Fig. 4.3 that the stability region is less when having less information about the ahead traffic conditions. But whenever we receive more information, the stable area also increases continuously. Through direct observation, by comparing Figs. 4.2 and 4.3, it is observed that the stable region with a control signal is greater than that without a control signal for the same values of the β and d. It is found from Fig. 4.3 that the stable area is enlarged whenever β and d increases ($0 \leq d \leq 0.5$) with the control signal, which depicts that the predictive effect has a positive impact on traffic dynamics with junction in 2D traffic system. This demonstrates that both factors are beneficial to minimize the traffic congestion in the 2D lattice model.

4.4 Results discussion

To check the capability of the proposed lattice model with the consideration of prior information as well as traffic diversion at junction node, numerical simulation is performed. The periodic boundary conditions are applied. As shown in Fig. 4.1, there are $M = 350$ nodes in x direction and $N = 200$ nodes in y direction. The density at the initial stage along the connecting roads to the junction point is assumed to be uniformly distributed: $\rho_{r,j}(0) = \rho_{r,j}(1) = \rho_0 = \rho_c = 0.25$; Δt is the unit time step, and it is taken as 0.1. The traffic flow diversion occurs at the node $(r = L, j = 1)$ with $L = 100$. The local density at site $(100, 1)$ is set as 0.35 to analyze a local disruption caused by a particular driver's

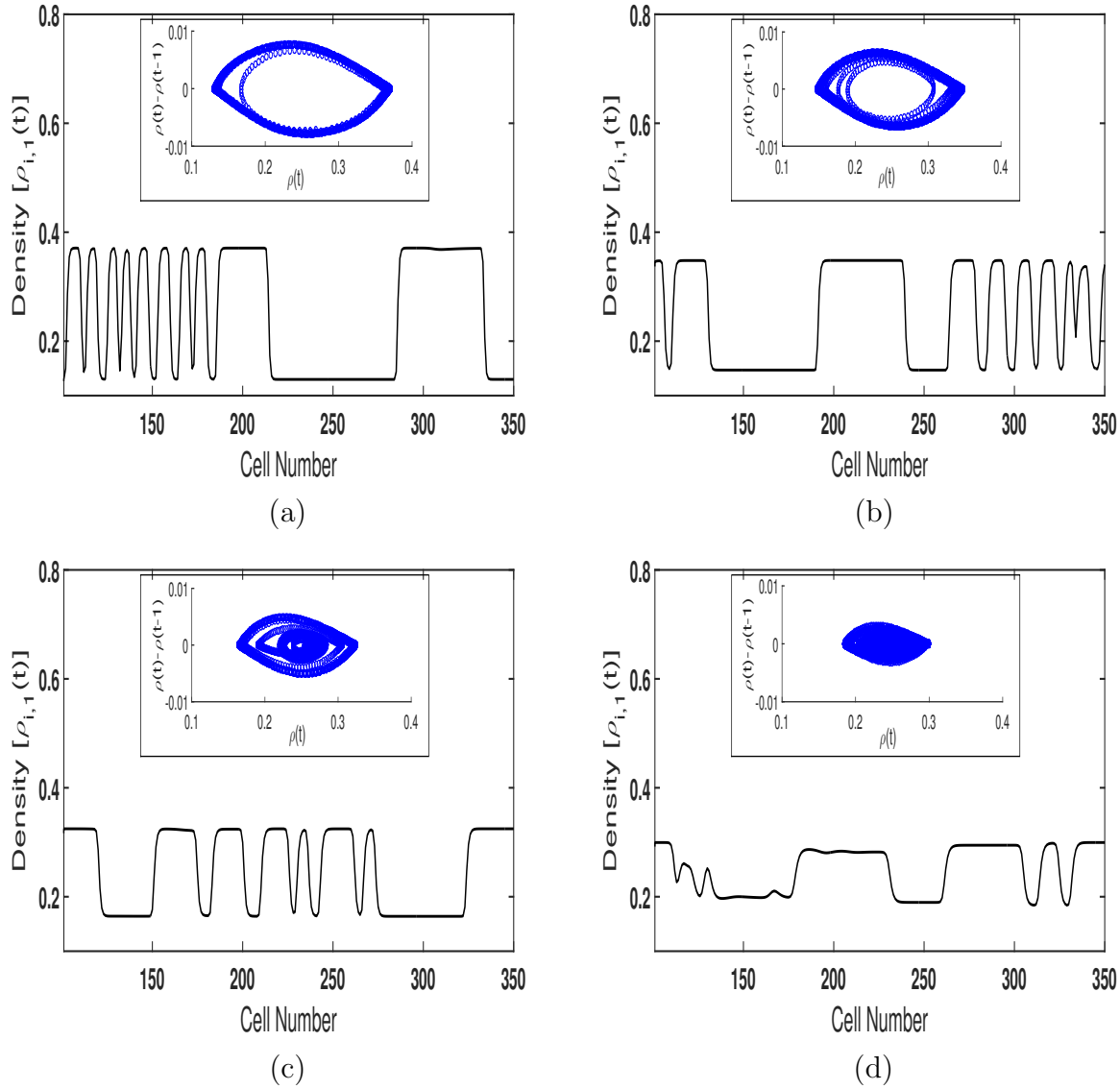

Figure 4.5: Density profiles at time $t = 10300s$ with $d = 1.0$, $a = 0.9$ for (a) $\beta = 0$, (b) $\beta = 0.3$, (c) $\beta = 0.6$, and (d) $\beta = 0.9$, respectively, in positive x-direction ($j = 1$). The inset profiles are drawn for density difference ($\rho(t) - \rho(t-1)$) versus density ($\rho(t)$).

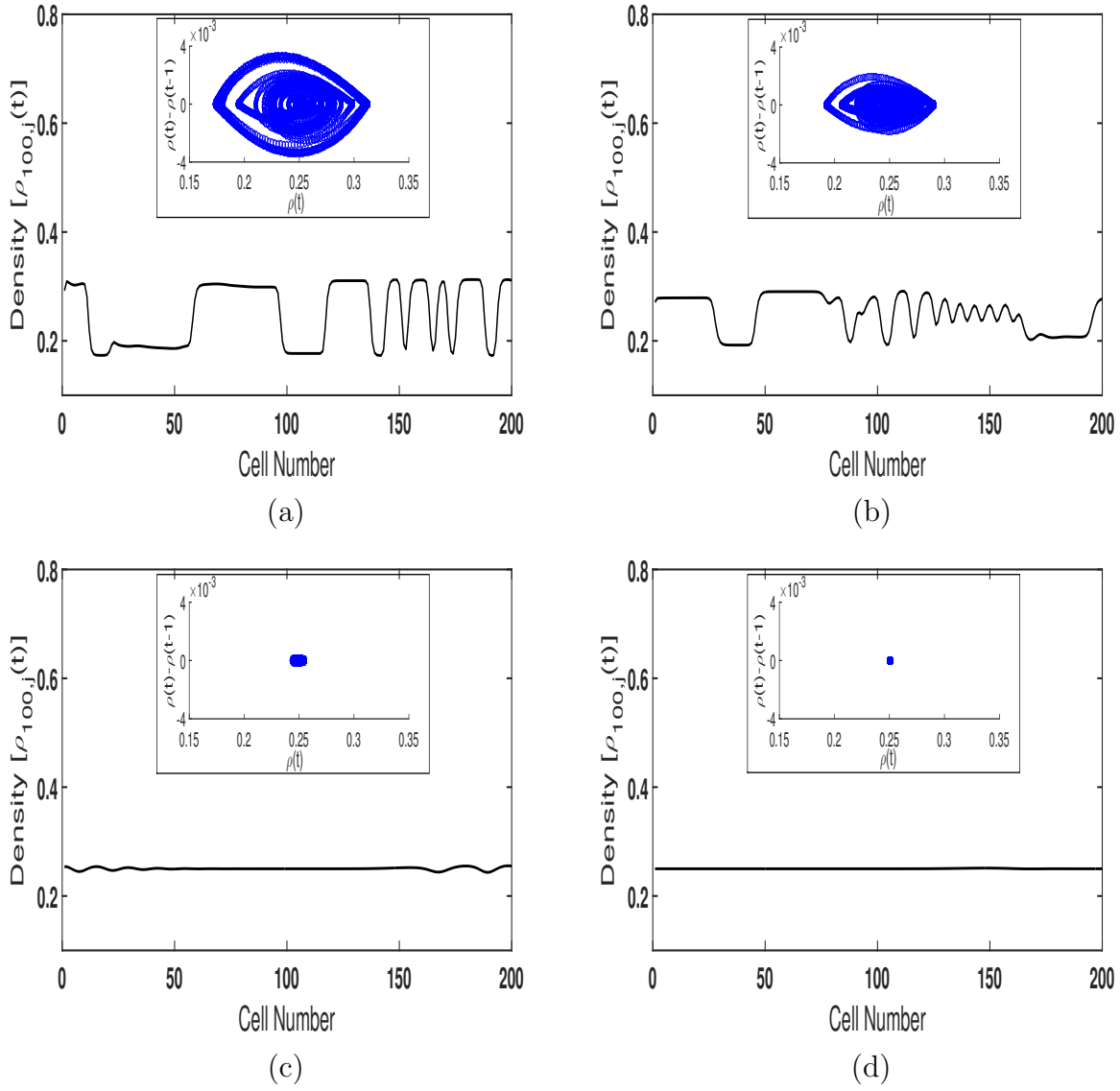

Figure 4.6: Density profiles at time $t = 10300s$ with $d = 0.2$, $a = 0.9$ for (a) $\beta = 0$, (b) $\beta = 0.3$, (c) $\beta = 0.6$, and (d) $\beta = 0.9$, respectively, in positive y-direction ($r = 100$). The inset profiles are drawn for density difference ($\rho(t) - \rho(t-1)$) versus density ($\rho(t)$).

delay in turning at the junction point, i.e., $\rho_{100,1}(0) = \rho_{100,1}(1) = 0.35$. In the following simulations, to validate theoretical findings and to check the influence of the parameters on the stability of traffic flow in the 2D vehicular system, the variations in the values of the β and d are analyzed.

The variations in the density profiles by taking different values of β in positive x-direction with traffic intensity d (where $j = 1$) and in positive y-direction with traffic intensity $(1-d)$ (where $r = 100$) are displayed in Figs. 4.4 - 4.7 without control signal. The parameter β is the coefficient of the prior information. The value of $\beta = 0$ indicates that there is no prior information, whereas $\beta > 0$ means that estimated information of the ahead traffic conditions in the next moment receive.

In Fig. 4.4, the results are shown for $d = 0$, which means no vehicles move straight ahead, and all vehicles turn left at the junction by taking different values of β ($\beta = 0, 0.3, 0.6, 0.9$). The traffic is always stable in x-direction as no vehicles go ahead. So, Fig. 4.4 represents the results only for y-direction. Similarly, for $d = 1$, all traffic moves straight ahead without turning at a junction with the prior information's consideration. The traffic is not affected and always stable in the y-direction as there is no disruption in the y-direction. Therefore, the results are shown only for x-direction in Fig. 4.5. In Fig. 4.4 and Fig. 4.5, the fluctuations occur in the density curves, and it is observed that with an increased value of β, the amplitude of these curves decreases, i.e., having more information about downstream traffic conditions helps maximize traffic flow.

Fig. 4.6 and Fig. 4.7 show the density curves for the values of $d = 0.2$ and $d = 0.8$, respectively, for distinct values of β. $d = 0.2$ means 20% traffic travel straight-ahead in x-direction, and the remaining 80% traffic turns left in y-direction from the junction. There will be a stable situation in the x-direction as only 20% of traffic goes in that direction. So, the results are displayed only for y-direction, as shown in Fig. 4.6. For $d = 0.8$, indicating that 80% traffic moves straight ahead and the turning proportion of the traffic is 20%. There are fewer vehicles traveling in the y-direction and will almost stable situation in that direction. So, for $d = 0.8$ in Fig. 4.7, the results are plotted only for the x-direction. It is found that the fluctuations of the density curves reduce with a rise in values of β, indicating that the stability of traffic flow becomes better, especially for a higher value of β. With a large value of β, it models the more prior information of the downstream traffic conditions. For $d = 0.5$, that means half (50%) traffic goes straight ahead, and half (50%) traffic turns to the left. For $d = 0.5$, the traffic will always be stable for all the values of β as the stability condition is satisfied. Therefore, results are not shown for $d = 0.5$. From the density profiles (Figs. 4.4 - 4.7), it is found that the stability of traffic flow enhances whenever β increases, i.e., the disruption in the straight-ahead direction (x-direction) and

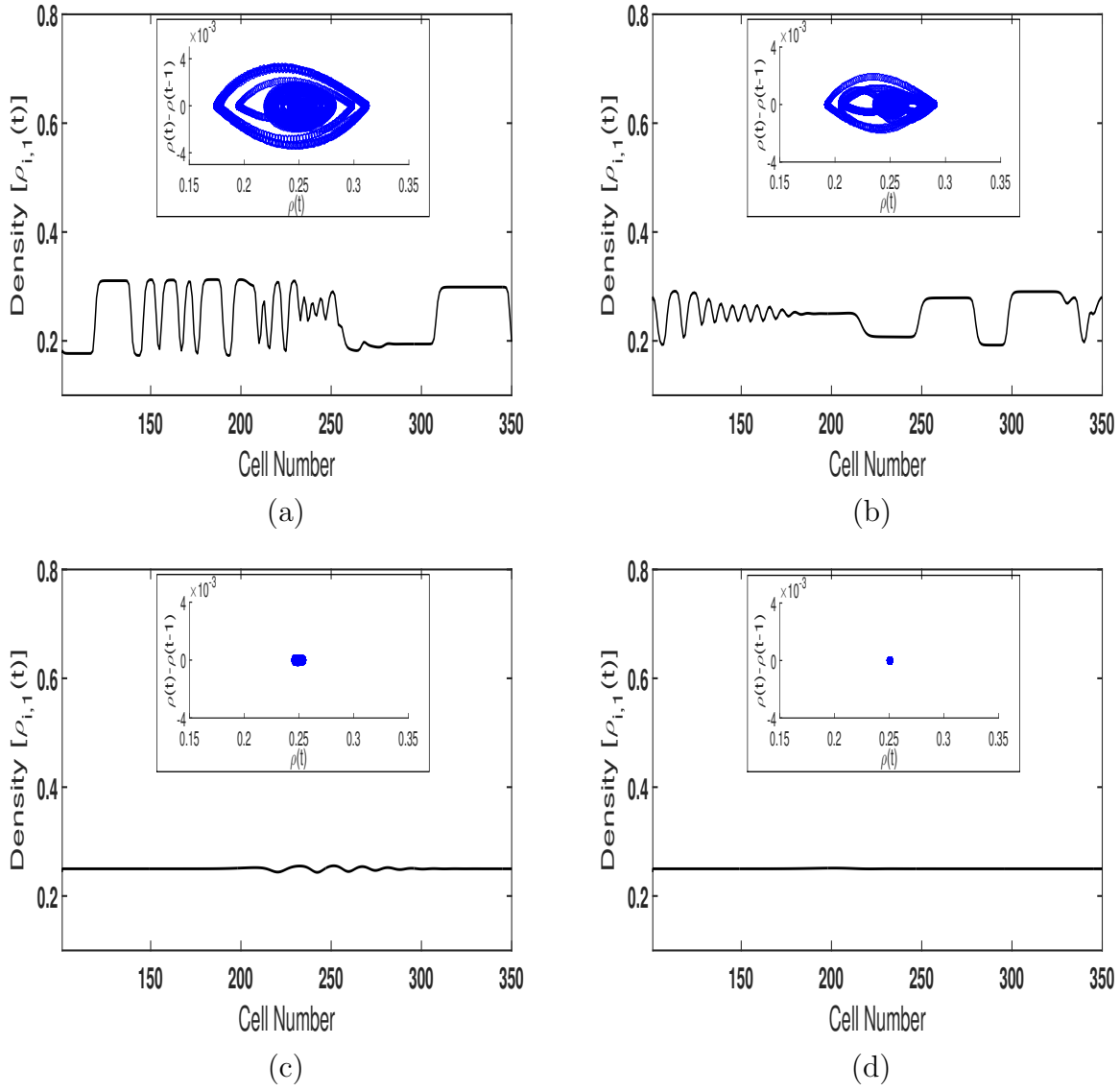

Figure 4.7: Density profiles at time $t = 10300s$ with $d = 0.8$, $a = 0.9$ for (a) $\beta = 0$, (b) $\beta = 0.3$, (c) $\beta = 0.6$, and (d) $\beta = 0.9$, respectively, in positive x-direction ($j = 1$). The inset profiles are drawn for density difference ($\rho(t) - \rho(t-1)$) versus density ($\rho(t)$).

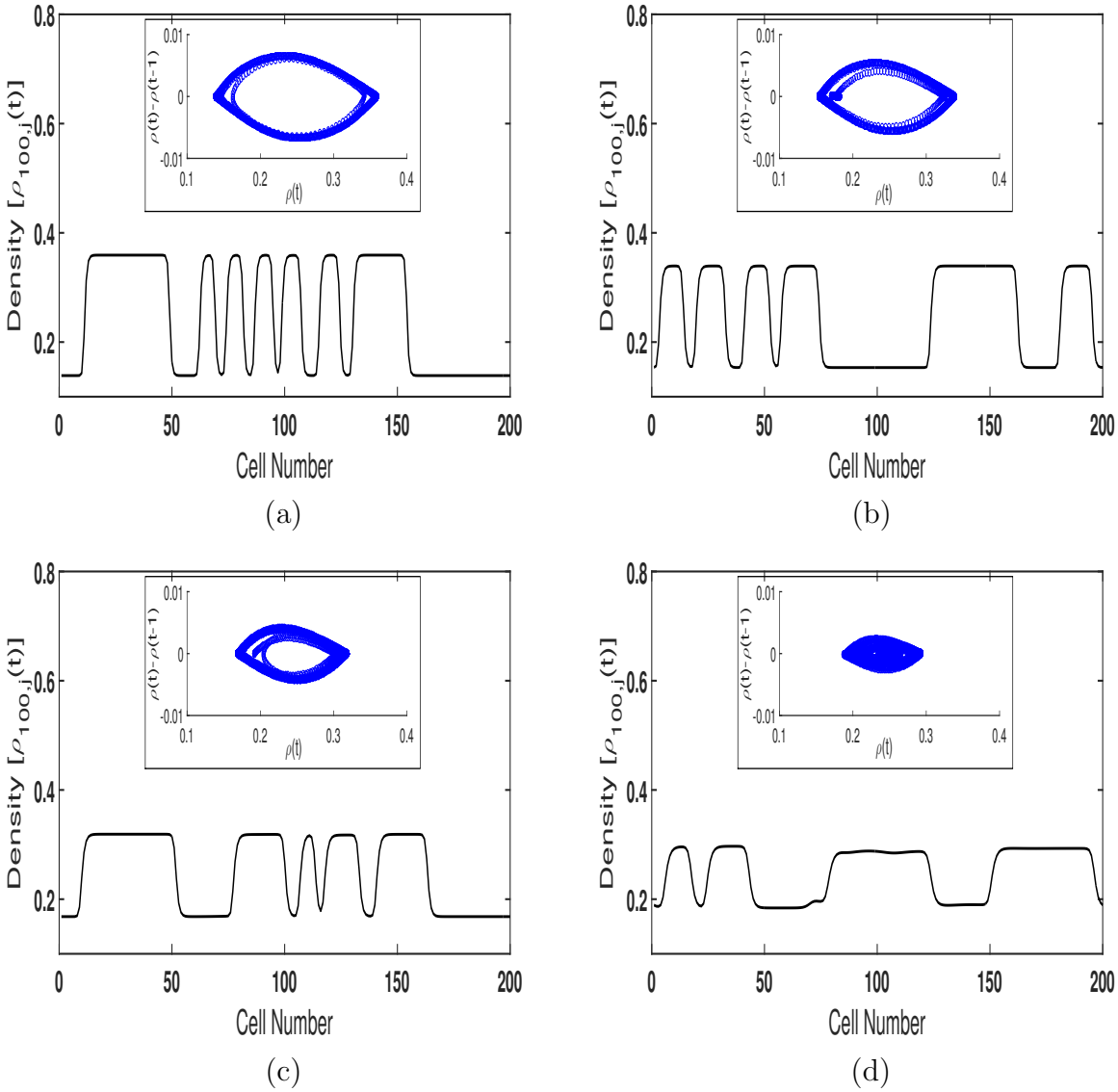

Figure 4.8: Density profiles at time $t = 10300s$ with $d = 0$, $a = 0.8$ for (a) $\beta = 0$, (b) $\beta = 0.3$, (c) $\beta = 0.6$, and (d) $\beta = 0.9$, respectively, in positive y-direction ($r = 100$). The inset profiles are drawn for density difference ($\rho(t) - \rho(t-1)$) versus density ($\rho(t)$).

left-turning direction (y-direction) will decrease if more prior information of downstream traffic conditions is received.

The phase plots are drawn for density difference ($\rho(t) - \rho(t-1)$) versus density ($\rho(t)$) to ensure the periodic behavior of traffic flow, in the inset of Figs. 4.4 - 4.7, for $t = 5000 - 10300s$. In the inset of Figs. 4.4 - 4.5, the limit cycle is shown generated by a set of dispersed points demonstrate the periodic behavior of traffic. The right and the left end points in the loop describe the jammed state of traffic and the free flow traffic, respectively. It is observed that with an increase in the value of β, the area of the loop begins to diminish. In the inset of Fig. 4.6 and Fig. 4.7, for the smaller values of β, the closed loop is formed by the collection of dispersed points that describes the periodic behavior of traffic. The region of the loop decreases whenever the value of β increases, eventually transforming into a solitary point for a higher value of β, as displayed in Fig. 4.6(d) and Fig. 4.7(d). It is observed from the results that prior information has a positive impact on the traffic network.

In Fig. 4.8 and Fig. 4.9, the results are displayed for $d = 0$ and $d = 0.2$, respectively, by considering different values of β ($\beta = 0, 0.3, 0.6, 0.9$) when control signal is considered. For $d = 0$, the traffic is always stable in x-direction as no vehicles move straight. So, Fig. 4.8 represents the results only for y-direction as all vehicles turn left at the junction. In Fig. 4.8, the fluctuations arise inside the density curves. It is found that with an elevated value of β, the amplitude of density curves decreases, i.e., the stability of traffic flow improves. For $d = 0.2$, there will be a stable situation in the x-direction since 20% of traffic goes in this direction. So, in Fig. 4.9, the results are drawn only for y-direction since 80% traffic turns left in this direction from the junction. It is seen that the fluctuations in the density curves decrease with increasing β values, i.e., having a lot of info regarding downstream traffic conditions helps maximize the traffic flow.

The phase plots are plotted for density difference ($\rho(t) - \rho(t-1)$) versus density ($\rho(t)$), in the inset of Figs. 4.8 - 4.9, for $t = 5000 - 10300s$. In the inset of Fig. 4.8, the limit cycle is shown as generated by a set of dispersed points demonstrating the periodic behavior of traffic. The right and the left endpoints in the loop describe the jammed state of traffic and the free-flow traffic, respectively. It is observed that with a rise in the value of β, the area of the loop starts decreasing in size. In the inset of Fig. 4.9, for the smaller values of β, the closed loop is formed by the collection of spread points that describes the periodic behavior of traffic. The loop area decreases every time the β goes up and eventually turns into a solitary point for a higher β, as displayed in Fig. 4.9(d). It is seen that prior information positively affects traffic dynamics.

Here, after observing all the simulation results, we found that they all are in good agreement

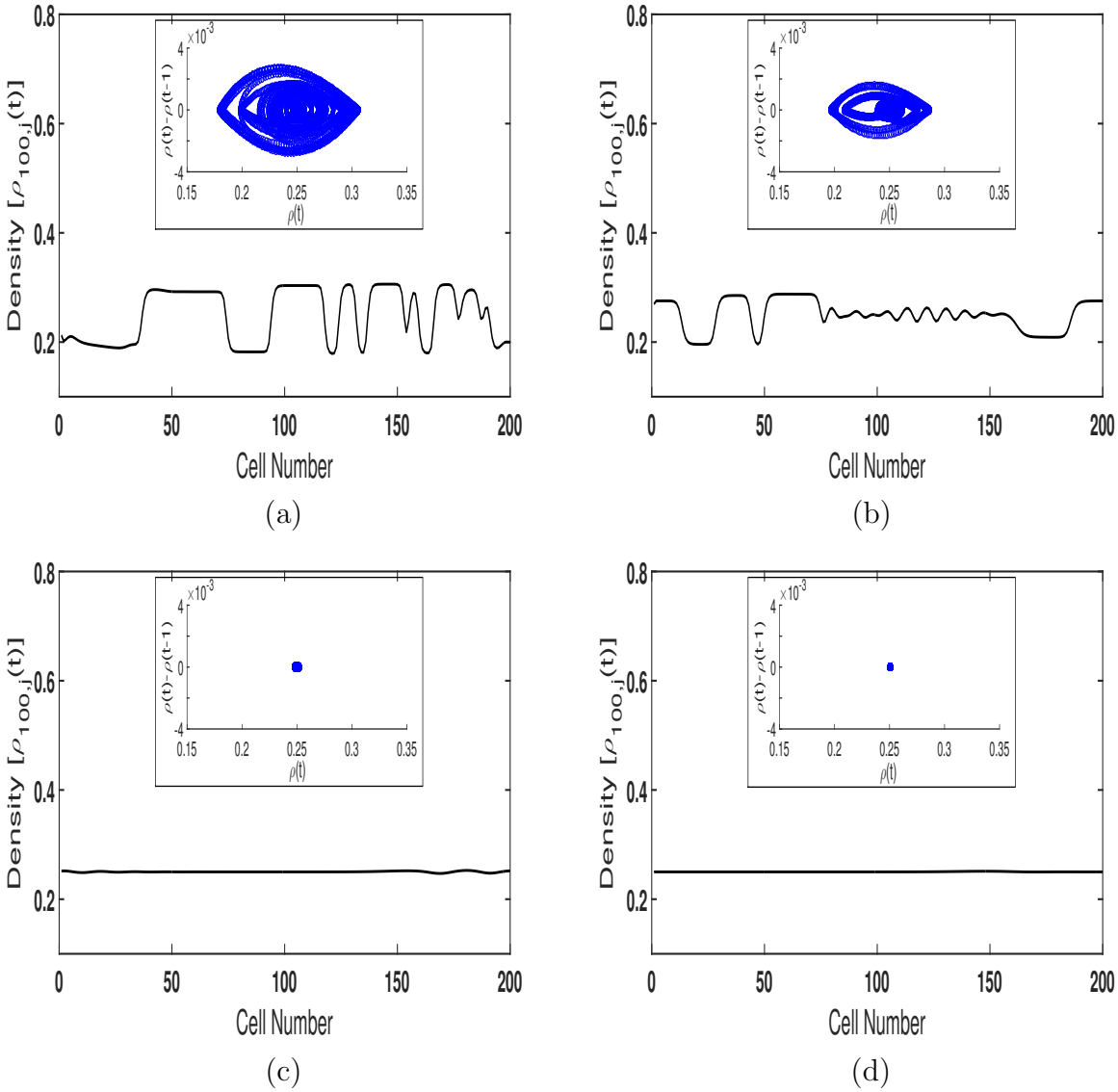

Figure 4.9: Density profiles at time $t = 10300s$ with $d = 0.2$, $a = 0.8$ for (a) $\beta = 0$, (b) $\beta = 0.3$, (c) $\beta = 0.6$, and (d) $\beta = 0.9$, respectively, in positive y-direction ($r = 100$). The inset profiles are drawn for density difference ($\rho(t) - \rho(t-1)$) versus density ($\rho(t)$).

with the theoretical predictions. Thus, we can conclude that traffic flow stability improves by taking the prior information (predictive effect) into account with the junction point in the 2D lattice model. It also confirms the features of real traffic situations as well.

4.5 Conclusion

4.5.1 Outcomes:

- A two-dimensional (2D) lattice model is proposed by incorporating the effect of the prior information (predictive effect) with the junction road to portray the traffic features on the road network.
- Considering the predictive effect, the behavior of traffic flow is investigated theoretically using the control method for linear stability analysis.
- From the junction, traffic diverges in various directions, which is related to the actual traffic condition. When drivers receive advanced knowledge of downstream traffic conditions, the traffic flow stability improves, as seen by the results.
- The stability condition is revised when the control signal is applied in the proposed lattice model. The parameter β is found to play an important role in traffic flow stability and to suppress traffic congestion in all directions for 2D traffic dynamics.
- To test the reliability of theoretical findings, numerical simulations are carried out.
- By observing the results of both the theoretical analysis and the numerical simulations, it is found that the prior information is beneficial to transportation networks with junction roads. The findings in this study can assist readers in better comprehending the complex phenomenon of traffic flow.

4.5.2 Future scope:

- Although the proposed model considers the prior information for two diverted lanes (road section 2 and 3) in a 2D unidirectional traffic system yet various factors influencing the traffic dynamics, such as driver's behavior [112,120,123,160], anticipation effect [94,95,118], etc. can be incorporated to make it directly applicable in a real scenario.
- Moreover, the proposed work can also be extended to incorporate the merging/diverging of lanes in a multi-lane system.

Chapter 5

Effects of uncertainty about historical information on traffic dynamics

Traffic congestion is increasingly high in the transportation network. Traffic jams waste a lot of money and time for the people who travel from one place to another by vehicle. However, the transportation network is a complex structure. Many factors involved in traffic dynamics affect traffic flow, including the driver's psychological tendency, weather information, road construction, serious road accidents, etc. In addition, if the management of the transport system will not be improved, congestion will likely worsen over the next few decades as travel demand continues to increase. Therefore, various traffic flow models such as car-following and continuum models [49,59,134,140,145] exist to understand the dynamics of the vehicular network. Moreover, the lattice models [83,86,87,91,92,119] have become famous in the last few decades because of their simplicity.

However, due to psychological uncertainty and unpredictable features of human behavior, car-following models have long struggled to precisely and objectively reflect drivers' behavior. Therefore, to better explain the uncertainty effect in car-following models, Zhang et al. [137] proposed a car-following model to describe the driving system involving the uncertainty about velocity and proved that the uncertainty of the vehicle's speed has a significant impact on traffic flow stability. Further, Wang et al. [167] extended the heterogeneous car-following model by considering the drivers' different psychological headways and concluded that when the psychological headway is larger, it leads to more stability at lower traffic densities and more instability at higher traffic densities. In addition, An et al. [139] proposed a new car-following model that considers driver characteristics on complex roadways, with factors such as experienced attribution, inexperienced attribution, and driver perception headway error. Moreover, the car-following model was extended by Li et al. [141] considering two factors, the driver's desire for smooth driving and self-stabilizing control with velocity uncertainty, demonstrating that these factors enhanced the stability of traffic flow.

In the current state of the traffic network, vehicles have interconnected and maintained

The content of this chapter is communicated in the SCI journal.

adequate distance to avoid a collision. They adjust their speed and position according to surrounding traffic or based on information about ahead traffic. The information may be based on previous traveling time, previous density, or other historical sources. This information may significantly affect driving performance. Based on this fact, some research has been done in the lattice model, including historic density difference [97], historic optimal velocity difference [98], historic flux effect [115], and historical evolution information [99]. It was concluded that historical information plays a paramount role. Driving is an ongoing process, and the driver behaves as per traffic information during a period of time rather than a fixed historical time. For that, the historical information in the integral form was investigated in lattice models as given in References [168–171], and results showed that this factor impacts the traffic flow stability. In this situation, the traffic density or flow can be affected in two ways, first by the driver's features like age, gender, psychology, and degree of intoxication, and secondly, according to the environmental factors. Moreover, many researchers believe that complex uncertainties such as equipment malfunctions, network fluctuations, and traffic disruption may affect the information that we obtain from intelligent transportation systems (ITS). In addition, a variety of reasons can cause network quality changes. Consequently, in areas with poor network connectivity, the device's network will randomly fluctuate, affecting the quality of traffic information we get through the internet. However, the factors included in the lattice models mentioned earlier are limited, and they can still not demonstrate the influence of uncertain traffic situations in the vehicular network. Inspired by the above viewpoints and filling the research gap, the author tries to develop a new lattice model considering the effect of uncertainty about historical density information.

The chapter is arranged in sequence; a new hydrodynamic lattice model allowing for historical density information with some uncertainties is proposed in Section 5.1. The stability condition is achieved through linear stability analysis in Section 5.2. The mKdV equation is derived using nonlinear stability analysis in Section 5.3. In order to confirm the results of the theoretical study, numerical simulations are performed in Section 5.4, and a conclusion with a future scope is given in Section 5.5.

5.1 Lattice model

The first hydrodynamic traditional lattice model for unidirectional traffic flow was developed by Nagatani [83]. The model equations (continuity equation and evolution equation)

are mentioned as follows:

$$\partial_t \rho_j(t) + \rho_0(\rho_j(t)v_j(t) - \rho_{j-1}(t)v_{j-1}(t)) = 0, \tag{5.1}$$

$$\partial_t(\rho_j(t)v_j(t)) = a[\rho_0 V(\rho_{j+1}(t)) - \rho_j(t)v_j(t)], \tag{5.2}$$

where, $v_j(t)$ and $\rho_j(t)$ are the velocity and local density at time t on lattice site j, respectively; ρ_0 is the average density; a is the sensitivity of drivers; $V(.)$ is the optimal velocity function.

On the traffic network roads, drivers show their driving characteristics and skills after getting the historical information, then dictate their driving status. But, this information may be affected by factors such as bad network connectivity, equipment impairment, traffic disturbances, etc. The uncertainty in the historical density information may impact the movement of traffic flow. Investigating the effect of uncertain downstream traffic information on vehicular dynamics is more practical and more important. Therefore, after implementing the aforementioned factor, the improved evolution equation is constructed as

$$\partial_t(\rho_j(t)v_j(t)) = a[\rho_0 V(\rho_{j+1}(t) + \zeta\rho_{j+1}(t - \tau_0))] - a\rho_j(t)v_j(t), \tag{5.3}$$

where, τ_0 is the historical time; $\rho_{j+1}(t - \tau_0)$ is the historic density at site $j + 1$ at time $(t - \tau_0)$; ζ is a coefficient that reflects uncertainty about the historical density information of ahead site and a large absolute value of ζ represents a higher level of uncertainty; i.e., $\zeta > 0$. Here, the optimal velocity function (V(.)) is dependent on the actual density and uncertain density.

Remark 1: For $\zeta = 0$, the proposed model is equivalent to Nagatani's traditional model [83].

Retaining the first order terms from Eq. (5.3) after using Taylor series approximation and then abolishing the velocity $v_j(t)$ in Eqs. (5.1) and (5.3), the Eq. (5.4) appears for the density is:

$$\begin{aligned}\partial_t^2 \rho_j(t) + a\partial_t \rho_j(t) + a\rho_0^2\Big[V(\chi\rho_{j+1}(t)) - V(\chi\rho_j(t))\Big] \\ - a\rho_0^2(\chi - 1)\tau_0[\partial_t\rho_{j+1}(t)V'(\chi\rho_{j+1}(t)) - \partial_t\rho_j(t)V'(\chi\rho_j(t))] = 0,\end{aligned} \tag{5.4}$$

where, $1 + \zeta = \chi$ to facilitate reading. For $\chi > 1$ defines the more uncertainty of traffic information. $V(.)$ is taken for the optimal velocity function, which is determined by the

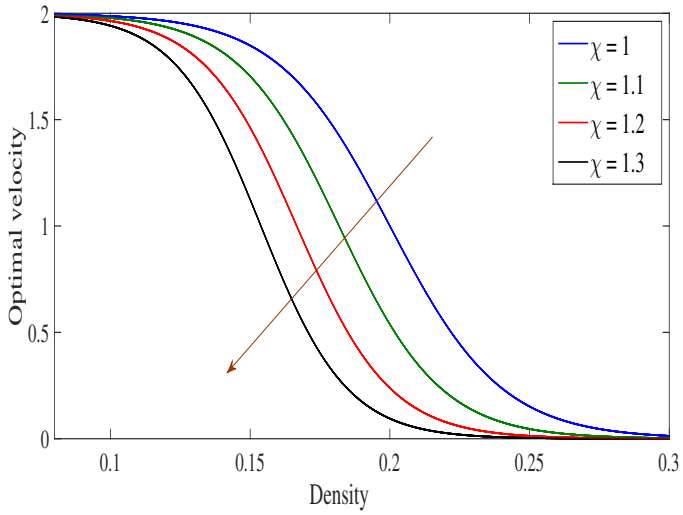

Figure 5.1: Variation of the optimal velocity versus density when uncertain factors happen.

uncertain density ($\chi\rho_{j+1}(t)$), and it is given as

$$V(\chi\rho_{j+1}(t)) = \frac{v_{max}}{2}\Big[\tanh\Big(\frac{2}{\rho_0} - \frac{\chi\rho_{j+1}(t)}{\rho_0^2} - \frac{1}{\rho_c}\Big) + \tanh\Big(\frac{1}{\rho_c}\Big)\Big], \tag{5.5}$$

where $v_{max} = 2$; ρ_c is the critical density; $\rho_0 = \rho_c = 0.2$. As shown in Figure 5.1, when the value of $\chi = 1$, then this optimal velocity function is the same as given in Ref. [83]. With an increase in the value of χ, the curve of optimal velocity function decreases, indicating the higher effect of the uncertain factors.

5.2 Linear stability analysis

This section investigates the impact of uncertainty about historical density information on the jamming transition of traffic flow using linear stability analysis. In the initial stage, the traffic is taken to move with a constant density (ρ_0) and resulting in constant optimal velocity ($V(\chi\rho_0)$) for the steady-state solution. Let the small perturbation in the form of $y_j(t)$ to the steady-state density is

$$\rho_j(t) = \rho_0 + y_j(t). \tag{5.6}$$

The replacement version of Eq. (5.4), after substituting Eq. (5.6) into it, is

$$\begin{aligned}\partial_t^2 y_j(t) + a\partial_t y_j(t) + a\chi\rho_0^2 V'(\chi\rho_0)[y_{j+1}(t) - y_j(t)] \\ - a(\chi-1)\tau_0\rho_0^2 V'(\chi\rho_0)[\partial_t y_{j+1}(t) - \partial_t y_j(t)] = 0.\end{aligned} \tag{5.7}$$

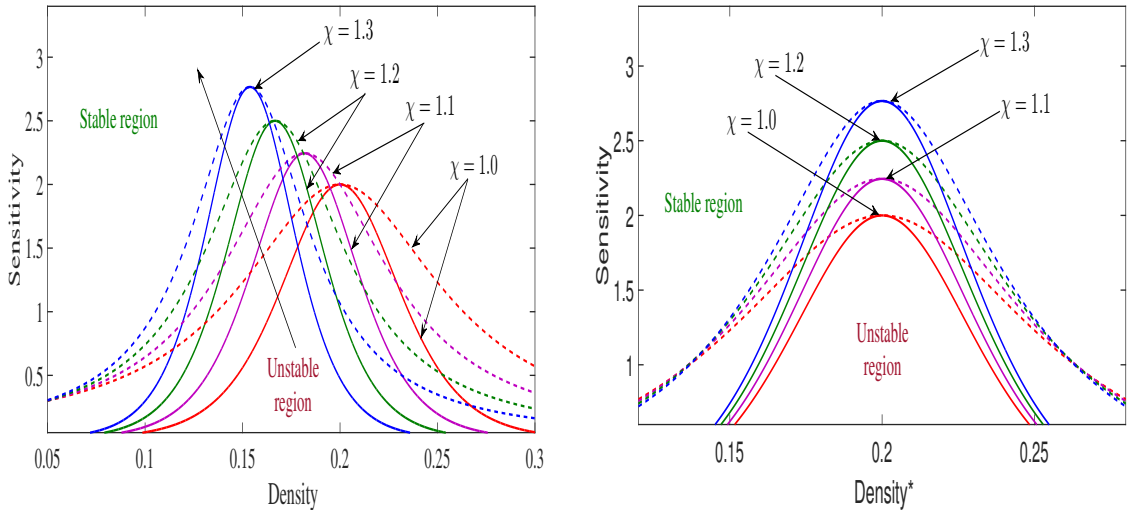

Figure 5.2: Phase diagrams of (a) Density ($\rho_j(t)$) versus sensitivity (a) and (b) Density* ($\rho_j(t)^* = \chi\rho_j(t)$) versus sensitivity ($a$) for different values of χ, where $\chi = 1$ to $\chi = 1.3$ by taking interval 0.1.

By expanding $y_j = \exp(ikj + \omega t)$ in Eq. (5.7), the transforming equation is as:

$$\omega^2 + a[1 - (\chi - 1)\tau_0\rho_0^2 V'(\chi\rho_0)(\exp(ik) - 1)]\omega + a\chi{\rho_0}^2 V'(\chi\rho_0)(\exp(ik) - 1) = 0. \quad (5.8)$$

Insert $\omega = i\omega_1$ into the Eq. (5.8), where ω_1 is a real number and makes its real part and imaginary part equal zero; we get

$$-\omega_1^2 + a\rho_0^2\chi V'(\chi\rho_0)(\cos(k) - 1) + a\rho_0^2(\chi - 1)\tau_0 V'(\chi\rho_0)\sin(k)\omega_1 = 0, \quad (5.9)$$

and,

$$a\omega_1 + a\rho_0^2\chi V'(\chi\rho_0)\sin(k) - a\rho_0^2(\chi - 1)\tau_0 V'(\chi\rho_0)(\cos(k) - 1)\omega_1 = 0. \quad (5.10)$$

By solving Eq. (5.10) for ω_1, we obtain

$$\omega_1 = \frac{-\rho_0^2\chi V'(\chi\rho_0)\sin(k)}{1 - \rho_0^2(\chi - 1)\tau_0 V'(\chi\rho_0)(\cos(k) - 1)}. \quad (5.11)$$

Assuming $\sigma = 1 - \rho_0^2(\chi - 1)\tau_0 V'(\chi\rho_0)(\cos(k) - 1)$ and then we achieve the following equation after keeping the value of ω_1 in Eq. (5.9):

$$a = \frac{-\rho_0^2\chi V'(\chi\rho_0)(1 + \cos(k))/\sigma^2}{1 + \rho_0^2(\chi - 1)\tau_0 V'(\chi\rho_0)(1 + \cos(k))/\sigma}, \quad (5.12)$$

the neutral stability condition is achieved, taking $k \to 0$, as given below

$$a = \frac{-2\chi{\rho_0}^2 V'(\chi\rho_0)}{1 + 2\tau_0(\chi - 1)\rho_0^2 V'(\chi\rho_0)}. \tag{5.13}$$

Here, the stability is influenced by coefficient χ, which reflects the uncertainty about the historical density. Note that for $\chi = 1$, the proposed model coincides with Nagatani's basic model [83].

5.3 Nonlinear stability analysis

The mKdV equation is constructed through a nonlinear stability analysis. The slow variables X for space and T for time are defined, and the assumption about density is also given below:

$$X = \epsilon(j + pt), \quad T = \epsilon^3 t, \quad \rho_j(t) = \rho_c + \epsilon S(X, T); \tag{5.14}$$

p is an unknown parameter that needs to be found.

Putting Eq. (5.21) into Eq. (5.4) and expanding Eq. (5.4) after using Taylor series expansion up to the fifth order of ϵ, one obtains:

$$\begin{aligned}\epsilon^2 h_1 \partial_X S + \epsilon^3(h_2\partial_X^2 S + h_3 \partial_X S^2) + \epsilon^4(\partial_T S + h_4\partial_X^3 S + h_5\partial_X^2 S^2 + h_6\partial_X S^3) \\ + \epsilon^5(h_7\partial_T\partial_X S + h_8\partial_X^4 S + h_9\partial_X^3 S^2 + h_{10}\partial_X^2 S^3) = 0.\end{aligned} \tag{5.15}$$

The h_i coefficients are exhibited in Table 5.1; where $V' = V'(\chi\rho_c) = \frac{\partial V(\rho)}{\partial \rho}\Big|_{\rho=\chi\rho_c}$. By substituting $p = -\chi{\rho_0}^2 V'(\rho_c^*)$, where $\rho_c^* = \chi\rho_c$ and $a_c = a(1 + \epsilon^2)$ into above equation, we achieve

$$\epsilon^4(\partial_T S - b_1\partial_X^3 S + b_2\partial_X S^3) + \epsilon^5(b_3\partial_X^2 S + b_4\partial_X^4 S + b_5\partial_X^2 S^3) = 0. \tag{5.16}$$

Here, the values of coefficients b_i are displayed in Table 5.2. $T = \frac{1}{b_1}T'$ and $S = \sqrt{\frac{b_1}{b_2}}S'$ are utilized to transform Eq. (5.16) into a conventional mKdV equation, then Eq. (5.16) turns into following form

$$\partial_{T'} S' - \partial_X^3 S' + \partial_X S' + \frac{\epsilon}{b_1}\Big[b_3\partial_X^2 S' + b_4\partial_X^4 S' + \frac{b_1 b_5}{b_2}\partial_X^2 S'\Big] = 0. \tag{5.17}$$

After omitting the term $O(\epsilon)$, the solution of Eq. (5.17) is as:

$$S_0'(X, T) = \sqrt{\mu}\tanh\Big(\sqrt{\frac{\mu}{2}}(X - \mu T)\Big), \tag{5.18}$$

Table 5.1: Values of h_i coefficients

coefficients	values	coefficients	values
h_1	$p + \chi {\rho_0}^2 V^{'}$	h_6	$\frac{\chi^3 \rho_0^2 V^{'''}}{6}$
h_2	$\frac{\chi {\rho_0}^2 V^{'}}{2} + \frac{p^2}{a} - \tau_0 p(\chi - 1)\rho_0^2 V^{'}$	h_7	$\frac{2p}{a} - \tau_0(\chi - 1)\rho_0^2 V^{'}$
h_3	$\frac{\chi^2 \rho_0^2 V^{''}}{2}$	h_8	$\frac{\chi {\rho_0}^2 V^{'}}{24} - \frac{\tau_0 p(\chi-1)\rho_0^2 V^{'}}{6}$
h_4	$\frac{\chi \rho_0^2 V^{'}}{6} - \frac{\tau_0 p(\chi-1)\rho_0^2 V^{'}}{2}$	h_9	$\frac{\chi^2 {\rho_0}^2 V^{''}}{12} - \frac{\tau_0 p\chi(\chi-1)\rho_0^2 V^{''}}{4}$
h_5	$\frac{\chi^2 \rho_0^2 V^{''}}{4} - \frac{\tau_0 p\chi(\chi-1)\rho_0^2 V^{''}}{2}$	h_{10}	$\frac{\chi^3 {\rho_0}^2 V^{'''}}{12} - \frac{\tau_0 p\chi^2(\chi-1)\rho_0^2 V^{'''}}{6}$

Table 5.2: Values of b_i coefficients

coefficients	values
b_1	$-\frac{\chi \rho_0^2 V^{'}}{6} + \frac{\tau_0 p(\chi-1)\rho_0^2 V^{'}}{2}$
b_2	$\frac{\chi^3 \rho_0^2 V^{'''}}{6}$
b_3	$-\frac{\chi {\rho_0}^2 V^{'}}{2} + \tau_0 p(\chi - 1)\rho_0^2 V^{'}$
b_4	$\frac{{\rho_0}^2 V^{'}}{24}\big[\chi - 4\tau_0 p(\chi - 1)\big] + \big[\frac{2p}{a_c} + \tau_0(\chi - 1)\big] b_1$
b_5	$\frac{\chi^2 {\rho_0}^2 V^{'''}}{12}\big[\chi - 2\tau_0 p(\chi - 1)\big] - \big[\frac{2p}{a_c} + \tau_0(\chi - 1)\big] b_2$

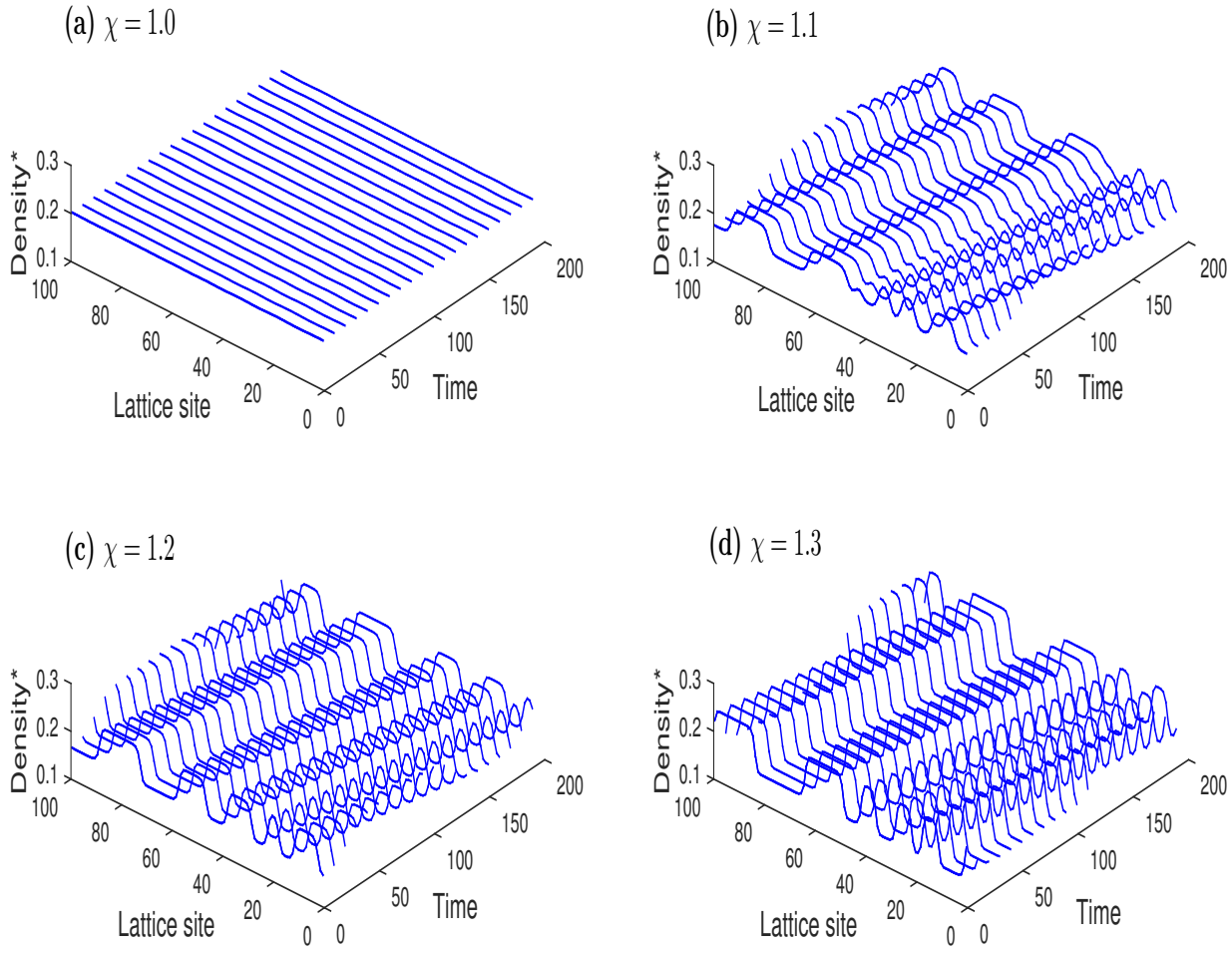

Figure 5.3: Spatio-temporal evolutions of density waves after $t = 9,800s$ with $\rho_0 = 0.2$, $a = 2.1$ for different values of χ.

where, μ is the propagation velocity and can be determined by solving the condition: $(S_0', M[S_0']) \equiv \int_{-\infty}^{\infty} dX S_0' M[S_0'] = 0$, where $M[S_0'] = \frac{1}{b_1}[b_3\partial_X^2 S' + b_4\partial_X^4 S' + \frac{b_1 b_5}{b_2}\partial_X^2 S'^3]$. Through the above modifications, the suitable choice of μ can be obtained as:

$$\mu = \frac{5b_2b_3}{2b_2b_4 - 3b_1b_5}. \tag{5.19}$$

Hence, the kink-antikink solution is

$$\rho_j^* = \rho_c + \alpha \tanh\Big(\sqrt{\frac{\mu}{2}}(X - \mu b_1 T)\Big), \quad \alpha(\text{amplitude}) = \sqrt{\frac{b_1\epsilon^2\mu}{b_2}},\ \epsilon^2 = \Big(\frac{a_c}{a} - 1\Big). \tag{5.20}$$

The kink-antikink solution of Eq. (5.20) denotes the coexisting phase, including freely

moving and congested phases both, which can be defined by $\rho_j^* = \rho_c - \alpha$ and $\rho_j^* = \rho_c + \alpha$, respectively. Moreover, the stability curves for different values of $\chi(\chi = 1.0, 1.1, 1.2, \text{and}, 1.3)$ are drawn (see Figure 5.2) to explore the implications of the uncertain historical density. The neutral and the coexisting stability curves are represented by the solid and dotted curves, respectively, produced from linear and nonlinear stability analyses. In the phase plot (ρ, a), the region above the curves is stable and below unstable. The remaining parameter's values are taken as $\rho_0 = \rho_c = 0.2$ and $\tau_0 = 0.1$. It can be seen that the apex of the curves rises gradually with an increase in the value of $\chi \geq 1$, which signifies that the stability of traffic flow significantly decreased. The phase plot shows that the traffic flow evolves into a jam situation when uncertainty occurs in vehicular dynamics.

5.4 Numerical simulations

In this section, the constructed density evolution equation (5.4) is used in discrete form for numerical computations is given below

$$\rho_j(t+2\Delta t) = (2 - a\Delta t)\rho_j(t+\Delta t) - (1 - a\Delta t)\rho_j(t) - a\rho_0^2\Delta t^2\big[V(\chi\rho_{j+1}(t)) - V(\chi\rho_j(t))\big] + a\rho_0^2(\chi - 1)\tau_0\Delta t\big[[\rho_{j+1}(t+\Delta t) - \rho_{j+1}(t)]V'(\chi\rho_{j+1}(t)) - [\rho_j(t+\Delta t) - \rho_j(t)]V'(\chi\rho_j(t))\big]. \tag{5.21}$$

Here, $\Delta t = 0.1$ is used for the time step. The total number of lattice sites are N ($N = 100$, $j = 1, 2, 3, \ldots N$). The density at the initial stage over space is assumed to be uniformly distributed: $\rho_j(0) = \rho_j(1) = \rho_0$. The local densities at site $j = 50$ and $j = 51$ are set as $\rho_j(0) = \rho_j(1) = \rho_0 - 0.005$ and $\rho_j(0) = \rho_j(1) = \rho_0 + 0.005$, respectively. Periodic boundary conditions are applied. The other parameters are considered as $a = 2.1$, $\tau_0 = 0.1$, and $\rho_c = 0.2$. In addition, for numerical computations, the value of χ (uncertain coefficient of historical density ($\chi \geq 1$)) is changed to investigate the results of theoretical findings where $\chi = 1,\ 1.1,\ 1.2,$ and 1.3.

The spatiotemporal evolutions are shown in Fig. 5.3 corresponding to the values of χ after time $t = 9800s$. In these patterns, the visualization of the impact of uncertain factors can be seen. In Fig. 5.3(a), it is found that for a small value of χ ($\chi = 1$), the traffic flow remains uniform as the stability condition is satisfied (Eq. (5.13)). Further, it can be seen from Fig. 5.3(b)-(d) that for the high value of χ, the solution occurs in terms of kink-antikink soliton waves, and fluctuations increases as the value of χ increases, which leads to the more instability of traffic flow. The soliton waves propagate in the backward direction, which discloses the vehicular flow evolves into a jam situation.

Moreover, by taking the same values of parameters corresponding to the panels of Fig. 5.3,

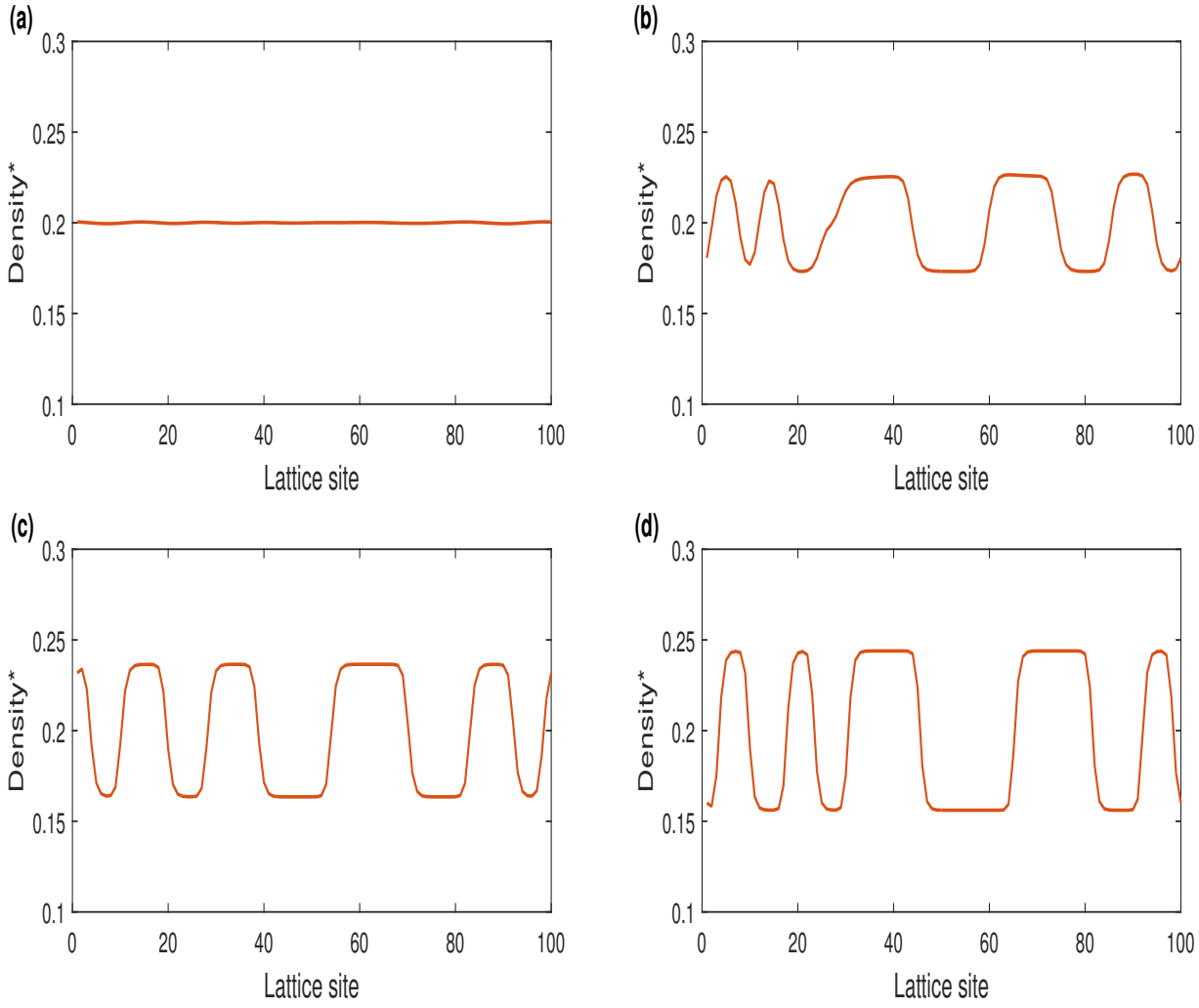

Figure 5.4: Density profiles at time $t = 10000s$ for different values of χ corresponding to the panels of Fig. 5.3.

the density profiles are plotted in Fig. 5.4 at time $t = 10000s$. Density profiles display the clearance of the traffic situations. In Fig. 5.4(a), as the stability condition is fulfilled for $\chi = 1$, so, there is no negative effect of χ occurs. Further, with a rise up in the value of χ, the disturbances are created that can be seen in Fig. 5.4(b)-(d). It is observed that the fluctuations continuously rise over time when the value of χ increases. As the higher value of χ, more instability is obtained. The results show that the uncertainty about historical density significantly impacts the traffic flow stability.

Fig. 5.5 portrays the plots between the instant flow ($J_j(t)$) and density ($\rho_j(t)^*$) by taking the parameter values same as in Fig. 5.3. The fundamental theoretical and simulation results are represented by the solid curve and scattered points, respectively. In Fig. 5.5(a), for $\chi = 1.0$, the scattered points lied on the solid line defining that the traffic flow is uniform, while in Fig. 5.5(b)-(d), the hysteresis loop is generated around density $\rho_0 = 0.2$ with an increase the value of χ. The lower and upper parts of the closed-loop display the coexisting phase associated with the behavior of traffic dynamics portraying kink-antikink density wave amplitudes, as illustrated in Fig. 5.3(b)-(d). The scattered points which are not on solid lines represent the dispersion between the theoretical and simulations results, i.e., the traffic situation converts from uniform to a congested state corresponding to the values of χ. The numerical results show that uncertainty of historical density information negatively impacts traffic flow stability, and the results also verify the theoretical findings.

5.5 Conclusion and future scope

The traffic flow may be affected by uncertain factors in the transportation system. Many drivers try to adjust speed based on past travel experience or driving skills to the smooth steady. Still, uncertain factors may affect the historic density information. Therefore, this chapter demonstrates a new lattice model that considers the effect of uncertainty (χ) of historical density information. The stability condition of new lattice model is derived applying linear stability analysis. The mKdV equation is obtained by nonlinear stability analysis. It is found that the traffic jam occurs by increasing the value of χ, which signifies that traffic flow leads to an unstable situation. Furthermore, numerical simulations of the new model have been conducted to examine the impact of uncertainty. It is observed that the variations between fundamental results and simulation results occur with the higher value of χ as the stability condition is not satisfied. Overall results show that the uncertainty about downstream historical density significantly influences traffic flow stability.

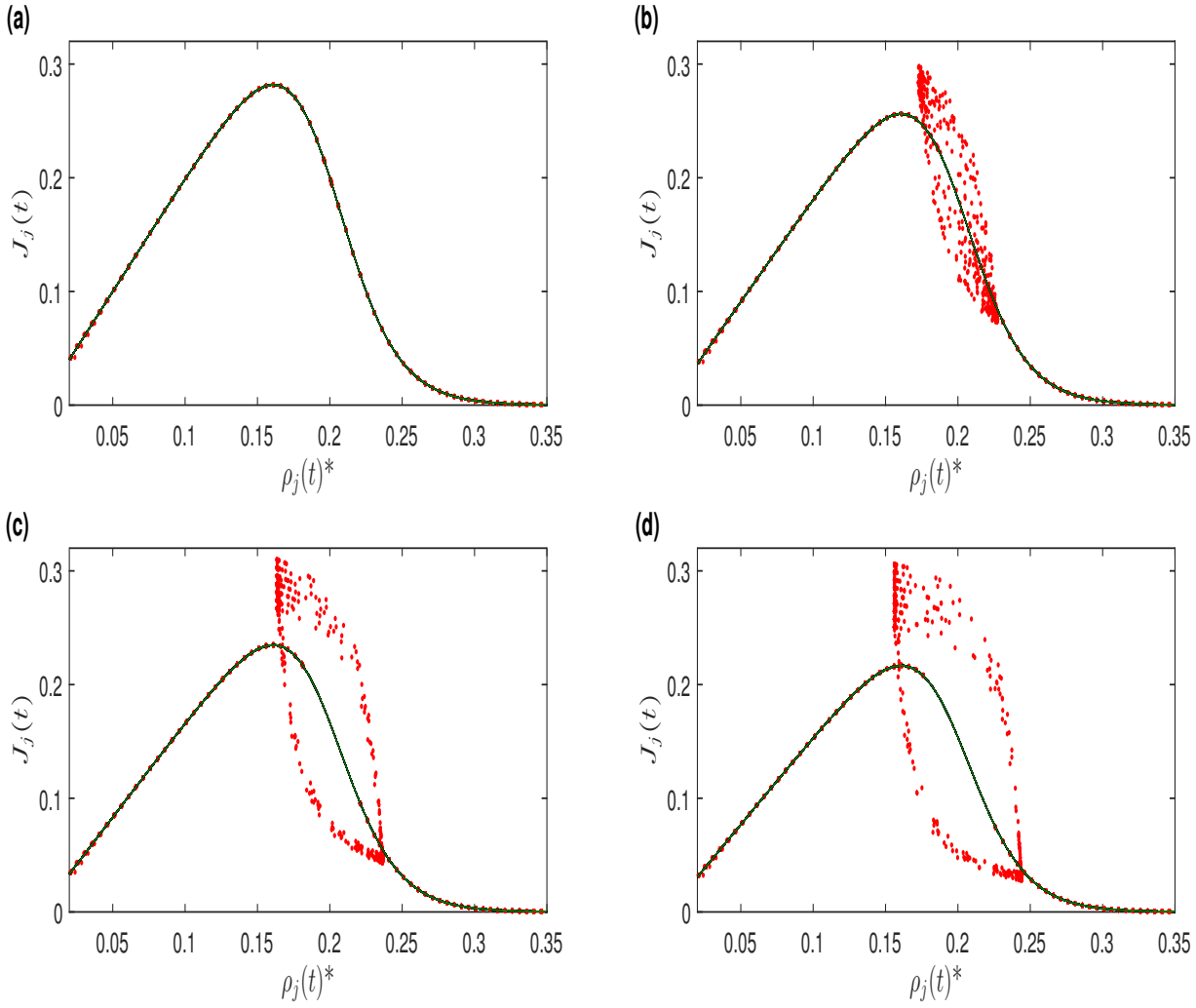

Figure 5.5: Instant flow versus Density with $a = 2.1$ for different values of χ corresponding to the panels of Fig. 5.3.

Considering the uncertainty effect, the proposed lattice model is only for a one-dimensional vehicular system. The proposed model can be further modified for two-lane roads or higher dimensional systems, taking various important factors related to drivers, forecasting, environmental factors, etc.

Chapter 6

Lattice hydrodynamic area occupancy model

Traffic networks consisting of traffic control devices, streets, highways, flyovers, bridges, etc., provide a convenient environment for travelers. Nowadays, in developing countries like India, traffic management is one of the major issues as the number of automobiles increases daily. Additionally, the vehicles are not only exceptionally heterogeneous but also do not follow lane discipline leading to a disordered traffic system. Consequently, phantom traffic jams frequently occur, resulting in severe problems in terms of traffic safety, traffic efficiency, energy consumption, etc. In the recent past, a large number of efforts [6,62,107,127,172] were devoted to analyzing and understanding the complex nonlinear traffic phenomena such as non-equilibrium phase transition and nonlinear waves, but a majority of them focus only on the lane-based traffic system.

While modeling the vehicular traffic flow on a network, it is generally assumed that the vehicles follow the leading vehicles with lane and queue discipline in homogeneous and ordered traffic. But the actual traffic flow in developing countries is neither homogeneous nor ordered. On Indian roadways, various vehicles with varying sizes and operational characteristics are commonly seen. These numerous vehicles are categorized into several classes: Motorized Two Wheelers (Eg. Bike), Motorized Three-Wheelers (Eg. Auto-Rickshaw), Light Commercial Vehicles (LCV), Car, and Truck, and so on, which represents "inhomogeneity" or "heterogeneity" in the traffic system. An investigation of vehicle interaction (both lateral and longitudinal) is required to capture such traffic flows. In this context, firstly, the speed and position of following motorists depend on the vehicles ahead (leading motorists). Secondly, if traffic is disordered and inhomogeneous, i.e., if there is no lane discipline, then the same section length of the road may be filled by several vehicles at the same time based on available space. So, there are two primary issues in modeling: (i) reflecting the influence of varied vehicle sizes and speeds and (ii) the area occupied by various vehicles.

The majority of the lattice models [85–87,89–92,100,112,120,123,153,158,166,168,173] presented in Chapter 1 are lane-based traffic models, which presume that all vehicles travel

The content of this chapter has been published in Physica A: Statistical Mechanics and its Applications, 607: 128184, (2022).

on the road with identical characteristics. But in mixed traffic, the high number of oversized vehicles quickly leads to congestion and instability because of less sensitivity and larger size. The larger vehicles have more reaction time as compared to smaller ones. In this context, to explore the nature of heterogeneity, Kaur and Sharma [132] proposed the generalization of the lattice model from homogeneous to heterogeneous considering two types of vehicles having different sensitivities. It is concluded that small vehicles have a high sensitivity in a mixed traffic stream than larger vehicles, which improves traffic flow stability.

Moreover, vehicles have different speeds according to their size. For example, Cars and Bikes have different speed limits on roads. Several kinds of vehicles travel without lane discipline in disorderly heterogeneous traffic networks. Vehicles adjust their velocity after seeing the available space ahead and move forward by using some lateral gap between them to set location according to their size in mixed traffic. However, a single large vehicle uses more space than a small vehicle in a hybrid traffic system. Whereas at that time, two-to-three small vehicles may occupy that same space. The size and speed of diverse vehicles may directly impact traffic flow efficiency. When larger vehicles outnumber smaller vehicles, larger vehicles can exacerbate the volatility of mixed traffic flow. In addition, vehicles significantly increase road capacity in heterogeneous traffic compared to homogeneous traffic. So, we can't ignore regions covered by vehicles of various sizes to better comprehend natural heterogeneous traffic occurrences. Therefore, it needs to consider the area occupied by different vehicles instead of taking only traffic intensity for heterogeneity traffic situations, where the norm of lane-based traffic is often not strictly followed. Based on this phenomenon, the concept of area occupancy was introduced in Refs. [71–73] in which different characteristics corresponding to distinct kinds of vehicles are explained. To our knowledge, no one has examined the lattice model with the effect of area occupancy for heterogeneous traffic, despite the fact that it is closely linked to the actual traffic scenario. Therefore, a new lattice hydrodynamic area occupancy (LHAO) model has been developed to ensure a better understanding of the vehicles with varying percentages, sizes, and speeds.

This chapter explores the vehicles' heterogeneity behavior that is arranged in sequence as follows; In Section 6.1, basic models and some definitions related to the proposed model are explained, whereas in Section 6.2, a new lattice model is constructed by incorporating the effect of area occupancy. The stability analysis is conducted for the proposed model in Section 6.3 to obtain the stability condition. In Section 6.4, the mKdV equation is achieved using nonlinear stability analysis. Numerical simulations are done to demonstrate the theoretical results in Section 6.5. Finally, the chapter concludes with possible research

outcomes, and a summary is drawn in Section 6.6.

6.1 Lattice Hydrodynamic Traffic Flow Models

6.1.1 Basic Lattice Model

Learning from the optimal velocity model [28] and continuum models [42,43], Nagatani proposed that the traffic flow can be optimized and an optimal state can be achieved and developed the first basic lattice hydrodynamic model [83] for a single lane traffic system. Let $\rho_j(t)$ and $v_j(t)$ represent the density and velocity on site-j at time t, respectively. The governing equations are given as follows:

$$\partial_t \rho_j(t) + \rho_0(\rho_j(t)v_j(t) - \rho_{j-1}(t)v_{j-1}(t)) = 0, \tag{6.1}$$

$$\partial_t(\rho_j(t)v_j(t)) = a[\rho_0 V(\rho_{j+1}(t)) - \rho_j(t)v_j(t)]. \tag{6.2}$$

The first equation is the conservation of vehicles representing the rate of change of density at site -j is proportional to the difference between the inflow $(\rho_{j-1}(t)v_{j-1}(t))$ and outflow $(\rho_j(t)v_j(t))$. The second equation denotes the flow evolution equation, which signifies the rate of change of flux at any site-j is also affected by the leading lattice site. Here, ρ_0 is the average density, $V(.)$ is the optimal velocity function, and a is the sensitivity coefficient which measures how strongly drivers behave according to the surrounding situation.

One of the important assumptions in the above basic lattice model is that all the vehicles are considered homogeneous, which is far from reality. In a traffic environment, vehicles may differ according to their size on the highway; in that case, drivers behave differently in the same traffic situations. To include this characteristic, later on, Kaur and Sharma [132] generalized the lattice model with optimal current difference effect (OCDE) by considering the heterogeneity in driver's behavior. The model incorporates different sensitivities corresponding to the vehicle's type and interactions. The governing equations corresponding to the heterogeneous traffic involving two different vehicle types are given as

$$\left.\begin{aligned} &\partial_t \rho_{1,j}(t) + \rho_0(\rho_{1,j}(t)v_{1,j}(t) - \rho_{1,j-1}(t)v_{1,j-1}(t)) = 0, \\ &\partial_t(\rho_{1,j}(t)v_{1,j}(t)) = a_1[\rho_0 c V(\rho_{j+1}(t)) - \rho_{1,j}(t)v_{1,j}(t)]. \end{aligned}\right\} \text{ small vehicles} \tag{6.3}$$

$$\left.\begin{aligned} &\partial_t \rho_{2,j}(t) + \rho_0(\rho_{2,j}(t)v_{2,j}(t) - \rho_{2,j-1}(t)v_{2,j-1}(t)) = 0, \\ &\partial_t(\rho_{2,j}(t)v_{2,j}(t)) = a_2[\rho_0(1-c)V(\rho_{j+1}(t)) - \rho_{2,j}(t)v_{2,j}(t)]. \end{aligned}\right\} \text{ large vehicles} \tag{6.4}$$

Here a_1 is sensitivity of small vehicles whereas a_2 is the larger ones. The parameter

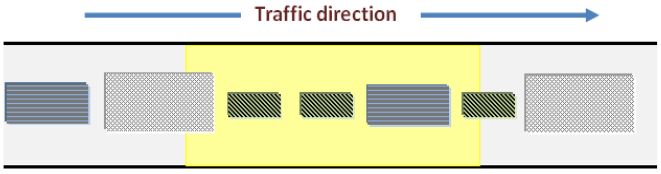

(a) With lane discipline

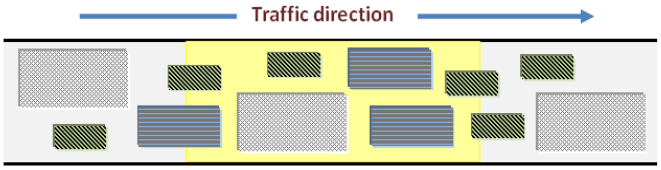

(b) Without lane discipline

Figure 6.1: Distinct vehicles in the heterogeneous transportation system.

$0 \leq c \leq 1$ is the small vehicles fraction while $1 - c$ denotes the larger vehicles fraction. Here, the optimal velocity function $(V(\rho_{j+1}(t)))$ is dependent on the total density at site -$j + 1$ at time t.

In developing countries, the majority of roads are one-lane, on which varieties of vehicles with different speeds and sizes can be seen. In such a heterogeneous traffic environment (Figure 6.1), the mixture of distinct vehicles impacts the traffic flow stability due to their different characteristics. When there is sufficient lateral space available ahead, small vehicles with high sensitivity adjust their speed to utilize this space by reacting immediately as compared to large vehicles with low sensitivity. Therefore, vehicles do not adhere to lane discipline in the above phenomenon and frequently depart from their centerline locations, as illustrated in Figure 6.1(b). The inclusion of various types of vehicles and their vast range of physical and dynamic features adds to the complexity. Moreover, for homogeneous traffic, the number of vehicles occupying a unit length of the road is referred to as traffic density. It is commonly calculated in terms of vehicles per lane per km of road length, ignoring the vehicle size and speed, and is, therefore, better suited to lane-disciplined homogenous traffic. But according to the actual traffic environment, we can't neglect the distinct features of different vehicles. So, it becomes necessary to incorporate vehicles area to study the realistic features of heterogeneous traffic, which are explained in the following part.

6.1.2 Area Occupancy (AO)

In order to account for the heterogeneity of traffic, dimensionless variable occupancy is used for a new measure of concentration [174]. When dealing with traffic that includes

a variety of vehicle kinds, such as motorized two-wheelers, motorized three-wheelers, and non-motorized vehicles, it's critical to include the vehicle's area to depict realistic traffic dynamics. In these traffic conditions, two or three different sizes of vehicles can travel side by side on a single lane. Moreover, occupancy is directly quantified by the percentage of time that the detection zone on the road is covered by all vehicles. Therefore, the length of the detection zone affects the occupancy detected by detectors. Thus, depending on the size and type of detectors, the recorded occupancy may change even with identical traffic for the same spot. As a result, the section length must be considered while measuring. In addition, occupancy fails to accurately portray heterogeneous traffic when different sizes of vehicles are available on the road in non-lane discipline situations because it accounts only for length, whereas the optimization of traffic is also affected by width. Therefore, to account for non-lane discipline, the whole width of the road segment must be considered. Hence, a widely used measure [71] for the concentration of heterogeneous traffic without lane discipline is:

$$\text{Area Occupancy(AO)} = \frac{\sum_i t_i A_i}{TA}. \tag{6.5}$$

Here, i is the vehicle number, t_i is for the time during the segment of road is occupied by the i^{th} vehicle; A_i is for the area occupied by the i^{th} vehicle of the road space during time t_i; A is for the total area of road segment under consideration; T is for the total observation time period. When the observation time is short for all the vehicles, i.e., $t_i = T$, then Eq. (6.5) becomes as [73]

$$\text{AO} = \frac{\sum_i A_i}{A}. \tag{6.6}$$

The aim of this article is to introduce the effects of area occupancy in the lattice hydrodynamic model. Therefore, for heterogeneous traffic, assume $l = 1,\ 2,\ 3, \ldots, m$ is the vehicle type on the road, where m is the total number of distinct kinds of vehicles. A_l denotes the area occupied by the vehicle of l^{th} type; $A = L \times W$ where, L and W be the length and width of the road segment under consideration, respectively; $\rho_j(t)$ is total density on site -j at time t. Then Eq. (6.6) changes to

$$\text{AO} = \frac{\sum_{l=1}^{m} c_l A_l}{W} \rho_j(t), \tag{6.7}$$

where c_l represents the fraction of l^{th} type of vehicle. Here $j = 1, 2, \ldots, N$ denotes the lattice site.

6.2 Lattice Hydrodynamic Area Occupancy (LHAO) Model

In this section, we propose a new LHAO model incorporating the idea of area occupancy for heterogeneous disorder unidirectional traffic in a one-lane system without on and off-ramps. The concept of area occupancy doesn't influence the conservation of law (continuity equation), while the evolution equation is improved by considering the effect of different sensitivities, speeds, and area occupancy for the distinct types of vehicles. Therefore, in this case, the continuity equations for each type of vehicle are given as follows

$$\left.\begin{aligned}
&\partial_t\rho_{1,j}(t)+\rho_0(\rho_{1,j}(t)v_{1,j}(t)-\rho_{1,j-1}(t)v_{1,j-1}(t))=0,\\
&\partial_t\rho_{2,j}(t)+\rho_0(\rho_{2,j}(t)v_{2,j}(t)-\rho_{2,j-1}(t)v_{2,j-1}(t))=0,\\
&\partial_t\rho_{3,j}(t)+\rho_0(\rho_{3,j}(t)v_{3,j}(t)-\rho_{3,j-1}(t)v_{3,j-1}(t))=0,\\
&\vdots\\
&\partial_t\rho_{m,j}(t)+\rho_0(\rho_{m,j}(t)v_{m,j}(t)-\rho_{m,j-1}(t)v_{m,j-1}(t))=0.
\end{aligned}\right\} \tag{6.8}$$

Here, $\rho_{l,j}(t)$ and $v_{l,j}(t)$, respectively, are the density and velocity of vehicle type l on site -j at time t. Furthermore, it's worth noting that all types of vehicles will interact with one another, and their presence will have an impact on each other. So, this has been integrated through the optimal velocity function in the evolution equation. The evolution equations corresponding to each type of vehicle with consideration of area occupancy explaining traffic heterogeneity are given below

$$\left.\begin{aligned}
&\partial_t(\rho_{1,j}(t)v_{1,j}(t))=a_1\big[c_1\rho_0V_1\big(\textstyle\sum_{l=1}^{m}\frac{c_lA_l}{W}\rho_{j+1}(t)\big)-\rho_{1,j}(t)v_{1,j}(t)\big],\\
&\partial_t(\rho_{2,j}(t)v_{2,j}(t))=a_2\big[c_2\rho_0V_2\big(\textstyle\sum_{l=1}^{m}\frac{c_lA_l}{W}\rho_{j+1}(t)\big)-\rho_{2,j}(t)v_{2,j}(t)\big],\\
&\partial_t(\rho_{3,j}(t)v_{3,j}(t))=a_3\big[c_3\rho_0V_3\big(\textstyle\sum_{l=1}^{m}\frac{c_lA_l}{W}\rho_{j+1}(t)\big)-\rho_{3,j}(t)v_{3,j}(t)\big],\\
&\vdots\\
&\partial_t(\rho_{m,j}(t)v_{m,j}(t))=a_m\big[c_m\rho_0V_m\big(\textstyle\sum_{l=1}^{m}\frac{c_lA_l}{W}\rho_{j+1}(t)\big)-\rho_{m,j}(t)v_{m,j}(t)\big],
\end{aligned}\right\} \tag{6.9}$$

where, c_l is the fraction of l^{th} type of vehicle with $\sum_{l=1}^{m}c_l=1$. The sensitivity of l^{th} type of vehicle is defined by a_l and inversely proportional to delay time as $a_l=\frac{1}{\tau_l}$. Here, $\rho_{j+1}(t)=\rho_{1,j+1}(t)+\rho_{2,j+1}(t)+\cdots+\rho_{m,j+1}(t)$ is the total density at time t on site -$j+1$. In the system of Eqs. (6.9), the optimal velocity function depends on the total density with area occupancy of all types of vehicles. Clearly, the small vehicles occupy an area lesser than the larger vehicles. When vehicles of a small type are high in mixed traffic, the optimal flow is higher because the area occupancy is high in this case. Moreover, combining each equation in the system of Eqs. (6.8) and (6.9) by one-to-one correspondence, we obtain

the density evolution equations for each type of vehicle as

$$\left.\begin{aligned}
&\rho_{1,j}(t+2\tau_1)-\rho_{1,j}(t+\tau_1)+c_1\tau_1\rho_0^2\Big(V_1\big(\textstyle\sum_{l=1}^{m}\frac{c_lA_l}{W}\rho_{j+1}(t)\big)-V_1\big(\sum_{l=1}^{m}\frac{c_lA_l}{W}\rho_j(t)\big)\Big)=0,\\
&\rho_{2,j}(t+2\tau_2)-\rho_{2,j}(t+\tau_2)+c_2\tau_2\rho_0^2\Big(V_2\big(\textstyle\sum_{l=1}^{m}\frac{c_lA_l}{W}\rho_{j+1}(t)\big)-V_2\big(\sum_{l=1}^{m}\frac{c_lA_l}{W}\rho_j(t)\big)\Big)=0,\\
&\rho_{3,j}(t+2\tau_3)-\rho_{3,j}(t+\tau_3)+c_3\tau_3\rho_0^2\Big(V_3\big(\textstyle\sum_{l=1}^{m}\frac{c_lA_l}{W}\rho_{j+1}(t)\big)-V_3\big(\sum_{l=1}^{m}\frac{c_lA_l}{W}\rho_j(t)\big)\Big)=0,\\
&\vdots\\
&\rho_{m,j}(t+2\tau_m)-\rho_{m,j}(t+\tau_m)+c_m\tau_m\rho_0^2\Big(V_m\big(\textstyle\sum_{l=1}^{m}\frac{c_lA_l}{W}\rho_{j+1}(t)\big)-V_m\big(\sum_{l=1}^{m}\frac{c_lA_l}{W}\rho_j(t)\big)\Big)=0.
\end{aligned}\right\} \tag{6.10}$$

In the above model equations, the properties of distinct types of vehicles are described through the different equations, whereas the purpose of mixed traffic is to depict traffic from a global perspective instead of focusing on individual vehicle characteristics. For simplicity, we assume $\tau_l = k_l\tau$; with $k_l \leq 1$ and $k_l < k_{l+1}$ as time delay corresponding to the small vehicles is less than that of the larger vehicles; $\tau\ (=1/a)$ is reaction time of mixed traffic. In addition, we adopt the modified version of the optimal velocity function [107] to incorporate the effect of AO, which is defined as

$$\begin{aligned}
V_l\Big(\sum_{l=1}^{m}\frac{c_lA_l}{W}\rho_j(t)\Big) =& \frac{v_{l,max}}{2}\Big[\tanh\Big(\frac{2}{\rho_0}-\frac{\sum_{l=1}^{m}\frac{c_lA_l}{W}\rho_j(t)}{\rho_0^2}-\frac{1}{\rho_c}\Big)+\tanh\Big(\frac{1}{\rho_c}\Big)\Big]\\
=& \frac{v_{l,max}}{2}f(B_l\rho_j(t)), \quad \text{where } B_l=\sum_{l=1}^{m}\frac{c_lA_l}{W},
\end{aligned} \tag{6.11}$$

where $v_{l,max}$ represents the maximum free-flow speed of the corresponding vehicle, i.e., the speed limit of l^{th} vehicle. Fig. 6.2 displays the optimal velocity curves versus density corresponding to two types of vehicles: small ($c_1 = c$) and large ($c_2 = 1-c$). It can be seen that both types of vehicles have an impact on one another. When small vehicles increase, the optimal velocity also increases as the fraction of larger vehicles continuously decreases, as shown in Fig. 6.2(a). In that case, small vehicles have the capability to move from one place to another by using the available lateral gap. When the proportion of small vehicles grows at a low level, the gap between the optimal velocity curve is less because larger vehicles are available more than small vehicles, which influences the traffic flow. In addition, when the proportion of small vehicles increases at a high level, the differences between optimal velocity curves become more, signifying an impact on the traffic flow. In contrast, from Fig. 6.2(b), it is clear that when the fraction of the larger vehicles increases, the optimal velocity decreases, and hence larger vehicles dominate the other ones. Moreover, due to their large size, they do not utilize the lateral space available ahead of them and do not move freely, resulting in a speed reduction. It can also be seen

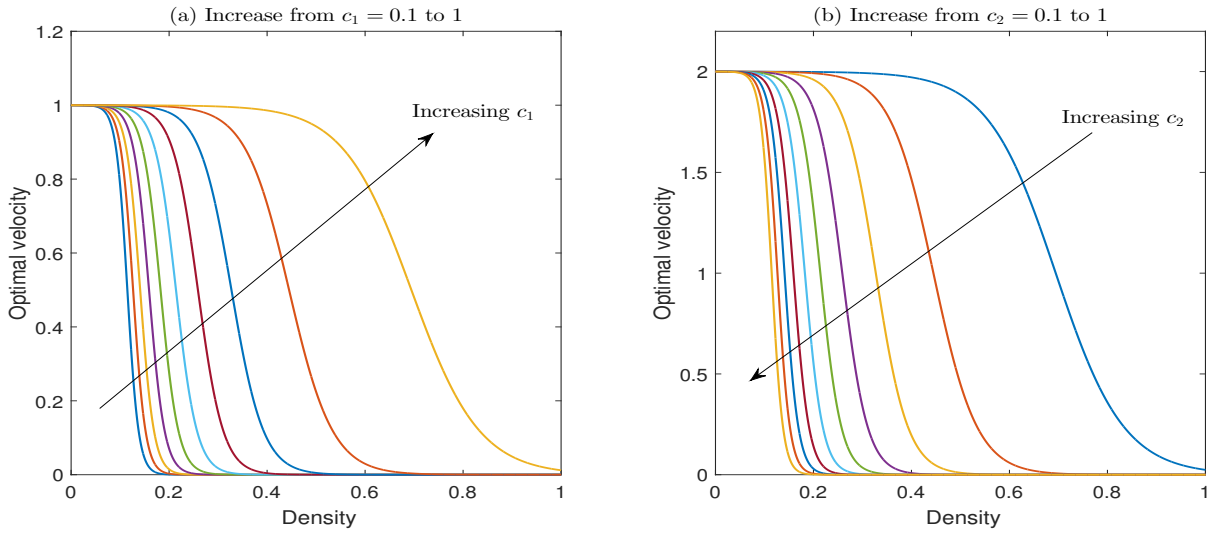

Figure 6.2: Variation of the optimal velocity versus density with $\rho_0 = \rho_c = 0.2$ for different values of fraction parameter corresponding to small (c_1) and large vehicles (c_2), where $A_1 = 1.08, A_2 = 7.14, v_{1,max} = 1.0, v_{2,max} = 2.0, W = 3.75$. The optimal velocity curves at intervals of 0.1 for: (a) increasing c_1 from $c_1 = 0.1$ to $c_1 = 1.0$ and (b) increasing c_2 from $c_2 = 0.1$ to $c_2 = 1.0$.

that when large vehicles increase at a low level, the difference between optimal velocity curves is more, which means smaller vehicles aid in smoothing traffic flow by utilizing lateral space at that time. For a high proportion of larger vehicles, the optimal velocity declines. Overall, Fig. 6.2 shows that small vehicles have a positive impact while large vehicles have a negative impact on the optimal velocity.

By combining density equations with each other in the system of Eqs. (6.10) by using Eq. (6.11), we get

$$\begin{aligned}
&[\rho_{1,j}((t+2\tau)+2\tau(k_1-1))+\rho_{2,j}((t+2\tau)+2\tau(k_2-1))+\cdots+\rho_{m,j}((t+2\tau)+2\tau(k_m-1))]\\
&-[\rho_{1,j}((t+\tau)+\tau(k_1-1))+\rho_{2,j}((t+\tau)+\tau(k_2-1))+\cdots+\rho_{m,j}((t+\tau)+\tau(k_m-1))]\\
&+\rho_0^2\Big[\frac{c_1\tau_1 v_{1,max}}{2}+\frac{c_2\tau_2 v_{2,max}}{2}+\cdots+\frac{c_m\tau_m v_{m,max}}{2}\Big]\big[f(B_l\rho_{j+1}(t))-f(B_l\rho_j(t))\big]=0.
\end{aligned} \tag{6.12}$$

As the values of k_l increase, the delay time increases, indicating that the vehicles become less responsive. Thus, by using Taylor series expansion for expression involving k_l and after neglecting the terms of the higher-ordered derivatives, the density evolution equation for m types of vehicles in mixed traffic is given in a simplified form as

$$\rho_j(t+2\tau)-\rho_j(t+\tau)+\tau\rho_0^2\sum_{l=1}^{m}\frac{c_l k_l v_{l,max}}{2}[f(B_l\rho_{j+1}(t))-f(B_l\rho_j(t))]=0. \tag{6.13}$$

Table 6.1: Special cases related to new LHAO model

Sr. no.	Cases	Explanation	Stability condition
1.	$m = 2$	two types of vehicles	
	$B_l = 1$	without area occupancy	$a > -3[c_1k_1 + c_2k_2]\rho_0^2 f'(\rho_0)$;
	$v_{l,max} = 2\ \forall l$	with same maximum speed	$\lambda = 0$ [132]
	$c_1 = c$ & $c_2 = 1 - c$ with $k_l = 1/q_l$	heterogeneous traffic	
2.	$m = 1$	one type of vehicles	
	$B_l = 1$	without area occupancy	$a > -3\rho_0^2 f'(\rho_0)$ [83]
	$v_{l,max} = 2\ \forall l$	with same maximum speed	
	$c_1 = 1$ with $k_1 = 1$	homogeneous traffic	

6.3 Linear Stability Analysis (Effect of small amplitude deviation)

In this section, a linear stability analysis is performed to investigate the impact of area occupancy on the jamming transition of mixed traffic flow. It is a useful technique for determining how a system reacts to small perturbations. Initially, the traffic is considered to move with a constant density ρ_0 and optimal velocity $V(\rho_0)$. Hence, the uniform steady-state solution for Eq. (6.13) is given as

$$\rho_j(t) = \rho_0, \quad v_j(t) = V(\rho_0). \tag{6.14}$$

Let $y_j(t)$ be a small perturbation and is introduced to the uniform density on site -j at time t, which leads to $\rho_j(t) = \rho_0 + y_j(t)$. Inserting this perturbed density term into Eq. (6.13) and linearizing it, we get the following equation

$$y_j(t + 2\tau) - y_j(t + \tau) + B_l C_l \tau {\rho_0}^2 [y_{j+1}(t) - y_j(t)] f'(B_l\rho_0) = 0, \tag{6.15}$$

where, $C_l = \sum_{l=1}^{m} \frac{c_l k_l v_{l,max}}{2}$. By applying Taylor expansion to Eq. (6.15) and putting the deviation as $y_j(t) = \exp(ikj + \omega t)$ in the Eq. (6.15), we get

$$e^{2\omega\tau} - e^{\omega\tau} + B_l C_l \tau {\rho_0}^2 [e^{ik} - 1] f'(B_l\rho_0) = 0. \tag{6.16}$$

Inserting $\omega = \omega_1(ik) + \omega_2(ik)^2$..... into Eq. (6.16), the first and second order terms of the coefficients (ik) and $(ik)^2$ are formulated as

$$\omega_1 = -B_l C_l {\rho_0}^2 f'(B_l\rho_0). \tag{6.17}$$

$$\omega_2 = -\frac{3}{2}\tau {\omega_1}^2 - \frac{B_l C_l}{2} {\rho_0}^2 f'(B_l\rho_0). \tag{6.18}$$

Table 6.2: List of parameters

Sr. no.	Parameters	Representations	MTW (c_1)	Car (c_2)
1.	A_l	area occupied [72]	1.08	7.14
2.	$v_{l,max}$	free flow speed	1.0	2.0
3.	k_l	reaction coefficient	0.7	0.8

If the inequality $\omega_2 < 0$, the uniform steady state flow becomes unstable for long wavelength waves; on the other side, it becomes stable if $\omega_2 > 0$. Moreover, at $\omega_2 = 0$, the neutral stability condition is achieved for the steady state of heterogeneous traffic flow, which is as

$$\tau = \frac{1}{a} = -\frac{1}{3B_l C_l \rho_0^2 f'(B_l \rho_0)}. \tag{6.19}$$

The stability condition for the heterogeneous traffic flow is given as

$$a > -3B_l C_l \rho_0^2 f'(B_l \rho_0). \tag{6.20}$$

The proposed LHAO model is general; therefore, the special cases are discussed in Table 6.1 related to existing lattice models. In addition, the values of parameters are given in Table 6.2, which are used through results.

6.4 Nonlinear Stability Analysis (Effect of long-wavelength deviation)

Long-wavelength modes in heterogeneous traffic flow on coarse-grained scales are used to explore the evolution features of traffic congestion at the critical point. Moreover, to construct the mKdV equation, the reduction perturbation method is used. The slow variables X for space and T for time are considered with a small positive scaling parameter $\epsilon(0 < \epsilon \ll 1)$, and the assumption about density is also given as below:

$$X = \epsilon(j + pt), \quad T = \epsilon^3 t, \quad \rho_j(t) = \rho_c + \epsilon S(X, T); \tag{6.21}$$

p is an unknown parameter that needs to be found.

When Eq. (6.21) is substituted into Eq. (6.13), and then Eq. (6.13) is expanded using Taylor series expansion to the fifth order of ϵ, the result is

$$\begin{aligned}\epsilon^2 h_1 \partial_X S + \epsilon^3(h_2 \partial_X^2 S + h_3 \partial_X S^2) + \epsilon^4(\partial_T S + h_4 \partial_X^3 S + h_5 \partial_X^2 S^2 + h_6 \partial_X S^3) \\ + \epsilon^5(h_7 \partial_T \partial_X S + h_8 \partial_X^4 S + h_9 \partial_X^3 S^2 + h_{10} \partial_X^2 S^3) = 0.\end{aligned} \tag{6.22}$$

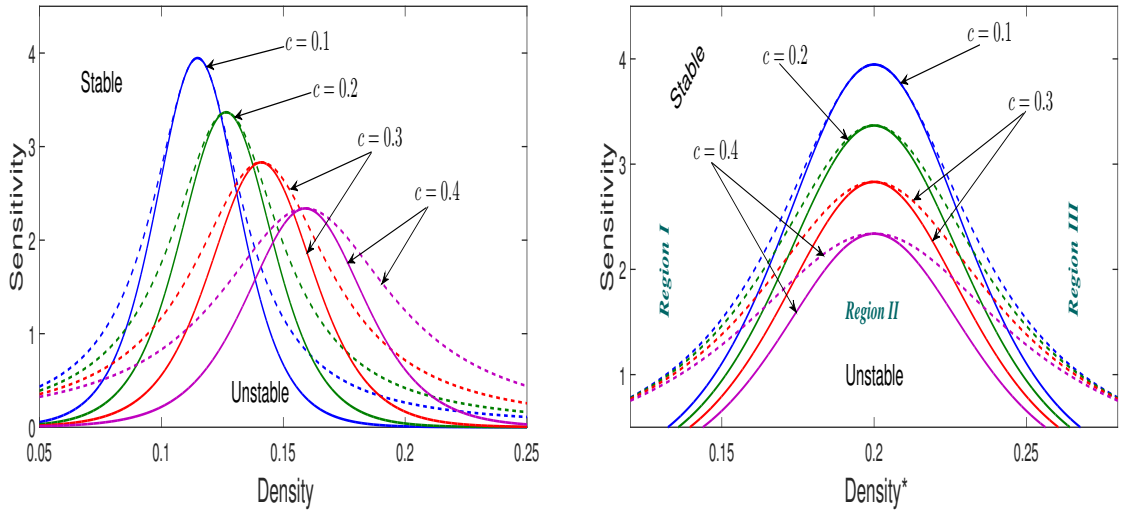

Figure 6.3: Phase diagrams of (a) Density ($\rho_j(t)$) versus sensitivity (a) and (b) Density* ($\rho_j(t)^* = B_l\rho_j(t)$) versus sensitivity ($a$) for different values of fraction parameter c when only two types of vehicles are considered as $c_1 = c$ and $c_2 = 1 - c$.

The h_i coefficients are shown in Table 6.3. By substituting $p = -B_l C_l {\rho_0}^2 f^{'}(\rho_c^*)$ where $\rho_c^* = B_l\rho_c$ and $\tau = \tau_c(1+\epsilon^2)$ into above equation, we achieve

$$\epsilon^4(\partial_T S - b_1\partial_X^3 S + b_2\partial_X S^3) + \epsilon^5(b_3\partial_X^2 S + b_4\partial_X^4 S + b_5\partial_X^2 S^3) = 0. \tag{6.23}$$

The values of coefficients b_i, which are named as in Eq. (6.23), are displayed in Table 6.4. $T = \frac{1}{b_1}T'$ and $S = \sqrt{\frac{b_1}{b_2}}S'$ are utilized to transform Eq. (6.23) into a conventional mKdV equation, then Eq. (6.23) turns into following form

$$\partial_{T'} S' - \partial_X^3 S' + \partial_X {S'}^3 + \frac{\epsilon}{b_1}\left[b_3\partial_X^2 S' + b_4\partial_X^4 S' + \frac{b_1 b_5}{b_2}\partial_X^2 {S'}^3\right] = 0. \tag{6.24}$$

The kink-antikink solution of the standard mKdV equation is achieved after omitting the term $O(\epsilon)$ as:

$$S_0'(X,T) = \sqrt{\mu}\tanh\left(\sqrt{\frac{\mu}{2}}(X - \mu T)\right), \tag{6.25}$$

where, μ is the propagation velocity and can be determined by solving the condition: $(S_0', M[S_0']) \equiv \int_{-\infty}^{\infty} dX S_0' M[S_0'] = 0$, where $M[S_0'] = \frac{1}{b_1}[b_3\partial_X^2 S' + b_4\partial_X^4 S' + \frac{b_1 b_5}{b_2}\partial_X^2 {S'}^3]$. Through the above modifications, the suitable choice of μ can be obtained as:

$$\mu = \frac{5b_2 b_3}{2b_2 b_4 - 3b_1 b_5}. \tag{6.26}$$

Hence, the kink-antikink solution is

Table 6.3: Values of h_i coefficients

coefficients	values	coefficients	values
h_1	$p + B_l C_l {\rho_0}^2 f'$	h_6	$\frac{B_l^3 C_l \rho_0^2 f'''}{6}$
h_2	$\frac{3p^2\tau}{2} + \frac{B_l C_l \rho_0^2 f'}{2}$	h_7	$3p\tau$
h_3	$\frac{B_l^2 C_l \rho_0^2 f''}{2}$	h_8	$\frac{5}{8}p^4\tau^3 + \frac{B_l C_l {\rho_0}^2 f'}{24}$
h_4	$\frac{7}{6}p^3\tau^2 + \frac{B_l C_l \rho_0^2 f'}{6}$	h_9	$\frac{B_l^2 C_l {\rho_0}^2 f''}{12}$
h_5	$\frac{B_l^2 C_l \rho_0^2 f''}{4}$	h_{10}	$\frac{B_l^3 C_l \rho_0^2 f'''}{12}$

Table 6.4: Values of b_i coefficients

coefficients	values
b_1	$-\frac{7}{6}p^3\tau_c^2 - \frac{B_l C_l \rho_0^2 f'}{6}$
b_2	$\frac{B_l^3 C_l \rho_0^2 f'''}{6}$
b_3	$\frac{3}{2}p^2\tau_c$
b_4	$\frac{5}{8}p^4\tau_c^3 + \frac{B_l C_l {\rho_0}^2 f'}{24} + 3p\tau_c b_1$
b_5	$\frac{B_l^3 C_l \rho_0^2 f'''}{12} - 3p\tau_c b_2$

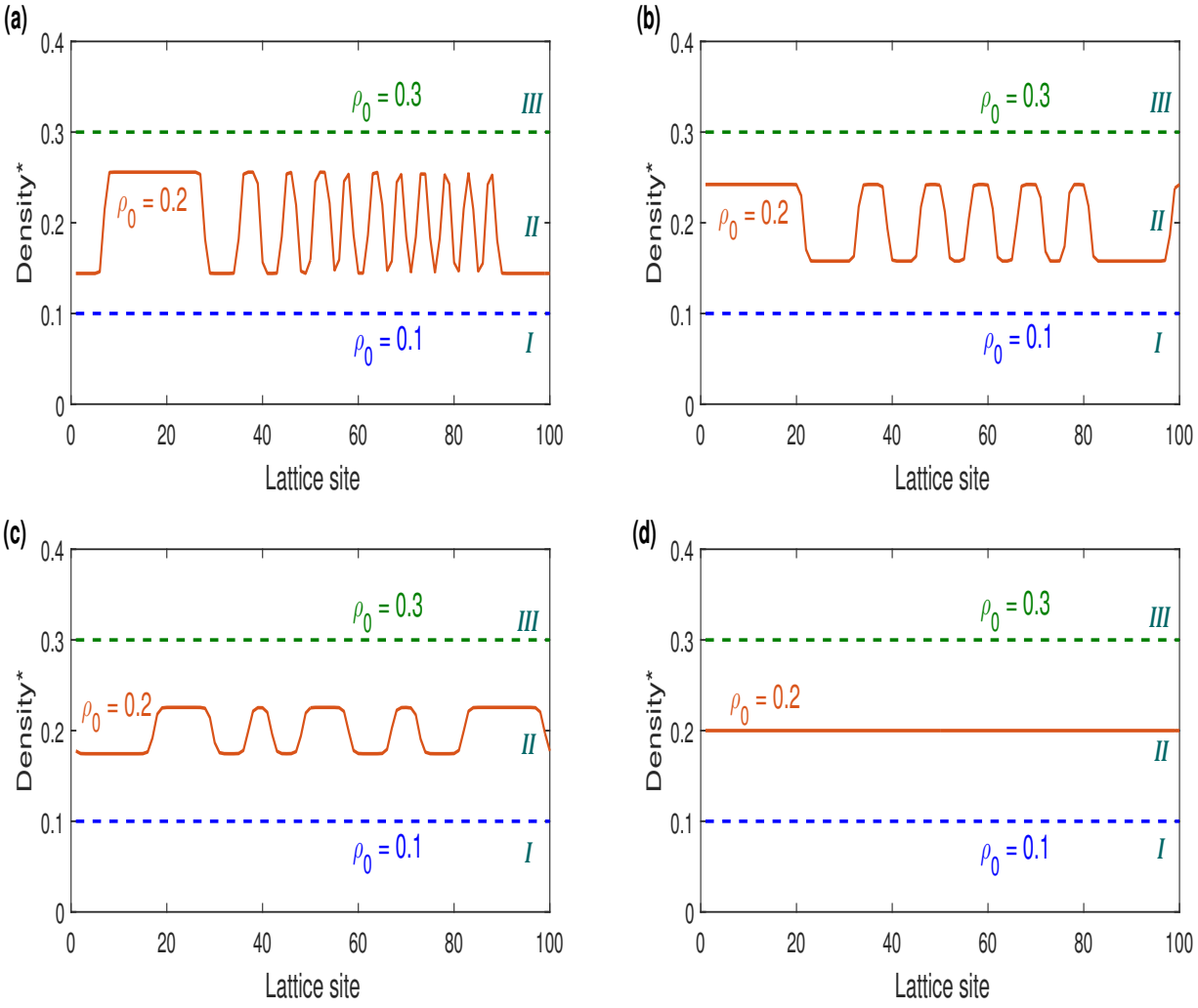

Figure 6.4: Density profiles with $a = 2.5$ at time $t = 25000$s for (a) $c = 0.1$, (b) $c = 0.2$, (c) $c = 0.3$, and (d) $c = 0.4$, respectively.

$$\rho_j^* = \rho_c + \alpha \tanh\Big(\sqrt{\frac{\mu}{2}}(X - \mu b_1 T)\Big), \quad \alpha(\text{amplitude}) = \sqrt{\frac{b_1\epsilon^2\mu}{b_2}},\ \epsilon^2 = \Big(\frac{\tau}{\tau_c} - 1\Big). \quad (6.27)$$

In the density-sensitivity (ρ, a) phase space, the kink-antikink soliton solution (6.27) is derived from the mKdV equation and describes the coexisting phase comprising of jammed and freely moving phases, as defined by $\rho_j^* = \rho_c \pm \alpha$.

In a further study, we have considered two types of vehicles ($m = 2$), i.e., $c_1 = c$ and $c_2 = 1 - c$. In Fig. 6.3, the phase plots are drawn for different values of c. The solid lines represent the neutral stability curves, and the dotted lines denote the coexisting curves derived from linear and nonlinear stability analysis, respectively, as displayed in Fig. 6.3. It is observed that the apex of curves decreases as the value of parameter c increases, which demonstrates that the traffic system becomes more stable as the fraction of high-sensitivity vehicles in vehicular systems increases. This is true because, in real-world traffic jams, smaller vehicles have higher sensitivity than larger vehicles and try to occupy the available space using lateral gaps to avoid congestion, which helps optimize the traffic flow, known as the area occupancy effect. In addition, the results show that the greater proportion of small vehicles is beneficial to diminishing traffic congestion in the vehicular system.

6.5 Numerical Simulations

To investigate the impact of area occupancy and to confirm the theoretical predictions (linear and nonlinear stability analysis) for the proposed heterogeneous disorder traffic flow model, numerical simulations are performed for a closed hypothetical road section. The initial conditions are chosen as homogeneous except near the central lattice, where a small perturbation is given as

$$\rho_j(0) = \rho_j(1) = \begin{cases} \rho_0; & j \neq \frac{N}{2}, \frac{N}{2} - 1 \\ \rho_0 + \Delta\rho; & j = \frac{N}{2} - 1 \\ \rho_0 - \Delta\rho; & j = \frac{N}{2} \end{cases}, \quad (6.28)$$

where $\Delta\rho = 0.005$ is the initial disturbance; N ($N = 100$) represents the total number of lattice sites; The value of sensitivity (a) is taken as 2.5 for numerical simulations.

Here, we have considered two types of vehicles with different area occupancy, where $c_1 = c$ and $c_2 = 1 - c$ represent the small and large types of vehicles, respectively. Therefore, in the numerical simulations, the effect of the fraction parameter (c) for heterogeneity is

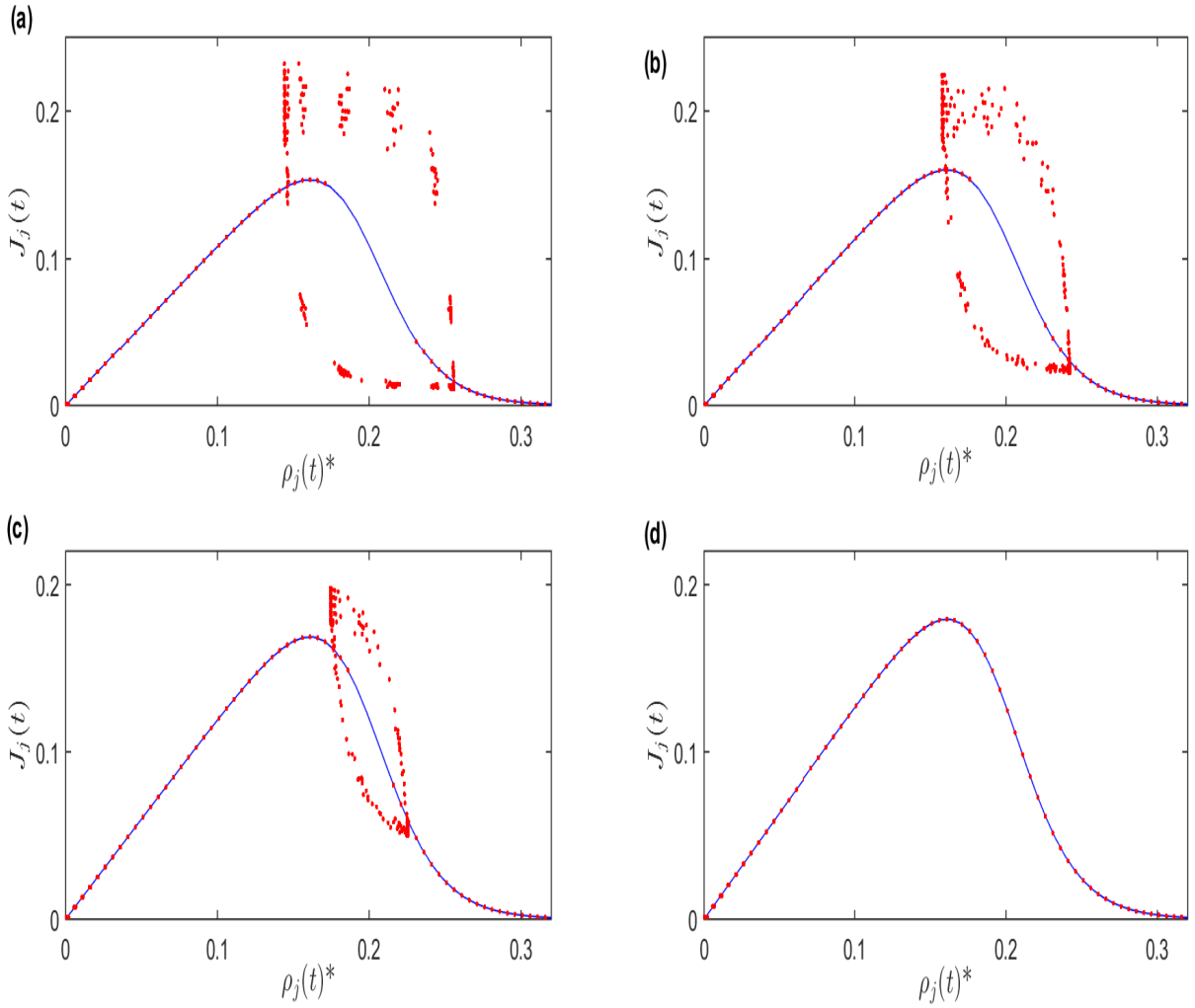

Figure 6.5: Instant flow ($J_j(t)$) versus density ($\rho_j(t)^*$) with $a = 2.5$ for (a) $c = 0.1$, (b) $c = 0.2$, (c) $c = 0.3$, and (d) $c = 0.4$, respectively.

analyzed by taking distinct initial densities. The results are shown after a sufficiently long time, i.e., $t = 25000$s.

Fig. 6.4(a)-(d) exhibits the density profiles corresponding to different values of c at fixed time $t = 25000$s. As shown in Fig. 6.4, the scenario for $\rho_0 = 0.1$ falls inside the stability region's domain (Region 1), and so no traffic congestion occurs in this case. However, with an increase in the value of ρ_0, i.e., $\rho_0 = 0.2$, the transition from Region 1 to Region 2 occurs. Further, for $\rho_0 = 0.3$, traffic situations are in the stable region's domain (Region 3), and traffic jams don't occur. Moreover, when $a > a_c$, the stability condition is satisfied, which we can see from our results at the value of $\rho_0 = 0.1$ and $\rho_0 = 0.3$. As illustrated in Fig. 6.4(a)-(c), when $a < a_c$ at $\rho_0 = 0.2$, the density curves arise in the form of kink–antikink soliton waves. However, as the value of c increases, the fluctuating amplitude of the kink-antikink waves substantially minimizes. When $c = 0.4$ at $\rho_0 = 0.2$, the stability criterion is fulfilled (Eq. 6.20), and the fluctuations of the density wave approaches zero, as shown in Fig. 6.4(d), where the initial disturbance dissipates. As a result, it is concluded that an increase in the small types of vehicles improves traffic flow stability, reduces traffic jams, and optimizes traffic flow.

Further, the effect of area occupancy by different types of vehicles is shown in Fig. 6.5. The plots show the profiles of instant current ($J_j(t)$) versus density ($\rho_j(t)^*$) by taking different values of c at time $t = 25000$s. In Fig. 6.5, the solid curve signifies the heterogeneous optimal traffic flow, which shows the relation between optimal flow and density. The red points are achieved from the simulation results. For the domain of the stable region (Region 1 and 3), the simulation results are the same as the theoretical results. In contrast, a group of dispersed points creates the limit cycle (closed-loop) that demonstrates the instability of traffic flow (Region 2). In Fig. 6.5(a)-(c), the hysteresis loop is formed around $\rho_0 = 0.2$ as the stability condition is not satisfied. The coexisting phase related to the dynamics of vehicles displaying the kink antikink density wave fluctuations is represented by the loop's lower and above-scattered points. The greater size of the closed loop represents the instability of traffic flow. It is noticed that the hysteresis loop starts to decline inward with an increase in the value of c, eventually convergent to a single point as illustrated in Fig. 6.5(d), indicating that the traffic flow has stabilized. This reaffirms that an increase in small vehicles can improve traffic flow stability.

The effect of heterogeneous traffic with area occupancy on the fundamental diagram is explored. Fig. 6.6 exhibits average flow-density patterns over a suitably long duration of time, i.e., $t = 20,000 - 25,000$s. The solid blue lines portray theoretical findings, and the red dots reflect simulation results. As we can see from Fig. 6.6 that the results achieved analytically and numerically are well-matched to each other in Regions 1 and 3 ($a > a_c$).

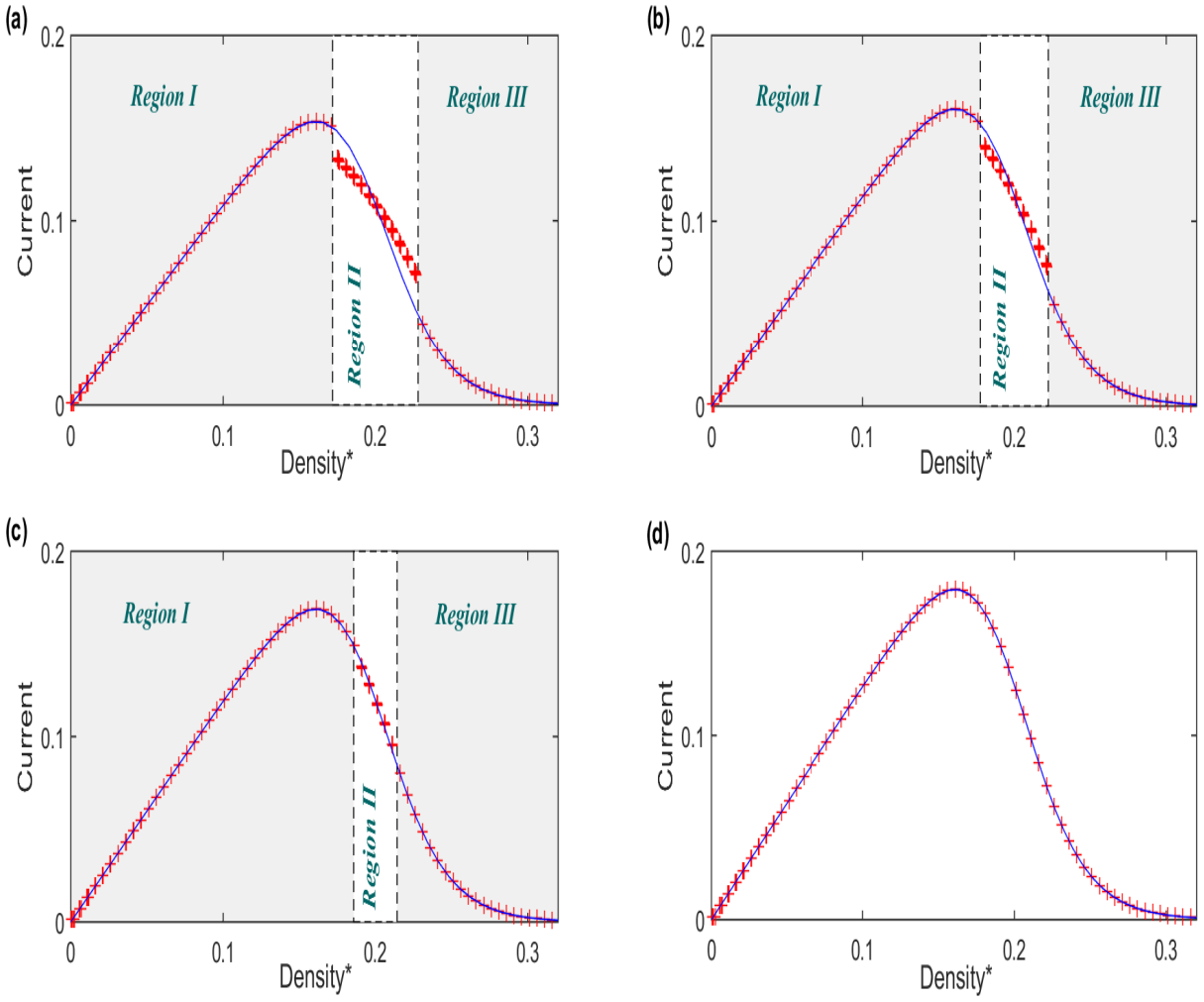

Figure 6.6: Plots of Current versus density with $a = 2.5$ for (a) $c = 0.1$, (b) $c = 0.2$, (c) $c = 0.3$, and (d) $c = 0.4$, respectively.

However, there are some variations between the results in Regions 2 for different values of c. The deviation signifies the traffic jam. It is found from Figure 6.6(a)-(c) that the variation occurs cause of kink-antikink density waves are generated in Fig. 6.4 as the stability condition is not satisfied ($a < a_c$). It's worth noting that when the value of c is increased, the variation from the theoretical curve diminishes and evolves into the uniform traffic flow, as displayed by Fig. 6.6(d).

In a disordered heterogeneous traffic environment, small vehicles can utilize the lateral gaps between the vehicles leading to a higher traffic flow rate [175]. As a result, it is found that the area occupancy effect plays a significant role in the non-lane-based heterogeneous traffic system. It is concluded that high numbers of small vehicles aid in optimizing the traffic flow.

6.6 Conclusion

In an actual traffic environment, vehicles with different characteristics can be seen on roadways. Due to heterogeneity behavior, vehicles do not adhere to lane discipline, resulting in a disordered traffic system. Besides previous studies, we concentrate on the area occupied by several types of vehicles in heterogeneous traffic. Therefore, the main aim of this chapter is to develop a lattice-based traffic model for a disordered heterogeneous traffic system prevalent in developing countries like India.

6.6.1 Research outcomes

The mixed traffic behavior is analyzed by taking different vehicles' fractions, sizes, and speeds. Moreover, stability analysis in terms of linear and nonlinear analysis and numerical simulations using finite difference schemes have been performed to illustrate the numerous interactions between various types of vehicles on traffic dynamics. In the traffic environment, the existence of one type of vehicle impacts the other vehicles' performance because of differences between their characteristics, including speed, fraction, and size as

- each type of vehicle has a different optimal speed on the road
- an increase in the number of one kind of vehicle affects the traffic efficiency
- diverse vehicles utilize the lateral space according to their size.

Vehicles react according to ahead traffic conditions. When lateral space is available ahead, small vehicles adjust their speed and position to utilize this space by immediately reacting

compared to large vehicles. Moreover, as evidenced by the theoretical results, when the proportion of small vehicles with high sensitivity grows, so does the stable region. The numerical solutions occur in terms of kink-antikink density waves, and the fluctuations can be seen when the stability condition is not satisfied. It is observed that some deviations arise between fundamental curves and simulation results. However, when we take the higher fraction of small vehicles, the variations completely disappear as the stability condition is satisfied. Numerical simulations confirm the theoretical predictions. It is concluded that small vehicles have more capability than larger vehicles to optimize the traffic flow and minimize traffic congestion. The theoretical and numerical results show that traffic flow stability improves whenever the number of small vehicles increases.

6.6.2 Future scope

- In the transportation system, vehicles can overtake each other based on speed and available road space. One limitation of this work is that it has only considered a one-lane traffic system without incorporating the effect of overtaking, whereas this factor may influence heterogeneous traffic efficiency.
- The proposed area occupancy model may be extended by considering the implications of overtaking [101,105], multi-lane [119,121], and two-dimensional [128,129] traffic dynamics in the future.

Chapter 7

Summary and future scope

This last chapter aims to summarize the thesis's key results and provide an outlook for future research. The traffic-related problems faced by road users, such as environmental issues and traffic jams, can be handled by implementing Intelligent Transportation Systems (ITSs). The present thesis's context is the modification, improvement, and evaluation of LH model, including the actual phenomena that exist in transportation with homogeneous and heterogeneous characteristics of vehicles.

7.1 Summary

The primary objective of mathematical traffic modelers is to represent aspects seen on roadways using a combination of analytic approaches and cutting-edge simulation. To understand the traffic flow phenomenon, traffic models are used, which have mainly categorized as microscopic and macroscopic approaches. Another class of models (the combination of microscopic and macroscopic models) known as the lattice hydrodynamic (LH) model has become famous for its simplicity and computational efficiency. The most significant contribution of the LH model is that the formation of traffic congestion can be shown in density waves. Moreover, the LH model is theoretically investigated via nonlinear and linear stability analysis. Additionally, the reduction perturbation technique is employed to obtain the kink-antikink density solution to the mKdV equation to reflect the congestion around the critical point. Furthermore, the presented work is motivated by the benefits of lattice hydrodynamic traffic flow models in representing and evaluating traffic features more realistically.

In the sequences of thesis contribution, in Chapter 1, an introduction to traffic flow theory is given. Various modeling techniques representing important characteristics of traffic flow are briefly detailed. The advantages and limitations of existing traffic models are presented. Afterward, the lattice model came into existence by incorporating the advantages of microscopic and macroscopic models and which is discussed. Additionally, the lattice model is able to comprehensively analyze the micro details of traffic through global variables, overcoming the limitations of existing models. Further, extensions over the lattice

model are also discussed by considering actual traffic phenomena.

In vehicular networks, ITS significantly impacts traffic dynamics. It provides prior information about downstream situations of traffic, which helps in the optimization of traffic flow and suppressing congestion. It was found that the predictive effect needs to be incorporated into the lattice hydrodynamic model. Hence, Chapters 2, 3, and 4 deal with checking the impact of the predictive effect on traffic dynamics by considering different road networks. In Chapter 2, the influence of predictive effect with passing is examined. Through theoretical analysis, it is found that the traffic flow stability is increased whenever more information about traffic conditions has received (an increment in the value of the predictive effect's coefficient). The results show that the connection between passing and predictive effect proves beneficial to suppress congestion. The different phase transitions occur in the case of the small and high values of the passing coefficient. Moreover, the influence of the predictive effect has proven positive for any value of the passing coefficient. Numerical simulations are conducted to check the reliability of theoretical findings and found consistent with theoretical ones.

In Chapter 3, the lane-changing behavior in a vehicular two-lane network is considered for investigating the influence of predictive effect with OCDE. Lane change happens when the upstream density on the first lane is lesser than the downstream density on another. Further, the phase diagrams are obtained through stability analysis (linear and nonlinear analysis) to show the importance of predictive effect on vehicular dynamics in both cases: with lane-changing and without lane-changing. It is observed from the results that the information about downstream traffic conditions plays an important role in stabilizing the traffic flow on two-lane highway with the consideration of OCDE when lane changing is permitted. Simulations are done, and the obtained results are compared with the analytical results and found consistent.

One-lane or multi-lane roads may be linked with other roads by the nodes (junctions). According to the situation, drivers can change their driving behavior while using their skills in advance with the help of prior information. Drivers can alter the route based on their destination at the junction. Therefore, Chapter 4 is devoted to analyzing the impact of prior information on a two-dimensional (2D) traffic system with the junction using a lattice approach. It is assumed that after crossing the junction point, some traffic from upstream may either go straight or turn left. Through the stability analysis, the traffic behavior is investigated with and without using a control signal. The results show that when drivers receive prior information about downstream traffic conditions, the traffic flow stability is increased in all directions. To test the reliability of theoretical findings, numerical simulations are carried out. It is concluded that prior knowledge is proven to

be helpful for two-dimensional traffic systems with junction roads.

Uncertain factors in the transportation system may have an impact on traffic flow. Many drivers attempt to adapt their speed to the smooth-steady depending on previous travel experience or historical information. Therefore, Chapter 5 demonstrates the effect of uncertainty about historical density information in the lattice model. The new lattice model is analyzed by stability analysis. It has been found that when uncertain factors happen while collecting and receiving traffic information, then traffic flow evolves into an unstable scenario. Further, numerical simulations of the new model have been performed to examine the effect of uncertain factors and validate the theoretical findings. Results show that the traffic flow stability is significantly influenced by uncertain historical density information, which impacts traffic behavior negatively.

All the proposed models in previous Chapters describe the homogeneous traffic phenomena, whereas heterogeneity between vehicles also exists. Chapter 6 reflects the heterogeneous traffic behavior, i.e., a lattice-based area occupancy model is developed for disordered heterogeneous traffic. Two types of vehicles (small and large) have been considered in investigating the impact of heterogeneity among vehicles by taking their different characteristics, such as velocity, occupied area, and sensitivity. Larger vehicles are assumed to have more reaction time than small vehicles. Small vehicles alter their speed and position to use the available lateral space ahead by reacting immediately because of high sensitivity compared to large vehicles. Moreover, the results have been displayed by theoretically taking different proportions of vehicles. The results depict that the traffic flow stability increases when a proportion of high-sensitivity (small) vehicles grows. Additionally, to justify the theoretical findings, numerical simulations are performed. It is found that small vehicles having less size and high sensitivity help enhance traffic stability.

The proposed lattice hydrodynamic models with different aspects have been theoretically and numerically analyzed under hypothetical test scenarios in this thesis. Moreover, the special cases related to the new proposed LH model are discussed that may recover the existing models in the literature. Furthermore, the outcomes from the proposed models are compared to existing ones. The models provided in this thesis have been proven to be an improvement over previous research. We anticipate that our work will contribute to a better understanding of traffic flow dynamics.

7.2 Future scope

Possible future research directions are suggested on the basis of the proposed models in this thesis;

- In a traffic environment, two types of tollgates exist: manual and electronic. In comparison to manual tollgates, electronic tollgates are quite important. As a result, the lattice model may be used to evaluate the influences of both kinds.
- The predictive effect on a vehicular network is examined by considering limited road types (Chapter 2. 3 and 4). However, multi-lane, curved, and higher dimensional roads are also available in traffic phenomena. Therefore, the presented models can be further extended for mentioned types of roads.
- The influence of key aspects of traffic dynamics, such as fuel and energy usage, etc., might be examined by utilizing the proposed homogeneous and heterogeneous traffic lattice models.
- Sometimes, the roads are partially blocked due to construction or another reason which leads to diverted traffic resulting in impacts on the traffic flow. Therefore, numerous road features, including blockages and bottlenecks, need to investigate. Additionally, the proposed work may be expanded to include lane merging and diverging in a multi-lane traffic network.
- The heterogeneity between vehicles has been studied (Chapter 6), whereas different characteristics of drivers (experienced/inexperienced, timid/aggressive, etc.) also exist, which play a significant role in the traffic stream. Further, new LH models can be analyzed for heterogeneity of drivers, heterogeneous lane changing and heterogeneous passing rates, etc.
- Due to the rapidly growing autonomous vehicle sector, the traffic system may soon become a mixture of the manual (human driving) and autonomous (self-driving) vehicles. Accident rates that could occur as a result of driver distraction decrease with the help of autonomous vehicles. Hence, the lattice model may be qualitatively improved by incorporating the notion of self-driving vehicles.
- Finally, experimental investigation can be conducted to verify existing models' results.

Bibliography

[1] R. Kaur, S. Sharma, Analysis and modeling of some traffic characteristics using lattice hydrodynamic approach, PhD thesis (2021).

[2] V. L. Knoop, Introduction to traffic flow theory: An introduction with exercises, Delft University of Technology (2018).

[3] B. S. Kerner, Complex dynamics of traffic management, Springer, 2019.

[4] T. Nagatani, The physics of traffic jams, Reports on progress in physics 65 (9) (2002) 1331.

[5] D. Helbing, Traffic and related self-driven many-particle systems, Reviews of Modern Physics 73 (4) (2001) 1067.

[6] D. Chowdhury, L. Santen, A. Schadschneider, Statistical physics of vehicular traffic and some related systems, Physics Reports 329 (4-6) (2000) 199–329.

[7] D. Helbing, H. J. Herrmann, M. Schreckenberg, D. E. Wolf, Traffic and granular flow'99: social, traffic, and granular dynamics, Springer Science & Business Media, 2012.

[8] M. Treiber, A. Kesting, Traffic flow dynamics: data, models and simulation, Physics Today 67 (3) (2014) 54.

[9] I. Prigogine, R. Herman, Kinetic theory of vehicular traffic, Tech. rep. (1971).

[10] W. Leutzbach, Introduction to the theory of traffic flow, Vol. 47, Springer, 1988.

[11] C. F. Daganzo, Requiem for second-order fluid approximations of traffic flow, Transportation Research Part B: Methodological 29 (4) (1995) 277–286.

[12] V. Tyagi, S. Darbha, K. R. Rajagopal, A review of the mathematical models for traffic flow, International Journal of Advances in Engineering Sciences and Applied Mathematics 1 (1) (2009) 53–68.

[13] S. Darbha, K. R. Rajagopal, V. Tyagi, A review of mathematical models for the flow of traffic and some recent results, Nonlinear analysis: Theory, methods & applications 69 (3) (2008) 950–970.

[14] F. van Wageningen-Kessels, Multi-class continuum traffic flow models: analysis and simulation methods, Delft University of Technology (2013).

[15] M. Rose, Modeling of freeway traffic (2004).

[16] R. Herman, K. Gardels, Vehicular traffic flow, Scientific American 209 (6) (1963) 35–43.

[17] D. C. Gazis, Mathematical theory of automobile traffic: Improved understanding and control of traffic flow has become a fast-growing area of scientific research., Science 157 (3786) (1967) 273–281.

[18] R. Rothery, Transportation research board (trb) special report 165, Traffic Flow Theory (1998).

[19] G. F. Newell, Nonlinear effects in the dynamics of car following, Operations Research 9 (2) (1961) 209–229.

[20] L. A. Pipes, An operational analysis of traffic dynamics, Journal of Applied Physics 24 (3) (1953) 274–281.

[21] R. E. Chandler, R. Herman, E. W. Montroll, Traffic dynamics: studies in car following, Operations Research 6 (2) (1958) 165–184.

[22] R. Herman, Car-following and steady state flow, in: Theory of Traffic Flow Symposium Proceedings, 1959, pp. 1–13.

[23] R. Herman, R. B. Potts, Single lane traffic theory and experiment (1959).

[24] D. C. Gazis, R. Herman, R. B. Potts, Car-following theory of steady-state traffic flow, Operations Research 7 (4) (1959) 499–505.

[25] D. C. Gazis, R. Herman, R. W. Rothery, Nonlinear follow-the-leader models of traffic flow, Operations Research 9 (4) (1961) 545–567.

[26] M. Bando, K. Hasebe, K. Nakanishi, A. Nakayama, A. Shibata, Y. Sugiyama, Phenomenological study of dynamical model of traffic flow, Journal de Physique I 5 (11) (1995) 1389–1399.

[27] M. Bando, K. Hasebe, A. Nakayama, A. Shibata, Y. Sugiyama, Structure stability of congestion in traffic dynamics, Japan Journal of Industrial and Applied Mathematics 11 (2) (1994) 203–223.

[28] M. Bando, K. Hasebe, A. Nakayama, A. Shibata, Y. Sugiyama, Dynamical model of traffic congestion and numerical simulation, Physical Review E 51 (2) (1995) 1035.

[29] T. Nagatani, Stabilization and enhancement of traffic flow by the next-nearest-neighbor interaction, Physical Review E 60 (6) (1999) 6395.

[30] R. Jiang, Q. Wu, Z. Zhu, Full velocity difference model for a car-following theory, Physical Review E 64 (1) (2001) 017101.

[31] G. H. Peng, X. H. Cai, C. Q. Liu, B. F. Cao, M. X. Tuo, Optimal velocity difference model for a car-following theory, Physics Letters A 375 (45) (2011) 3973–3977.

[32] C. Chen, H. X. Ge, R. J. Cheng, Self-stabilizing analysis of an extended car-following model with consideration of expected effect, Physica A: Statistical Mechanics and its Applications 535 (2019) 122423.

[33] S. Jiao, S. Zhang, B. Zhou, L. Zhang, L. Xue, Dynamic performance and safety analysis of car-following models considering collision sensitivity, Physica A: Statistical Mechanics and its Applications 564 (2021) 125504.

[34] G. H. Peng, H. D. He, W. Z. Lu, A new car-following model with the consideration of incorporating timid and aggressive driving behaviors, Physica A: Statistical Mechanics and its Applications 442 (2016) 197–202.

[35] H. Y. Wen, Y. Rong, C. B. Zeng, W. W. Qi, The effect of driver's characteristics on the stability of traffic flow under honk environment, Nonlinear Dynamics 84 (3) (2016) 1517–1528.

[36] Z. Li, X. Xu, S. Xu, Y. Qian, A heterogeneous traffic flow model consisting of two types of vehicles with different sensitivities, Communications in Nonlinear Science and Numerical Simulation 42 (2017) 132–145.

[37] B. Yu, H. Zhou, L. Wang, Z. Wang, S. Cui, An extended two-lane car-following model considering the influence of heterogeneous speed information on drivers with different characteristics under honk environment, Physica A: Statistical Mechanics and its Applications 578 (2021) 126022.

[38] C. Zhai, W. Wu, S. Luo, Heterogeneous traffic flow modeling with drivers' timid and aggressive characteristics, Chinese Physics B 30 (10) (2021) 100507.

[39] S. Jin, D. Wang, P. Tao, P. Li, Non-lane-based full velocity difference car following model, Physica A: Statistical Mechanics and its Applications 389 (21) (2010) 4654–4662.

[40] Y. Li, L. Zhang, S. Peeta, H. Pan, T. Zheng, Y. Li, X. He, Non-lane-discipline-based car-following model considering the effects of two-sided lateral gaps, Nonlinear Dynamics 80 (1) (2015) 227–238.

[41] Y. Li, L. Zhang, H. Zheng, X. He, S. Peeta, T. Zheng, Y. Li, Nonlane-discipline-based car-following model for electric vehicles in transportation-cyber-physical systems, IEEE Transactions on Intelligent Transportation Systems 19 (1) (2017) 38–47.

[42] M. J. Lighthill, G. B. Whitham, On kinematic waves ii. a theory of traffic flow on long crowded roads, Proceedings of the Royal Society of London. Series A. Mathematical and Physical Sciences 229 (1178) (1955) 317–345.

[43] P. I. Richards, Shock waves on the highway, Operations Research 4 (1) (1956) 42–51.

[44] H. J. Payne, Model of freeway traffic and control, Mathematical Model of Public System (1971) 51–61.

[45] P. G. Michalopoulos, P. Yi, A. S. Lyrintzis, Development of an improved high-order continuum traffic flow model, Transportation Research Record (1365) (1992).

[46] G. Q. Liu, A. S. Lyrintzis, P. G. Michalopoulos, Modelling of freeway merging and diverging flow dynamics, Applied Mathematical Modelling 20 (6) (1996) 459–469.

[47] H. M. Zhang, A theory of nonequilibrium traffic flow, Transportation Research Part B: Methodological 32 (7) (1998) 485–498.

[48] A. Aw, M. Rascle, Resurrection of "second order" models of traffic flow, SIAM Journal on Applied Mathematics 60 (3) (2000) 916–938.

[49] R. Jiang, Q. S. Wu, Z. J. Zhu, A new continuum model for traffic flow and numerical tests, Transportation Research Part B: Methodological 36 (5) (2002) 405–419.

[50] H. M. Zhang, A non-equilibrium traffic model devoid of gas-like behavior, Transportation Research Part B: Methodological 36 (3) (2002) 275–290.

[51] Y. Xue, S. Q. Dai, Continuum traffic model with the consideration of two delay time scales, Physical Review E 68 (6) (2003) 066123.

[52] M. Papageorgiou, J.-M. Blosseville, H. Hadj-Salem, Macroscopic modelling of traffic flow on the boulevard périphérique in paris, Transportation Research Part B: Methodological 23 (1) (1989) 29–47.

[53] W. F. Phillips, A new continuum traffic model obtained from kinetic theory, in: 1978 IEEE Conference on Decision and Control including the 17th Symposium on Adaptive Processes, IEEE, 1979, pp. 1032–1036.

[54] P. Ross, Traffic dynamics, Transportation Research Part B: Methodological 22 (6) (1988) 421–435.

[55] H. Huang, T. Tang, Z. Gao, Continuum modeling for two-lane traffic flow, Acta Mechanica Sinica 22 (2) (2006) 131–137.

[56] D. H. Sun, G. H. Peng, A viscous continuum traffic flow model with consideration of the coupling effect for two-lane freeways, Chinese Physics B 18 (9) (2009) 3724.

[57] T. Q. Tang, C. Y. Li, H. J. Huang, H. Y. Shang, A new fundamental diagram theory with the individual difference of the driver's perception ability, Nonlinear Dynamics 67 (3) (2012) 2255–2265.

[58] T. Q. Tang, Y. P. Wang, G. Z. Yu, H. J. Huang, A stochastic lwr model with consideration of the driver's individual property, Communications in Theoretical Physics 58 (4) (2012) 583.

[59] T. Q. Tang, H. J. Huang, H. Y. Shang, An extended macro traffic flow model accounting for the driver's bounded rationality and numerical tests, Physica A: Statistical Mechanics and its Applications 468 (2017) 322–333.

[60] A. K. Gupta, I. Dhiman, Phase diagram of a continuum traffic flow model with a static bottleneck, Nonlinear Dynamics 79 (1) (2015) 663–671.

[61] T. Q. Tang, P. Li, X. B. Yang, An extended macro model for traffic flow with consideration of multi static bottlenecks, Physica A: Statistical Mechanics and its Applications 392 (17) (2013) 3537–3545.

[62] A. K. Gupta, V. K. Katiyar, Analyses of shock waves and jams in traffic flow, Journal of Physics A: Mathematical and General 38 (19) (2005) 4069.

[63] A. K. Gupta, A section approach to a traffic flow model on networks, International Journal of Modern Physics C 24 (05) (2013) 1350018.

[64] Q. T. Zhai, H. X. Ge, R. J. Cheng, An extended continuum model considering optimal velocity change with memory and numerical tests, Physica A: Statistical Mechanics and its Applications 490 (2018) 774–785.

[65] C. Zhai, W. T. Wu, A continuum model considering the uncertain velocity of preceding vehicles on gradient highways, Physica A: Statistical Mechanics and its Applications 588 (2022) 126561.

[66] T. Q. Tang, H. J. Huang, S. G. Zhao, H. Y. Shang, A new dynamic model for heterogeneous traffic flow, Physics Letters A 373 (29) (2009) 2461–2466.

[67] S. P. Hoogendoorn, Multiclass continuum modelling of multilane traffic flow (1999).

[68] D. Ngoduy, Macroscopic discontinuity modeling for multiclass multilane traffic flow operations. (2006).

[69] D. Ngoduy, R. Liu, Multiclass first-order simulation model to explain non-linear traffic phenomena, Physica A: Statistical Mechanics and its Applications 385 (2) (2007) 667–682.

[70] A. K. Gupta, I. Dhiman, Analyses of a continuum traffic flow model for a nonlane-based system, International Journal of Modern Physics C 25 (10) (2014) 1450045.

[71] V. T. Arasan, G. Dhivya, Measuring heterogeneous traffic density, International Journal of Civil and Environmental Engineering 2 (10) (2008) 236–240.

[72] C. Mallikarjuna, K. R. Rao, Area occupancy characteristics of heterogeneous traffic, Transportmetrica 2 (3) (2006) 223–236.

[73] R. Mohan, G. Ramadurai, Heterogeneous traffic flow modelling using second-order macroscopic continuum model, Physics Letters A 381 (3) (2017) 115–123.

[74] R. Mohan, G. Ramadurai, State-of-the art of macroscopic traffic flow modelling, International Journal of Advances in Engineering Sciences and Applied Mathematics 5 (2) (2013) 158–176.

[75] Y. Sugiyama, A. Nakayama, M. Fukui, K. Hasebe, M. Kikuchi, K. Nishinari, S.-i. Tadaki, S. Yukawa, Observation, theory and experiment for freeway traffic as physics of many-body system, in: Traffic and Granular Flow'03, Springer, 2005, pp. 45–58.

[76] Y. Sugiyama, M. Fukui, M. Kikuchi, K. Hasebe, A. Nakayama, K. Nishinari, S.-i. Tadaki, S. Yukawa, Traffic jams without bottlenecks-experimental evidence for the physical mechanism of the formation of a jam, New Journal of Physics 10 (3) (2008) 033001.

[77] A. Nakayama, M. Fukui, M. Kikuchi, K. Hasebe, K. Nishinari, Y. Sugiyama, S.-i. Tadaki, S. Yukawa, Metastability in the formation of an experimental traffic jam, New Journal of Physics 11 (8) (2009) 083025.

[78] M. Muramatsu, T. Nagatani, Soliton and kink jams in traffic flow with open boundaries, Physical Review E 60 (1) (1999) 180.

[79] D. A. Kurtze, D. C. Hong, Traffic jams, granular flow, and soliton selection, Physical Review E 52 (1) (1995) 218.

[80] B. S. Kerner, P. Konhäuser, Cluster effect in initially homogeneous traffic flow, Physical Review E 48 (4) (1993) R2335.

[81] K. Brauer, The korteweg-de vries equation: history, exact solutions, and graphical representation, University of Osnabrück/Germany1 (2000).

[82] T. S. Komatsu, S.-i. Sasa, Kink soliton characterizing traffic congestion, Physical Review E 52 (5) (1995) 5574.

[83] T. Nagatani, Modified kdv equation for jamming transition in the continuum models of traffic, Physica A: Statistical Mechanics and its Applications 261 (3-4) (1998) 599–607.

[84] U. Makhloga, Improving india's traffic management using intelligent transportation systems (2022).

[85] T. Wang, R. Zang, K. Xu, J. Zhang, Analysis of predictive effect on lattice hydrodynamic traffic flow model, Physica A: Statistical Mechanics and its Applications 526 (2019) 120711.

[86] C. Tian, D. H. Sun, M. Zhang, Nonlinear analysis of lattice model with consideration of optimal current difference, Communications in Nonlinear Science and Numerical Simulation 16 (11) (2011) 4524–4529.

[87] D. H. Sun, M. Zhang, T. Chuan, Multiple optimal current difference effect in the lattice traffic flow model, Modern Physics Letters B 28 (11) (2014) 1450091.

[88] G. H. Peng, S. H. Yang, H. Z. Zhao, New feedback control model in the lattice hydrodynamic model considering the historic optimal velocity difference effect, Communications in Theoretical Physics 70 (6) (2018) 803.

[89] H. X. Ge, R. J. Cheng, The "backward looking" effect in the lattice hydrodynamic model, Physica A: Statistical Mechanics and its Applications 387 (28) (2008) 6952–6958.

[90] C. T. Jiang, R. J. Cheng, H. X. Ge, An improved lattice hydrodynamic model considering the "backward looking" effect and the traffic interruption probability, Nonlinear Dynamics 91 (2) (2018) 777–784.

[91] Q. Y. Wang, H. X. Ge, An improved lattice hydrodynamic model accounting for the effect of "backward looking" and flow integral, Physica A: Statistical Mechanics and its Applications 513 (2019) 438–446.

[92] X. Y. Qi, H. X. Ge, R. J. Cheng, Analysis of a novel lattice hydrodynamic model considering density integral and "backward looking" effect, Physica A: Statistical Mechanics and its Applications 525 (2019) 714–723.

[93] G. H. Peng, A new lattice model of traffic flow with the consideration of individual difference of anticipation driving behavior, Communications in Nonlinear Science and Numerical Simulation 18 (10) (2013) 2801–2806.

[94] A. K. Gupta, P. Redhu, Analyses of the driver's anticipation effect in a new lattice hydrodynamic traffic flow model with passing, Nonlinear Dynamics 76 (2) (2014) 1001–1011.

[95] G. H. Peng, H. Kuang, L. Qing, A new lattice model of traffic flow considering driver's anticipation effect of the traffic interruption probability, Physica A: Statistical Mechanics and its Applications 507 (10) (2018) 374–380.

[96] J. F. Tian, Z. Z. Yuan, B. Jia, M. H. Li, G. J. Jiang, The stabilization effect of the density difference in the modified lattice hydrodynamic model of traffic flow, Physica A: Statistical Mechanics and its Applications 391 (19) (2012) 4476–4482.

[97] G. H. Peng, S. H. Yang, H. Z. Zhao, A delayed-feedback control method for the lattice hydrodynamic model caused by the historic density difference effect, Physica A: Statistical Mechanics and its Applications 509 (11) (2018) 855–860.

[98] G. H. Peng, S. H. Yang, H. Z. Zhao, New feedback control model in the lattice hydrodynamic model considering the historic optimal velocity difference effect, Communications in Theoretical Physics 70 (6) (2018) 803–807.

[99] G. H. Peng, S. H. Yang, L. Qing, Feedback control pattern for a new lattice hydrodynamic model accounting for historic evolution information, International Journal of Control 93 (10) (2020) 2370–2377.

[100] N. Madaan, S. Sharma, Effects of multi-phase optimal velocity function on a lattice model accounting for driver's behavior, International Journal of Modern Physics B 33 (22) (2019) 1950248.

[101] T. Nagatani, Chaotic jam and phase transition in traffic flow with passing, Physical Review E 60 (2) (1999) 1535.

[102] A. K. Gupta, P. Redhu, Analyses of the driver's anticipation effect in a new lattice hydrodynamic traffic flow model with passing, Nonlinear Dynamics 76 (2) (2014) 1001–1011.

[103] P. Redhu, A. K. Gupta, Jamming transitions and the effect of interruption probability in a lattice traffic flow model with passing, Physica A: Statistical Mechanics And its Applications 421 (2015) 249–260.

[104] S. Sharma, Modeling and analyses of driver's characteristics in a traffic system with passing, Nonlinear Dynamics 86 (3) (2016) 2093–2104.

[105] A. K. Gupta, S. Sharma, P. Redhu, Effect of multi-phase optimal velocity function on jamming transition in a lattice hydrodynamic model with passing, Nonlinear Dynamics 80 (3) (2015) 1091–1108.

[106] R. Kaur, S. Sharma, Analyses of lattice hydrodynamic model using delayed feedback control with passing, Physica A: Statistical Mechanics and its Applications 510 (2018) 446–455.

[107] T. Nagatani, Jamming transitions and the modified korteweg–de vries equation in a two-lane traffic flow, Physica A: Statistical Mechanics and its Applications 265 (1-2) (1999) 297–310.

[108] T. Wang, Z. Y. Gao, X. M. Zhao, J. F. Tian, W. Y. Zhang, Flow difference effect in the two-lane lattice hydrodynamic model, Chinese Physics B 21 (7) (2012) 070507.

[109] G. H. Peng, X. H. Cai, C. Q. Liu, M. X. Tuo, A new lattice model of traffic flow with the anticipation effect of potential lane changing, Physics Letters A 376 (4) (2012) 447–451.

[110] G. H. Peng, A new lattice model of two-lane traffic flow with the consideration of optimal current difference, Communications in Nonlinear Science and Numerical Simulation 18 (3) (2013) 559–566.

[111] A. K. Gupta, P. Redhu, Analysis of a modified two-lane lattice model by considering the density difference effect, Communications in Nonlinear Science and Numerical Simulation 19 (5) (2014) 1600–1610.

[112] S. Sharma, Lattice hydrodynamic modeling of two-lane traffic flow with timid and aggressive driving behavior, Physica A: Statistical Mechanics and its Applications 421 (2015) 401–411.

[113] G. H. Peng, S. H. Yang, D. X. Xia, X. Q. Li, Impact of lattice's self-anticipative density on traffic stability of lattice model on two lanes, Nonlinear Dynamics 94 (4) (2018) 2969–2977.

[114] G. H. Peng, H. Kuang, H. Z. Zhao, L. Qing, Nonlinear analysis of a new lattice hydrodynamic model with the consideration of honk effect on flux for two-lane highway, Physica A: Statistical Mechanics and its Applications 515 (2) (2019) 93–101.

[115] G. H. Peng, H. Kuang, K. H. Bai, The impact of the individual difference on traffic flow under honk environment in lattice hydrodynamic model, Physica A: Statistical Mechanics and its Applications 526 (2019) 120772.

[116] X. Q. Li, K. L. Fang, G. H. Peng, A new lattice model accounting for multiple optimal current differences' anticipation effect in two-lane system, Physica A: Statistical Mechanics and its Applications 486 (2017) 814–826.

[117] A. K. Gupta, P. Redhu, Analyses of driver's anticipation effect in sensing relative flux in a new lattice model for two-lane traffic system, Physica A: Statistical Mechanics and its Applications 392 (22) (2013) 5622–5632.

[118] S. Sharma, Effect of driver's anticipation in a new two-lane lattice model with the consideration of optimal current difference, Nonlinear Dynamics 81 (1-2) (2015) 991–1003.

[119] N. Madaan, S. Sharma, A lattice model accounting for multi-lane traffic system, Physica A: Statistical Mechanics and its Applications 564 (2021) 125446.

[120] N. Madaan, S. Sharma, Influence of driver's behavior with empirical lane changing on the traffic dynamics, The European Physical Journal B 95 (1) (2022) 1–11.

[121] N. Madaan, S. Sharma, Delayed-feedback control in multi-lane traffic system, Physica A: Statistical Mechanics and its Applications 599 (2022) 127393.

[122] J. Zhou, Z. K. Shi, Lattice hydrodynamic model for traffic flow on curved road, Nonlinear Dynamics 83 (3) (2016) 1217–1236.

[123] R. Kaur, S. Sharma, Analysis of driver's characteristics on a curved road in a lattice model, Physica A: Statistical Mechanics and its Applications 471 (2017) 59–67.

[124] J. Zhou, Z. K. Shi, C. P. Wang, Lattice hydrodynamic model for two-lane traffic flow on curved road, Nonlinear Dynamics 85 (3) (2016) 1423–1443.

[125] Y. D. Jin, J. Zhou, Z. K. Shi, H. L. Zhang, C. P. Wang, Lattice hydrodynamic model for traffic flow on curved road with passing, Nonlinear Dynamics 89 (1) (2017) 107–124.

[126] T. Wang, R. J. Cheng, H. X. Ge, An extended two-lane lattice hydrodynamic model for traffic flow on curved road with passing, Physica A: Statistical Mechanics and its Applications 533 (2019) 121915.

[127] T. Nagatani, Jamming transition in a two-dimensional traffic flow model, Physical Review E 59 (5) (1999) 4857.

[128] A. K. Gupta, P. Redhu, Jamming transition of a two-dimensional traffic dynamics with consideration of optimal current difference, Physics Letters A 377 (34-36) (2013) 2027–2033.

[129] P. Redhu, A. K. Gupta, Phase transition in a two-dimensional triangular flow with consideration of optimal current difference effect, Nonlinear Dynamics 78 (2) (2014) 957–968.

[130] C. Zhai, W. T. Wu, A modified two-dimensional triangular lattice model under honk environment, International Journal of Modern Physics C 31 (06) (2020) 2050089.

[131] L. X. Li, R. J. Cheng, H. X. Ge, New feedback control for a novel two-dimensional lattice hydrodynamic model considering driver's memory effect, Physica A: Statistical Mechanics and its Applications 561 (2021) 125295.

[132] R. Kaur, S. Sharma, Analyses of a heterogeneous lattice hydrodynamic model with low and high-sensitivity vehicles, Physics Letters A 382 (22) (2018) 1449–1455.

[133] D. Kaur, S. Sharma, A. K. Gupta, Analyses of lattice hydrodynamic area occupancy model for heterogeneous disorder traffic, Physica A: Statistical Mechanics and its Applications 607 (2022) 128184.

[134] H. X. Ge, S. Q. Dai, L. Y. Dong, Y. Xue, Stabilization effect of traffic flow in an extended car-following model based on an intelligent transportation system application, Physical Review E 70 (6) (2004) 066134.

[135] T. Q. Tang, Q. Yu, K. Liu, Analysis of the traffic running cost in a two-route system with feedback strategy, Physica A: Statistical Mechanics and its Applications 466 (2017) 1–9.

[136] W. X. Zhu, H. M. Zhang, Analysis of mixed traffic flow with human-driving and autonomous cars based on car-following model, Physica A: Statistical Mechanics and its Applications 496 (2018) 274–285.

[137] G. Zhang, D. H. Sun, M. Zhao, X. Y. Liao, W. N. Liu, T. Zhou, An extended car-following model accounting for cooperation driving system with velocity uncertainty, Physica A: Statistical Mechanics and its Applications 505 (2018) 1008–1017.

[138] Y. Q. Sun, H. X. Ge, R. J. Cheng, An extended car-following model considering driver's memory and average speed of preceding vehicles with control strategy, Physica A: Statistical Mechanics and its Applications 521 (2019) 752–761.

[139] S. An, L. Xu, G. Chen, Z. Shi, A new car-following model on complex road considering driver's characteristics, Modern Physics Letters B 34 (16) (2020) 2050182.

[140] P. Liao, T. Q. Tang, T. Wang, J. Zhang, A car-following model accounting for the driving habits, Physica A: Statistical Mechanics and its Applications 525 (2019) 108–118.

[141] S. H. Li, T. Wang, R. J. Cheng, H. X. Ge, An extended car-following model considering the driver's desire for smooth driving and self-stabilizing control with velocity uncertainty, Mathematical Problems in Engineering 2020 (2020).

[142] C. Zhai, W. T. Wu, A continuous traffic flow model considering predictive headway variation and preceding vehicle's taillight effect, Physica A: Statistical Mechanics and its Applications 584 (2021) 126364.

[143] G. Y. Ma, M. H. Ma, S. D. Liang, Y. S. Wang, H. Guo, Nonlinear analysis of the car-following model considering headway changes with memory and backward looking effect, Physica A: Statistical Mechanics and its Applications 562 (2021) 125303.

[144] M. Ma, G. Y. Ma, S. D. Liang, Density waves in car-following model for autonomous vehicles with backward looking effect, Applied Mathematical Modelling 94 (2021) 1–12.

[145] W. Ren, R. J. Cheng, H. X. Ge, Bifurcation analysis of a heterogeneous continuum traffic flow model, Applied Mathematical Modelling 94 (2021) 369–387.

[146] P. Redhu, A. K. Gupta, Effect of forward looking sites on a multi-phase lattice hydrodynamic model, Physica A: Statistical Mechanics and its Applications 445 (2016) 150–160.

[147] P. Redhu, V. Siwach, An extended lattice model accounting for traffic jerk, Physica A: Statistical Mechanics and its Applications 492 (2018) 1473–1480.

[148] T. Q. Tang, T. Wang, L. Chen, H. J. Huang, Analysis of the equilibrium trip cost accounting for the fuel cost in a single-lane traffic system without late arrival, Physica A: Statistical Mechanics and its Applications 490 (2018) 451–457.

[149] T. Q. Tang, H. J. Huang, H. Y. Shang, Influences of the driver's bounded rationality on micro driving behavior, fuel consumption and emissions, Transportation Research Part D: Transport and Environment 41 (2015) 423–432.

[150] E. D. Angelis, Nonlinear hydrodynamic models of traffic flow modelling and mathematical problems, Mathematical and Computer Modelling 29 (7) (1999) 83–95.

[151] A. K. Gupta, V. K. Katiyar, A new anisotropic continuum model for traffic flow, Physica A: Statistical Mechanics and its Applications 368 (2) (2006) 551–559.

[152] G. H. Peng, H. Kuang, L. Qing, Feedback control method in lattice hydrodynamic model under honk environment, Physica A: Statistical Mechanics and its Applications 509 (11) (2018) 651–656.

[153] G. H. Peng, A new lattice model of two-lane traffic flow with the consideration of optimal current difference, Communications in Nonlinear Science and Numerical Simulation 18 (3) (2013) 559–566.

[154] G. H. Peng, H. D. He, W. Z. Lu, A new lattice model with the consideration of the traffic interruption probability for two-lane traffic flow, Nonlinear Dynamics 81 (1-2) (2015) 417–424.

[155] F. X. Sun, A. H. F. Chow, S. M. Lo, H. X. Ge, A two-lane lattice hydrodynamic model with heterogeneous lane changing rates, Physica A: Statistical Mechanics and its Applications 511 (2018) 389–400.

[156] G. H. Peng, S. H. Yang, D. X. Xia, X. Q. Li, A novel lattice hydrodynamic model considering the optimal estimation of flux difference effect on two-lane highway, Physica A: Statistical Mechanics and its Applications 506 (9) (2018) 929–937.

[157] G. H. Peng, S. H. Yang, H. Z. Zhao, L. Qing, The flux difference memory integral effect on two-lane stability in the lattice hydrodynamic model, International Journal of Modern Physics C 29 (9) (2018) 1850083.

[158] D. Kaur, S. Sharma, The impact of the predictive effect on traffic dynamics in a lattice model with passing, The European Physical Journal B 93 (3) (2020) 1–10.

[159] T. Wang, Z.-Y. Gao, X.-M. Zhao, J.-F. Tian, W.-Y. Zhang, Flow difference effect in the two-lane lattice hydrodynamic model, Chinese Physics B 21 (7) (2012) 070507.

[160] G. Zhang, D. H. Sun, W. N. Liu, M. Zhao, S. L. Cheng, Analysis of two-lane lattice hydrodynamic model with consideration of drivers' characteristics, Physica A: Statistical Mechanics and its Applications 422 (2015) 16–24.

[161] O. Biham, A. A. Middleton, D. Levine, Self-organization and a dynamical transition in traffic-flow models, Physical Review A 46 (10) (1992) R6124.

[162] T. Nagatani, Jamming transition in the traffic-flow model with two-level crossings, Physical Review E 48 (5) (1993) 3290.

[163] K. H. Chung, P. M. Hui, G. Q. Gu, Two-dimensional traffic flow problems with faulty traffic lights, Physical Review E 51 (1) (1995) 772.

[164] P. Redhu, A. K. Gupta, The role of passing in a two-dimensional network, Nonlinear Dynamics 86 (1) (2016) 389–399.

[165] Y. Liu, C. K. Wong, A two-dimensional lattice hydrodynamic model considering shared lane marking, Physics Letters A 384 (27) (2020) 126668.

[166] D. Kaur, S. Sharma, A new two-lane lattice model by considering predictive effect in traffic flow, Physica A: Statistical Mechanics and its Applications 539 (2020) 122913.

[167] J. F. Wang, F. X. Sun, R. J. Cheng, H. X. Ge, An extended heterogeneous car-following model with the consideration of the drivers' different psychological headways, Physica A: Statistical Mechanics and its Applications 506 (2018) 1113–1125.

[168] T. Wang, R. J. Cheng, H. X. Ge, Analysis of a novel lattice hydrodynamic model considering predictive effect and flow integral, Physica A: Statistical Mechanics and its Applications 527 (2019) 121425.

[169] C. Zhai, W. T. Wu, Lattice hydrodynamic modeling with continuous self-delayed traffic flux integral and vehicle overtaking effect, Modern Physics Letters B 34 (05) (2020) 2050071.

[170] X. Y. Qi, R. J. Cheng, H. X. Ge, Analysis of a novel two-lane lattice model with consideration of density integral and relative flow information, Engineering Computations 37 (8) (2020) 2939–2955.

[171] X. Y. Qi, H. X. Ge, R. J. Cheng, Analysis of a novel two-lane hydrodynamic lattice model accounting for driver's aggressive effect and flow difference integral, Mathematical Problems in Engineering 2020 (2020).

[172] T. Nagatani, Tdgl and mkdv equations for jamming transition in the lattice models of traffic, Physica A: Statistical Mechanics and its Applications 264 (3-4) (1999) 581–592.

[173] D. Kaur, S. Sharma, Prior information affecting traffic dynamics in a two dimensional (2d) network, The European Physical Journal B 94 (9) (2021) 1–12.

[174] P. Athol, Interdependence of certain operational characteristics withina moving traffic stream, Highway Research Record 72 (8) (1965) 58–87.

[175] R. Nair, H. S. Mahmassani, E. Miller Hooks, A porous flow approach to modeling heterogeneous traffic in disordered systems, Procedia-Social and Behavioral Sciences 17 (2011) 611–627.